APPENDIX T

Hydrodynamic Assessment of the Pit Lake
(Hydronumerics)

HydroNumerics

HydroNumerics

Project Martha

Martha Phase 4 Pit Extension

Pit Lake Limnology

Final Report

22 May 2018

Prepared for OceanaGold (NZ) Limited

HydroNumerics Pty Ltd
ABN 87 142 999 246
Suite 103, 757 Bourke St Docklands VIC 3008
www.hydronumerics.com.au

DOCUMENT SUMMARY

GENERAL INFORMATION	
Project Title	Project Martha Martha Phase 4 Pit Extension
Project Manager	Peter Yeates (Mb +61400 750 980) peter.yeates@hydronumerics.com.au
Document Title	Pit Lake Limnology
Document Type	Final Report
Authors	Peter Yeates and Patricia Okely
Document ID	HN_OG_Phase4PitLimnology_Report_Final.docx

CLIENT INFORMATION	
Client	OceanaGold (NZ) Limited
Contact	Kathy Mason
Details	kathy.mason@oceanagold.com

DOCUMENT HISTORY			
Prepared	Peter Yeates	Hydronumerics	22/05/2018
	Patricia Okely	Hydronumerics	
Reviewed	Chris Dallimore	Hydronumerics	10/05/2018
	Chris O'Neill	Hydronumerics	10/05/2018
		OceanaGold	27/03/2018
Submitted	Kathy Mason	Oceana Gold (NZ) Limited	22/05/2018

NOTICE

DISCLAIMER

The accuracy of information presented in this document is entirely dependent on the accuracy and completeness of supplied information. Hydronumerics Pty Ltd makes no warranty, representation or guarantee with respect to the accuracy and completeness of supplied information, shall have no liability to any person for any errors or omissions in the supplied information, and shall have no liability for loss or damage of any kind suffered or incurred by any person acting in reliance on the information in this document where the loss or damage arises from errors or omissions in the supplied information.

EXECUTIVE SUMMARY

Part of the consent process to extend mining activities at Waihi is rehabilitation of the Martha Phase 4 Pit, which includes filling the Martha Pit to create a pit lake (MPL). The pit lake is to provide recreation benefits to the local community.

Hydronumerics was contracted by OceanaGold (NZ) Limited to assess the physical limnology of MPL over decadal timeframes to determine the potential for stratification and mixing. To do so the three-dimensional Aquatic Ecosystem Model (AEM3D) was applied to simulate:

- Long time periods that incorporate stages of filling and post filling;
- The development of seasonal thermal stratification and subsequent mixing in response to meteorological conditions; and
- The dilution and fate of inflows from diverted river water, pit-wall run-off, rainwater and groundwater with different Total Dissolved Solids (TDS) and temperatures and their contribution to the stratification.

The predicted limnological behaviour is characterised by the following features:

- Strong seasonal stratification in the warmer months, followed by winter mixing that erodes the temperature stratification;
- In years with cooler and/or stormier autumn and winter months the mixing may extend more than 150 m below the surface. In years with warmer autumn and winter months, the extent of winter mixing is less than 100 m, and typically less than 75 m;
- Mixing to the full depth of the pit lake was not predicted because of development of density gradient (pycnocline) between the overlying pit water and water of high TDS that develops at depth;
- Deep mixing below 1000 m RL is predicted to occur in approximately 50% of years in the first 18 years after filling. The model results suggest sequential periods of years of deep and shallow mixing because of the legacy effects of years with warm autumn and winter conditions. Therefore, extended periods of no deep mixing are expected; and
- Over the next 16 years that were simulated the increased height of the pycnocline associated with the continual groundwater release into the base of the pit till reduce the depth of winter mixing.

Of the limitations and uncertainties associated with developing a predictive model of MPL, assumptions about the groundwater temperature are most likely to impact on the study outcomes. When groundwater is warm enough (estimated to be 24^{o}C) to overcome the density differences due to TDS, the mixing regime changes to include more frequent deep mixing.

These findings have a number of implications for concurrent water chemistry studies (AECOM, 2018). These include the chemistry associated with very long, and potentially indefinite, periods of isolation (i.e. a lack of refreshing from mixing processes) of the waters beneath the deep pycnocline from the waters above. In addition, long periods (possibly decades) of isolation of waters below 70 to 100 m and above the pycnocline will likely lead to substantial chemical change over time for these intermediate waters. Mixing deep waters into the surface waters during deep mixing years following a period of stratification has the potential to rapidly and substantially change the surface water chemistry and the chemistry of

the released water. A lack of mixing for long periods may also lead to deterioration in the surface water chemistry due to a lack of dilution of poor quality run-off waters.

Because MPL will take some time to adjust to a run-off, rainfall and groundwater dominated system, after a filling period dominated by the diversion of river flow, it is likely that the physical limnology will gradually change over decadal timeframes, with associated long term evolution of the water chemistry.

HydroNumerics

TABLE OF CONTENTS

LIST OF FIGURES

LIST OF TABLES

1 Project Overview

1.1 Martha Phase 4 Pit Lake

1.1.1 Location

Part of the consent process to extend mining activities at Waihi is rehabilitation of the Martha Phase 4 Pit. Rehabilitation includes filling the Martha Pit to create a pit lake (the Martha Pit Lake – hereafter referred to as MPL) that is to provide recreational benefits to the local community. The intended end-use of MPL includes primary contact through watercraft and swimming activities.

A regional depiction of the open pit (to be rehabilitated as MPL) in relation to the town of Waihi and associated mining structures is provided in Figure 1.1.

Figure 1.1 Regional view of the Martha Pit and related mining infrastructure (Source: Google Earth).

1.1.2 Bathymetry

At the completion of the Martha Phase 4 Pit cutback the pit shell characteristics will be:

- Floor level of approximately 875 m RL;
- Depth of approximately 275 m;
- Length (NE to SW) of approximately 950 m;
- Breadth (NW to SE) of approximately 715 m;
- Surface area of approximately 51 ha; and

- Total volume of approximately 43 million m^3.

A contour diagram of the pit is provided in Figure 1.2 below.

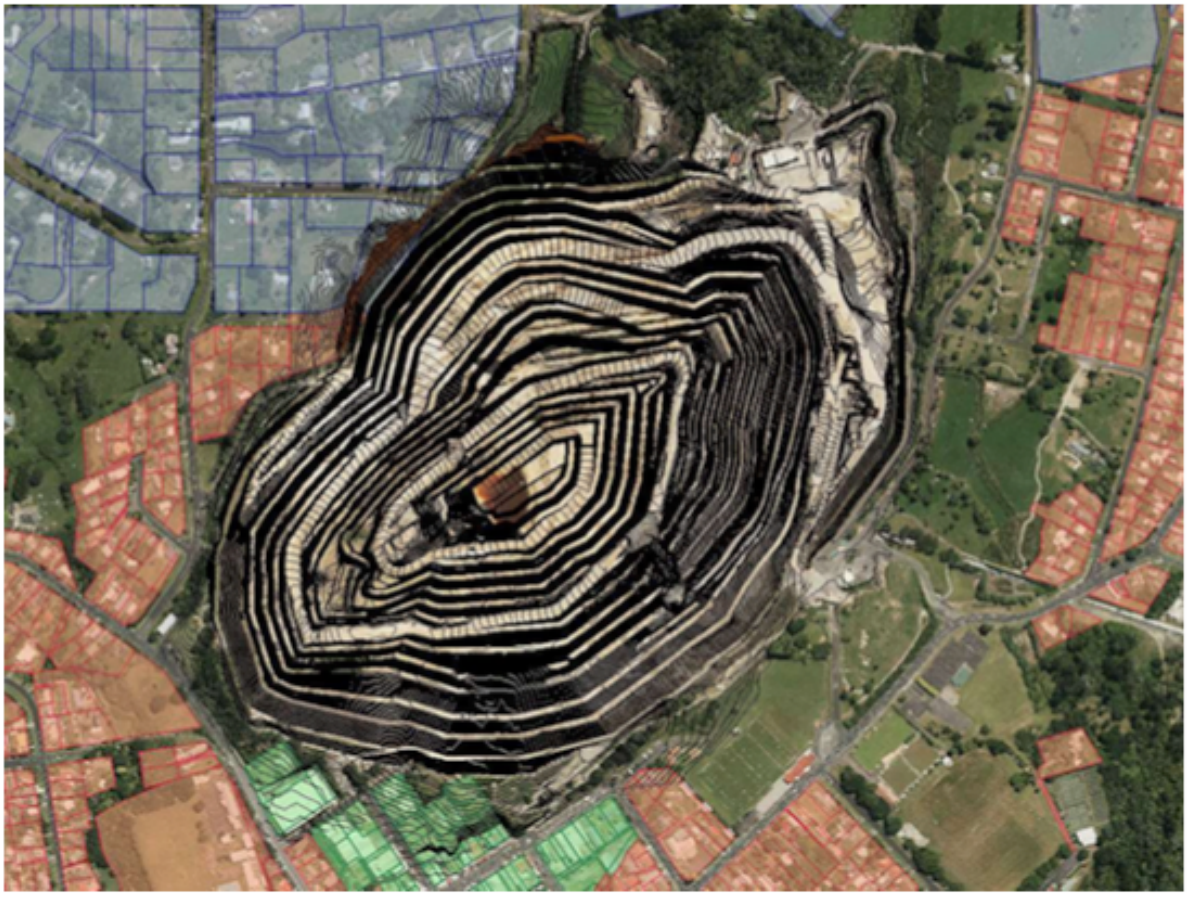

Figure 1.2 Martha Pit contours and surrounding township (Ocean Gold, 2017a)

1.1.3 Meteorology

Meteorological conditions at and near to the Martha mine pit are recorded at Waihi mine site, Golden Valley to the east, and Tauranga Airport to the south.

The meteorological conditions at Waihi consist of a humid-maritime climate with average annual precipitation of about 2 m that exceeds evaporation by approximately three-fold. Winds are frequently strong (in excess of 10 m/s) and there is only a moderate variation between minimum and maximum temperatures (with an average of 10 ^{o}C difference between winter and summer). Average summer daily temperatures peak at approximately 25 ^{o}C, during winter they peak at approximately 15 ^{o}C. Daily minimum temperatures are about 10 ^{o}C in summer and below zero in winter.

Whilst a detailed assessment of site meteorology is beyond the scope of this study, the meteorological data has been used and discussed in the context of the limnological modelling undertaken in Chapter 3. Detailed records of meteorological conditions are illustrated in the Appendix.

1.2 Study Objectives

Hydronumerics was contracted by Oceana Gold (NZ) Limited to deliver on the following project objectives:

a. Assess the hydrodynamic performance of the proposed MPL over decadal timeframes to determine the potential for stratification and mixing; the results of which will feed into a reassessment of the pit lake water quality;

b. Liaise with a geochemistry consultant to ensure that study outputs can and are properly incorporated into the lake water quality predictions;

c. Liaise with OGNZL staff and support OGNZL's consultation program as required; and

d. Respond to requests for further information from councils.

This technical report has been compiled to support a resource consent application by reporting on a study that has examined the expected physical limnology of the MPL. A three dimensional numerical model of the pit lake hydrodynamics was developed to assist with this study and the results of the modelling have been described in this report.

2 Physical Limnology of Pit Lakes

2.1 Overview

The limnology of pit lakes is influenced by a range of physical and biogeochemical processes that govern the quality of water in-situ and the quality of water released from a lake. In addition, the water quality may change over time due to changes in weather, hydrology, geochemistry and biological activity.

Predicting the limnology of pit lakes needs to take into account the spectrum of processes that are considered in the study of lakes and reservoirs, but for pit lakes a greater emphasis is typically applied to geochemical processes that relate to the mineralogy of the pit walls and groundwater recharge.

Castendyk and Eary (2009) provide a hierarchical framework for assessing water quality in pit lakes that considers sequential levels of knowledge. At a very fundamental level the pit geology (and shape), local climate and hydrology underpin the physical limnology (i.e. the hydrodynamics) of a pit lake (Figure 2.1). The physical limnology then provides a context for assessments of lake geochemistry and consequently potential management and mitigation decisions that ultimately impact on the water quality and end use.

This study is focussed only on assessing the physical limnology of the proposed MPL. In the sub-sections that follow we provide an overview of the physical limnology of pit lakes that provides the necessary background for a concise discussion about the predicted limnology of MPL. This includes examining case studies mine pit lakes that are reported in the literature and a review of previous limnological studies that have been undertaken for MPL.

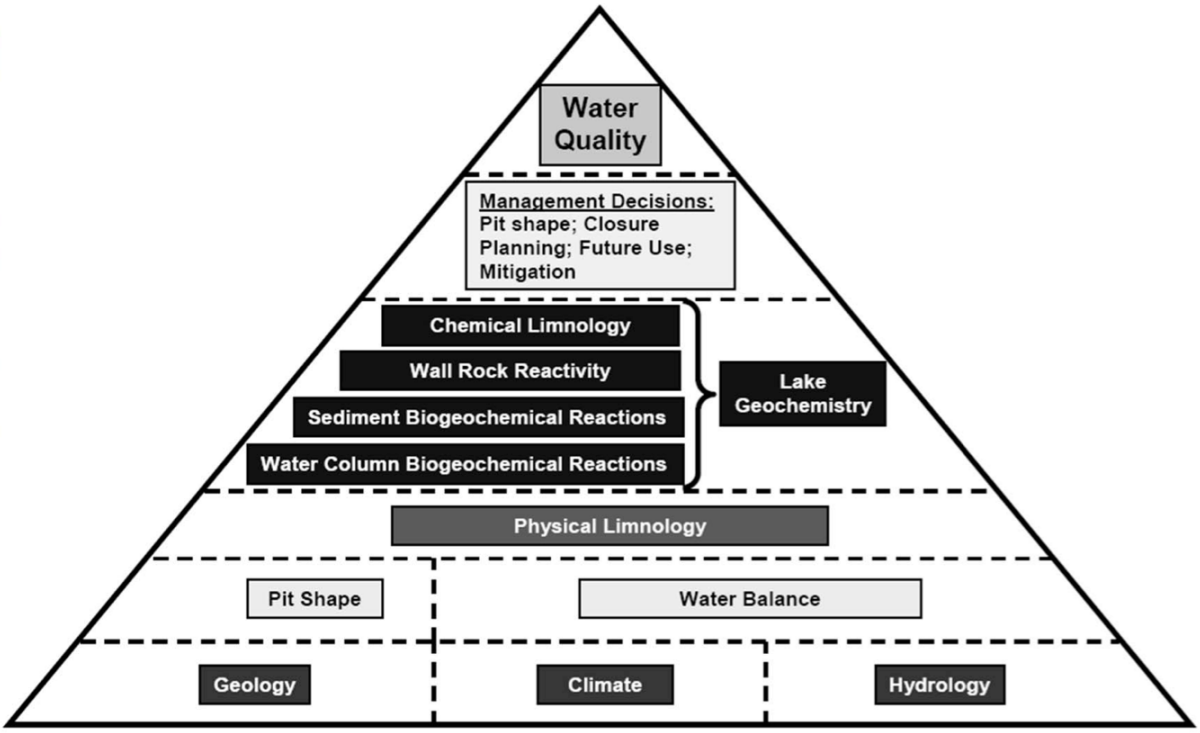

Figure 2.1 Conceptual relationships between components that impact on pit lake water quality, as presented in Castendyk and Eary (2009).

2.2 Stratification and Mixing

2.2.1 Stratification

Pit lakes differ from most natural lakes owing to steep sides and considerably higher depth to surface area ratios. Whilst most natural lakes have a relative depth (i.e. the ratio of depth to surface area) of less than 2%, pit lakes commonly have relative depths of between 10 and 40% (Doyle and Davies, 1999, cited from Zhao et al. 2009). The small surface area and extensive depth of mine pit lakes means that vertical density stratification of the pit lake water column is typically observed.

Vertical temperature gradients contribute to density stratification and develop in response to surface heating from the atmosphere during the warmer months. This leads to a stable density stratification whereby lighter warm water near the surface of the lake lies above cooler, heavier (i.e. more dense) water beneath. Temperature gradients erode during the winter months as the surface waters cool and mix with the water beneath. Mixing may be complete to the bottom of the lake leading to uniform temperature profiles. Alternatively, temperature gradients may persist during the cooler months (albeit with significantly reduced strength and at a deeper depths) if there is insufficient mixing to overcome the buoyancy forces associated with the density gradients. Mixing typically arises from external forcing at the surface from winds, cooling and inflows (see Chapter 2.2.2 for a description of mixing processes).

The clarity of water within a pit lake is an important parameter that influences the strength of temperature stratification. In turbid water there is a rapid absorption of light as it travels down from the lake surface (i.e. the water has a high light extinction coefficient) so that much of the solar radiation hitting the surface of the lake generates heat in a thin layer near the surface. Conversely, when water clarity is high (i.e. the light extinction coefficient is low) heat energy from the sun is distributed more deeply, which leads to weaker temperature gradients.

The clarity of the water will depend on the concentration of suspended material and dissolved constituents that absorb light (such as sediments and dissolved organic matter) and the concentration of biological constituents, including phytoplankton.

In addition to the density stratification that arises due to surface heating gradients, the temperature differences between the inflowing source waters, and the rate at which they fill the pit, will influence the temperature gradients that develop. Warm subsurface inflow (compared to the overlying water) such as groundwater seepage, or cold surface flows, will have a destabilizing effect that weakens vertical stratification and promotes mixing. Cold groundwater seepage or warm surface flows will strengthen temperature gradients.

The strength of the density stratification that develops in a pit lake is also a function of suspended and dissolved concentrations. Total dissolved solids (TDS) and electrolytic conductivity tend to increase with depth reaching values that are often several times higher than at the surface (Zhao et al. 2009). The differences in TDS in source water and/or the in-situ increase in TDS over time from pit-wall leachate can contribute to the vertical gradients in TDS and therefore strengthen density gradients leading to greater stability (i.e. resistance to mixing).

However the processes are not always simplistic; for example, high TDS surface run-off into an established pit lake may plunge vertically into the water column, promoting mixing and entrainment of surface or intermediate water that ultimately reduces the density gradient through the water column. As a result, the flow rates and the location of the inputs during and after filling are important factors that control the eventual density stratification. In the case of cold, high TDS groundwater seeping into the depths of a pit lake, coupled with low TDS river water and precipitation at the surface, strong vertical TDS gradients will form and increase the stability of the lake.

Because of the stable density stratification the water column in a pit lake will often develop as a series of layers. In the most basic case of a temperature stratified pit lake two distinct layers will form – the *epilimnion* at the surface that overlies the *hypolimnion* beneath. The epilimnion and hypolimnion are separated by gradients in an intermediate layer of water called the *metalimnion.* The *thermocline* refers to the region where temperature gradients are highest. The thickness of the metalimnion will depend largely on the extent of mixing that occurs between the epilimnion and hypolimnion and the intrusion of layers of intermediate density during inflow events.

2.2.2 Mixing

Mixing mechanisms in stratified lakes are varied and complex and an exhaustive review is not provided herein. Key vertical mixing processes that will potentially impact on the limnology of MPL are described briefly below.

Horizontal mixing in density-stratified waters typically occurs at rates that are significantly faster than vertical mixing because horizontal mixing is not impeded by the buoyancy forces encountered during vertical mixing. In small lakes with simple geometry, such as pit lakes, it is therefore reasonable to assume that horizontal gradients of water quality constituents do not persist and lateral heterogeneity is rapidly achieved. In contrast, vertical mixing rates are slowed by the density gradients and in the absence of mixing mechanisms that overcome buoyancy forces the vertical exchange of constituents through the metalimnion will potentially reduce to rates of molecular diffusion.

Wind shear and cooling at the surface are two key mechanisms that trigger vertical mixing. Turbulent kinetic energy is generated in the epilimnion from wind shear and wave action at the surface of the lake. This creates a turbulent front that penetrates down through the epilimnion and erodes the density gradients in the metalimnion. In doing so there is an exchange of water between the hypolimnion and epilimnion. Wind stress at the surface also imparts momentum into the epilimnion that creates currents and internal waves (see below for a description of internal waves). At locations in the lake where vertical velocity gradients develop (such as in the metalimnion and at the boundaries) internal shear may be high enough (compared to the buoyancy forces offered by the stable stratification) to create instabilities that generate turbulence and cause mixing.

During atmospheric cooling at night or in the cooler months, surface waters become colder (and therefore more dense) than the waters beneath to create an unstable density profile that adjusts vertically by developing convective mixing cells in which the denser water of higher density plunges and is replaced by warmer water from beneath. This leads to a cooling and deepening of the epilimnion. In lakes with complex bathymetry, differential heating and cooling over the lake surface due to changes in depth may induce secondary currents that exchange water masses further.

Weakening of the density stratification, and eventual complete mixing is usually the result of a combination of convective mixing and wind mixing processes that exchange epilimnion waters down into the hypolimnion. The depth of mixing will depend on the energy provided by the disruptive processes compared to the stabilising forces of the stratification. For example, during the peak of summer stratification, vertical mixing induced by a strong wind event may promote complete mixing within the epilimnion, but only entrain a small fraction of the cooler water beneath. Most of the turbulent mixing energy is dissipated as heat within the epilimnion. However, for the same wind stress applied in autumn, when the stratification is weaker, complete mixing through to the bottom of the lake may result.

Other mixing mechanisms that are likely to be less influential in MPL include internal waves and inflow entrainment. As wind stress at the surface imparts momentum into the epilimnion surface waters will be ‘pushed’ downwind to create a pressure gradient that tilts the

thermocline down at the downwind end of the lake and up at the upwind end. If sufficient deflection of the thermocline takes place, the hypolimnion waters can upwell at the upwind end of the lake and mixing of the epilimnion and hypolimnion occurs. When the wind stress is relaxed the thermocline will oscillate (i.e. an internal seiche will evolve) leading to internal and boundary shear that may contribute to mixing. Internal wave motions in lakes can be varied and complex depending on the bathymetric shape and size, rotational effects (i.e. Coriolis force), and the natural harmonic frequency of the lake compared to the frequency of the wind forcing.

Inflows may also act to adjust stratification. As inflows propagate through the lake they typically entrain ambient waters and create intrusions of intermediate density that adjust the stratification. Stratification may weaken in the case of flows of intermediate density that form intrusions with the density gradients in the metalimnion, or strengthen for overflows and underflows. Inflows that are cooler than ambient water temperature (or with high dissolved or suspended concentrations) are denser than ambient water and may under some conditions generate underflows that can displace hypolimnion waters and potentially strengthen stratification. In a similar way warmer inflows may be confined to the epilimnion and increase the epilimnion temperature.

Heat that is introduced at depth (e.g. through groundwater) may lead to an unstable density profile that promotes mixing as the plume rises through the water column. The same principles apply for fresh water introduced into brackish deep waters.

The stratification and mixing regime dictates the fate and transport of constituents that are either derived internally (e.g. sediment releases and primary productivity) or introduced from an external source (e.g. in catchment water, groundwater and atmosphere deposition). During stratification there is limited vertical exchange of internally derived constituents between the epilimnion and hypolimnion with the exception of particles in the epilimnion (such as detritus and suspended sediments) that settle deeper into the water column owing to their negative buoyancy. Other than slow molecule exchange, only gaseous release in the hypolimnion will propagate into the epilimnion in the absence of physical mixing or biological motility.

Because of the complex nature and transient behaviour of stratification and mixing, processes-based numerical models are typically required to account for the stratification and mixing processes that contribute to fate and transport on constituents within stratified water bodies.

2.2.3 Classifications

Basic classifications of stratification and mixing regimes have been offered in the limnological literature to differentiate between distinctly different hydrodynamic behaviors. Lakes that undergo a period of complete vertical mixing one or more times a year are classified as *holomictic* (Figure 2.2(a)). Complete mixing in a lake is often referred to as lake ‘turnover’, despite this term being a misleading description for a gradual mixing process that occurs in many lakes that experience seasonal cooling and complete mixing.

Holomictic lakes include:

- *Monomictic* lakes that undergo a single period of full mixing each year;
- *Dimictic* lakes that undergo two periods of complete mixing each year; and
- *Polymictic* lakes are shallow enough that seasonal stratification does not develop and therefore mix multiple times each year.

Deep temperate lakes such as those that occur in New Zealand are typically classified as monomictic and undergo an annual cycle of thermal stratification in spring and summer followed by complete mixing in autumn and winter (Spigel 1997).

In contrast to holomictic lakes, *meromictic* lakes do not mix completely. Mixing between the epilimnion and hypolimnion creates a so-called *mixolimnion* that by itself behaves much like a holomictic lake; however, the mixing excludes a deeper water fraction that sits below the hypolimnion, which is referred to as the *monimolimnion* (Figure 2.2b). While temperature gradients may contribute to a lack of mixing of the monimolimnion with the waters above, high dissolved solids concentrations generally contribute to a density gradient across a *chemocline* (between the hypolimnion and monimolimnion) that prohibits or slows deep vertical mixing (both partial and complete).

One further classification of lakes relevant to deep pit lakes is that of an *oligomictic* lake, which mixes completely, but only occasionally, and not every year. Complete mixing occurs during events, such as unusually cold and stormy weather, which can generate enough mixing energy to overcome the stable density stratification. In most years, however, winter mixing is only partial and complete mixing to the bottom of the lake does not occur. Oligomictic lakes may, for many years, behave the same way as meromictic lakes and only experience very occasional complete mixing events. These events are of particular interest because of the rapid changes in water quality that can occur when monimolimnetic waters are mixed into the remainder of the reservoir after a long period of physical isolation that is often accompanied by significant chemical change. In many instances the chemical change in the monimolimion follows from a change in redox conditions that occurs due to the lack of frequent downward mixing of oxygenated surface waters that replenish oxygen concentrations at depth. Whilst the same process occurs in the hypolimnion during summer stratification, winter mixing acts as an annual ‘re-set’ of chemical conditions in holomictic lakes; this is not the case in oligomictic lakes where de-oxygenation may persist for many years.

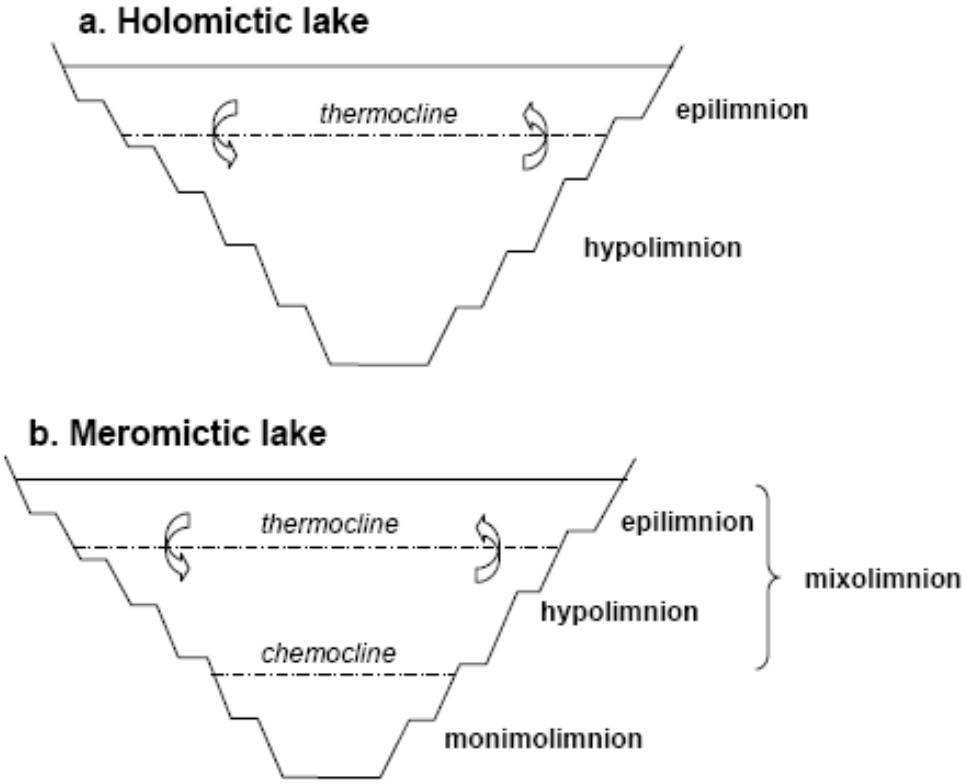

Figure 2.2 Limnological classifications of stratification and mixing regimes in an (a) *holomictic* pit lake, and (d) a *meromictic* pit lake (Soni et al. 2014). The arrows depict mixing between layers.

2.3 Pit Lake Studies

2.3.1 Literature Survey

A review of pit lake stratification relevant to MPL reported in published literature (see summary table in the Appendix) indicates that meromixis was observed in eight of the ten lakes with a total depth of more than 100 m. The two lakes reviewed that are more than 100 m deep and do not experience meromixis (from available observations) are Enterprise (Boland and Padovan 2002) in tropical northern Australia and Sleeper (Dowling et al. 2004) in Nevada, USA. Only six of the remaining 20 pit lakes with a depth of less than 100 m have been classified as meromictic.

Enterprise Pit Lake experiences considerably different climatic conditions to Waihi and, at 140 m deep, is significantly shallower than MPL. However, it should be noted that the lack of consistent measurements to the bottom of the Enterprise pit lake made it difficult for the authors to ascertain the true nature of the mixing regime; whilst they report observations of a seasonal deep mixing period, the full extent of the mixing was not well defined.

Sleeper Pit Lake is shallower than MPL and has the largest surface area to depth ratio (of 0.7 ha/m) of the meromictic pit lakes that were reported with depths from 100 to 200 m deep. Moreover, the authors note that surface cooling in late autumn is sufficient to promote a thermal inversion that gives rise to deep mixing and a homogeneous water column through the cooler months of the year. This is triggered by monthly average minimum temperatures (as recorded in nearby Winnemucca) that drop below zero from October to May.

Jewell (2009) summarises thermocline depth during summer stratification in pit lakes as a function of the length of the pit lake (see Figure 2.3). MPL has a length of approximately 1000 m, and so based on the relationship of Jewell (2009) the thermocline depth during summer stratification is expected to be approximately 10 m.

A simple comparison between MPL and existing pit lakes reported in the literature therefore suggests that meromictic behaviour in MPL is likely given the depth of the pit, small surface area to depth ratio and mild climate. MPL is likely to cycle between summer stratification (with a peak summer thermocline depth of approximately 10 m) and a winter mixed condition that does not include mixing to the bottom of the water column. A majority of the pit lakes reported in the literature less than 100 m deep have been classified as holomictic, which suggests that winter mixing in MPL may extend to 100 m or more below the surface.

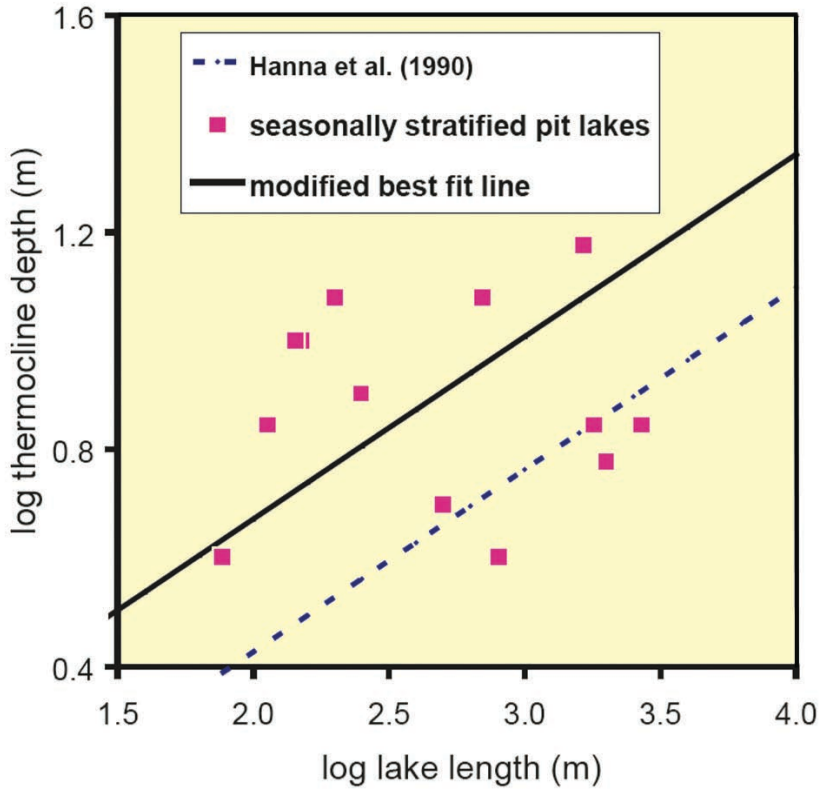

Figure 2.3 Thermocline depth as a function of pit lake length (Jewell, 2009).

2.3.2 Previous Studies

A prediction of the physical limnology of MPL was previously undertaken by Spigel (1997), who applied a 1D numerical model to assess thermal stratification and mixing in response to sixteen consecutive years of meteorological data collected at the town of Waihi. Two pit options were investigated, one with a total depth of 135 m and another with a total depth of 210 m. Only the findings from the deeper configuration are considered here given the new projected depth of MPL being over 210 m.

An example of simulated temperature profiles for 1983 are illustrated in Figure 2.4 for a case with a light extinction coefficient of 0.7 m^{-1} (low clarity) and 0.1 m^{-1} (high clarity). For the low water clarity case predictions show strong summer and spring stratification with an epilimnion of 5 to 20 m thick that is 20 to 21 ^{o}C. In the cooler months of autumn and winter the

stratification erodes until there is deep (and sometimes complete) mixing by August. The deep mixing period is then followed by a re-establishment of thermal stratification as the warmer weather returns. Temperatures in the hypolimnion are approximately 10 ^{o}C during stratification, and 10 ^{o}C through the water column during winter mixing. For the simulations with higher water clarity the temperature gradients in the metalimnion are considerably weaker and extend 20 to 30 m deep compared to 5 to 10 m for the low clarity case.

The modelling of Spigel (1997) suggested that:

- MPL will be strongly stratified every summer and remain weakly stratified during most winters;
- Complete mixing in the deep lake (210 m) will occur in 20 to 30% of all years modelled (i.e. every 3 to 5 years on average);
- Maximum depth of winter mixing during years when complete mixing did not occur is 150 m; and
- In years of incomplete winter mixing the minimum temperature difference between surface and bottom waters will be between 0.01 and 1.2 ^{o}C.

In addition to predictions described above, the following key observations were drawn from modelling results:

- Groundwater inflow may increase the frequency and duration of complete mixing. The extent of increase depends on the buoyancy effects associated with elevated groundwater temperatures and the degree to which temperature-induced buoyancy is offset by higher concentrations of dissolved solids in the groundwater compared to the lake;
- Model results were most sensitive to the magnitude of the extinction coefficient (i.e. the water clarity) and less sensitive to the basin size;
- Vertical mixing is most likely to follow a course of gradual mixed-layer deepening over the entire basin, as opposed to strong upwelling and sudden 'turnover'.

The modelling of Spigel (1997) suggests that the predicted oligomixis of MPL is atypical of New Zealand lakes (which are usually holomictic) and this is attributable to the large depth-to-surface area ratio of MPL and a maritime climate in Waihi of warm humid summers and mild winters.

Importantly, the modelling undertaken by Spigel (1997) did not take into account the contribution to stratification that is made by inflow waters with different salinity (or TDS). The results are therefore based only on the predicted temperature stratification in MPL and the influence of river diversion and rainfall (both of which have low TDS). The contribution from groundwater and surface run-off from the pit batters (which have far higher TDS) was not included in the model.

Nonetheless, the predicted temperature stratification regime remains consistent with the literature whereby the lakes cycles between a stratified summer condition with a shallow thermocline (approximately 5 to 10 m deep for the low water clarity case) and a weakly stratified winter mixed condition that is expected to reach a mixing depth of more than 100 m in most years with complete mixing occurring in some years. The predicted oligomictic behaviour differs from the meromixis typically observed in pit lakes of simular dimension, which may be because of the higher TDS inputs of groundwater and pit-wall run-off were omitted in the model so that a deep chemocline with stable density gradient does not develop.

More recent predictive modelling by Castendyk and Webster-Brown (2007) introduced some key modifications to the work done by Spigel (1997). Although Castendyk and Webster-

Brown (2007) applied the same model, they included elevated TDS of pit-wall run-off and groundwater inputs in the model. A series of sensitivity simulations were also performed over a range of potential values of TDS and temperature of the additional inflows. The simulated temperature, salinity and density profiles over time for the different scenarios are illustrated in Figure 2.5.

The model results show that the salinity and temperature assigned to water balance items during filling had an impact on the predicted mixing and stratification regimes, the most influential change being the temperature that was assigned to the groundwater contribution. Cold groundwater (assumed to be at 17^{o}C) produced the most stable density profile when compared to simulations with warm (and therefore more buoyant) groundwater. The effect of adjusting the salinity of the other inflows was more complex. The addition of higher salinity pit-wall run-off to the cold groundwater case weakened the density gradients, yet the pit lake stratification still persisted over the 6-year simulation. In the persistently stratified scenarios (i.e. those with cold groundwater) the depth of the mixolimnion in winter was approximately 150 m when the lake was full; the remaining water in the bottom 60 m did not mix, as shown by the persistent salinity and temperature gradients. When warmer (at 20^{o}C) groundwater was introduced, complete mixing was predicted in winter regardless of whether the pit-wall run-off was of high or low salinity.

The study of Castendyk and Webster-Brown (2007) concludes by providing a conceptual model for the filing of MPL, in which the resultant stratification is a function of the properties of the source waters during the filling period – in particular the density difference between the river water and the groundwater. A potential shortcoming of the study is the limited simulation period, which does not account for slow erosion of density gradients over time, or the impact of infrequent weather events.

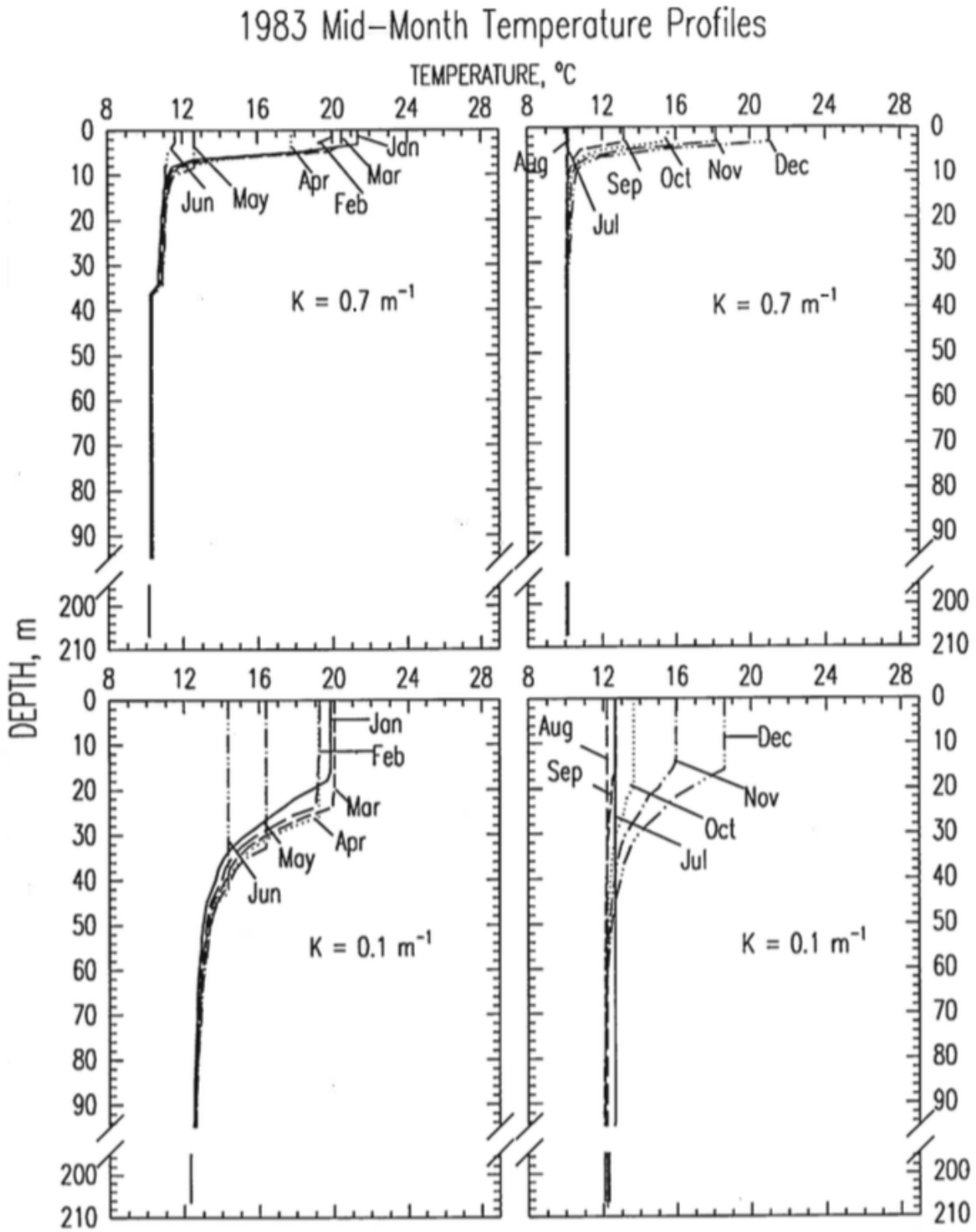

Figure 2.4 Simulated monthly temperature profiles in MPL for low clarity (top panels) and high clarify (bottom panels) from Spigel (1997).

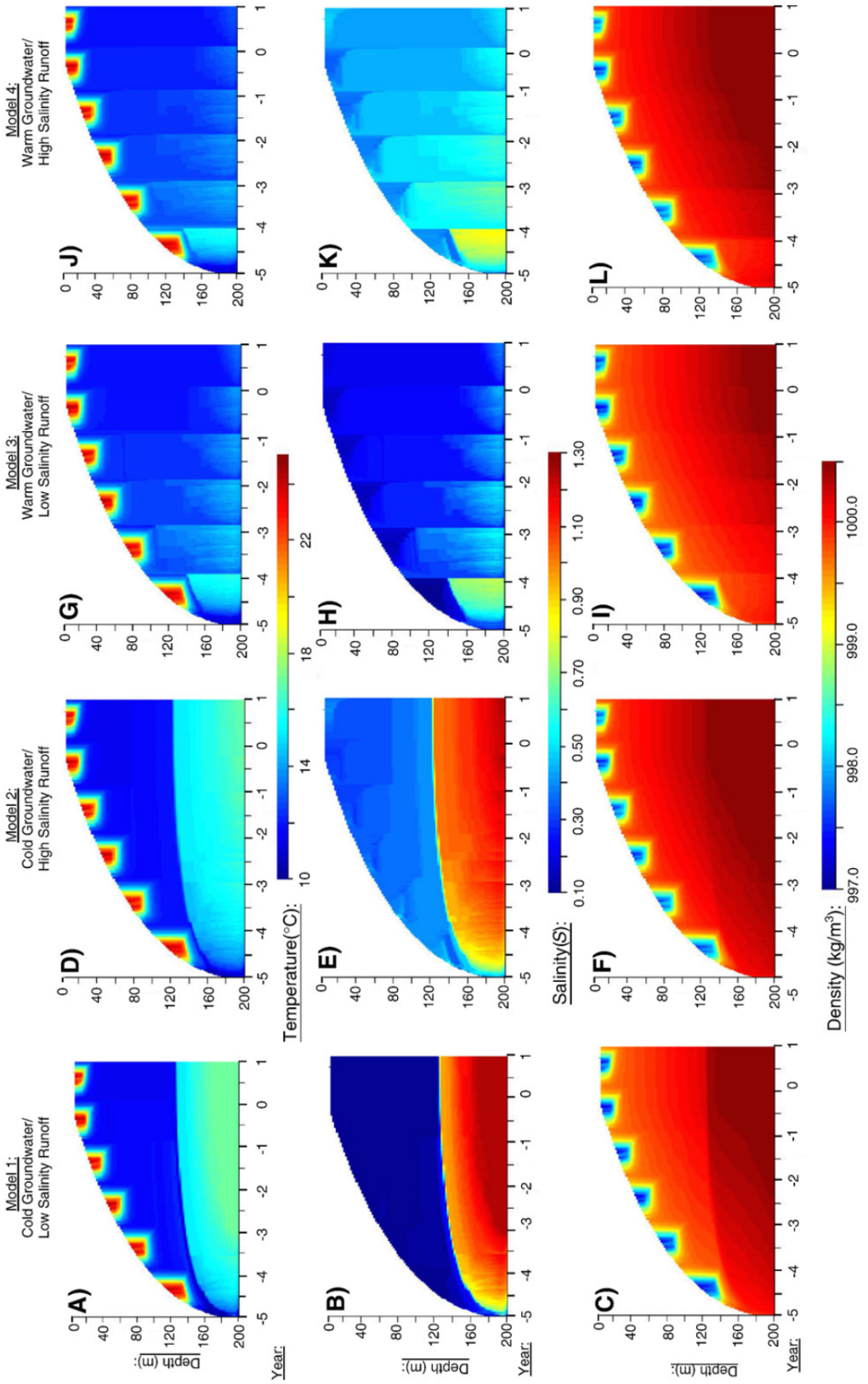

Figure 2.5 Temperature, salinity, and density profiles of four DYRESM models of the proposed MPL (Castendyk and Webster-Brown, 2007). Note the scenario descriptions in the figure panel titles.

3 Pit Lake Model

3.1 Overview

This section of the report describes the model that was applied to predict the hydrodynamics of MPL, the model configuration and simulations that have been undertaken. Based on the findings of the literature review there are a number of essential processes that needed to be incorporated into a model of MPL. These processes are:

- Development of seasonal thermal stratification and subsequent mixing in response to meteorological conditions;
- Account for inflows of different temperature and TDS and how they contribute to the strength of vertical density gradients, which are a culmination of vertical gradients in temperature, total suspended solids (TSS), TDS and pressure. This includes groundwater inputs;
- Track the dilution of the different flows that contribute to the water balance and provide information on the dilution to inform assessments of the resultant water quality; and
- Provide a means to simulate long time periods that incorporate stages of filling and post filling.

3.2 Model Description

3.2.1 Aquatic Ecosystem Model 3D

The Aquatic Ecosystem Model (AEM3D) is a three-dimensional hydrodynamic model used for forecasting the velocity, temperature and salinity distribution in natural water bodies that are subjected to external environmental forcing such as meteorological conditions, catchment flows and groundwater flows. AEM3D has been applied globally to numerous and varied environments including rivers, wetlands, lakes, reservoirs, estuaries and coastal regions. AEM3D is based on an earlier model – the so-called Estuary Lake and Coastal Ocean Model (ELCOM) - developed by the University of Western Australia. The numerical schemes in the model are described in peer-reviewed literature (e.g. Hodges et al. (2000). Whilst AEM3D can be used to simulate aquatic chemistry and biology, in this study only the physical properties (i.e. the hydrodynamics) of the pit lake have been modelled.

The transport equations in AEM3D are unsteady Reynolds-averaged Navier-Stokes equations and scalar transport equations with the Boussinesq approximation with non-hydrostatic pressure terms. The free surface solution is provided by vertical integration of the continuity equation applied to the Reynolds-averaged kinematic boundary condition. The flow equations are solved using the TRIM numerical scheme (Casulli and Cheng 1992), with modifications to improve accuracy, scalar conservation, numerical diffusion, and implementation of a mixed-layer turbulence closure scheme. Solutions are made on an Arakawa C-grid (orthogonal with the option of a varying width) within which flow velocity is defined on cell faces and the free-surface height and scalar concentrations are solved at the cell centre. The free-surface height in each column of grid cells moves vertically through the grid to improve computational efficiency and allows sharper vertical gradients to be maintained with coarse grid resolutions.

AEM3D computes solutions using the following steps:

1. Introduce surface heating/cooling in the surface layer;
2. Mix scalar concentrations and momentum using a mixed-layer model;

3. Introduce wind energy as a momentum source in the wind-mixed layer;
4. Solve the free-surface evolution and velocity field;
5. Apply horizontal diffusion of momentum;
6. Advection of scalars; and
7. Horizontal diffusion of scalars.

The most critical components for the MPL modelling are steps 1, 2 and 3 because they are the mechanisms that dictate the cycles of stratification and mixing. In Step 1 the heat exchange through the surface is governed by the bulk transfer models of Amorocho and Devries (1980), Imberger and Patterson (1981) and Jacquet (1983). The energy transfer across the free surface is separated into non-penetrative components of long-wave radiation, sensible heat transfer, and evaporative heat loss and complemented by penetrative shortwave radiation. Non-penetrative effects are introduced as sources of heat in the surface-mixed layer, whereas penetrative sources are introduced as heat in one or more grid layers on the basis of an exponential decay and a light extinction coefficient in accordance with Beer's Law. The extinction coefficient for the absorption of solar radiation can be set by the user for different wavelengths, or derived by the model based on the specific attenuation provided by dissolved and/or suspended constituents.

For the base case simulation undertaken in this study an extinction coefficient of 0.7 m^{-1} was used (as per Spigel 1997) and a test-case simulation was also undertaken with light extinction coefficient of 0.1 m^{-1}. The results of the tests are described in Chapter 3.5.

Vertical mixing, which is governed by step 2 and 3, is based on a turbulent kinetic energy (TKE) mixed-layer model that accounts for the different sources of mixing energy – convective mixing from surface heat exchange, wind-generated turbulence at the surface and shear due to velocity gradients (introduced in step 2). These processes contribute to a TKE budget that is applied to mix the water column, during which the available TKE is used to increase the potential energy (PE) of the water column by mixing heavier water beneath the surface mixed layer with lighter water within the surface mixed layer. The algorithm used to determine available TKE and mixing is generic (as opposed to site-specific) and process-based; the algorithm form and parameters are derived from process-scale laboratory work reported in the literature and scalable to the model grid size. As a result the mixing rates in AEM3D are not defined by the user and require no explicit calibration process. This in turn provides a means for robust prediction of the stratification and mixing in hypothetical lakes such as MPL.

3.3 Model Build

3.3.1 Bathymetry

Bathymetry for the MPL model was generated from CAD diagram (provided by OceanaGold as a DXF file) that mapped the depth and shape contours of the pit. This data was converted into Cartesian x, y, and z data points and geo-referenced. Figure 3.1 illustrates the high-resolution 10 x 10 m horizontal grid bathymetry. The high-resolution grid was sub-sampled to produce 40 x 40m and 80 x 80 m and lateral grid resolution with two preliminary vertical resolutions of 1 and 2.5 m.

Preliminary modelling tests where undertaken (see Table 3.1) to determine the grid size that provided simulation efficiency, in terms of computation run speed, and was able to simulate multiple years without a loss of model performance (when compared to higher resolution grids). The test configurations used a model time step of 30 seconds over a 20-year simulation period. Results of the test simulations are shown in Figure 3.2. After 2 decades of model simulation the coarse vertical grid size of 2.5 m (compared to 1 m) produced a deeper

thermocline and warmer profile. The 80 x 80 m and 40 x 40 m horizontal grids produced simulation results that were very similar, however the 40 x 40 m gridded model took almost 4 times longer to complete the simulation. Use of the finer horizontal grid model for multiple decadal simulations was deemed prohibitive (in terms of time) and therefore an 80 x 80 m horizontal grid with a 1 m vertical grid resolution was selected for the project. Moreover, the selected model configuration remained numerically stable for a larger time step of 60 seconds, increasing the real-to-runtime ratio to 1:8400, so that a 27-year simulation based on the water balance provided was able to be completed in 1.3 days.

The bathymetry, storage capacity and surface area curves are illustrated in Figure 3.3 and Figure 3.4.

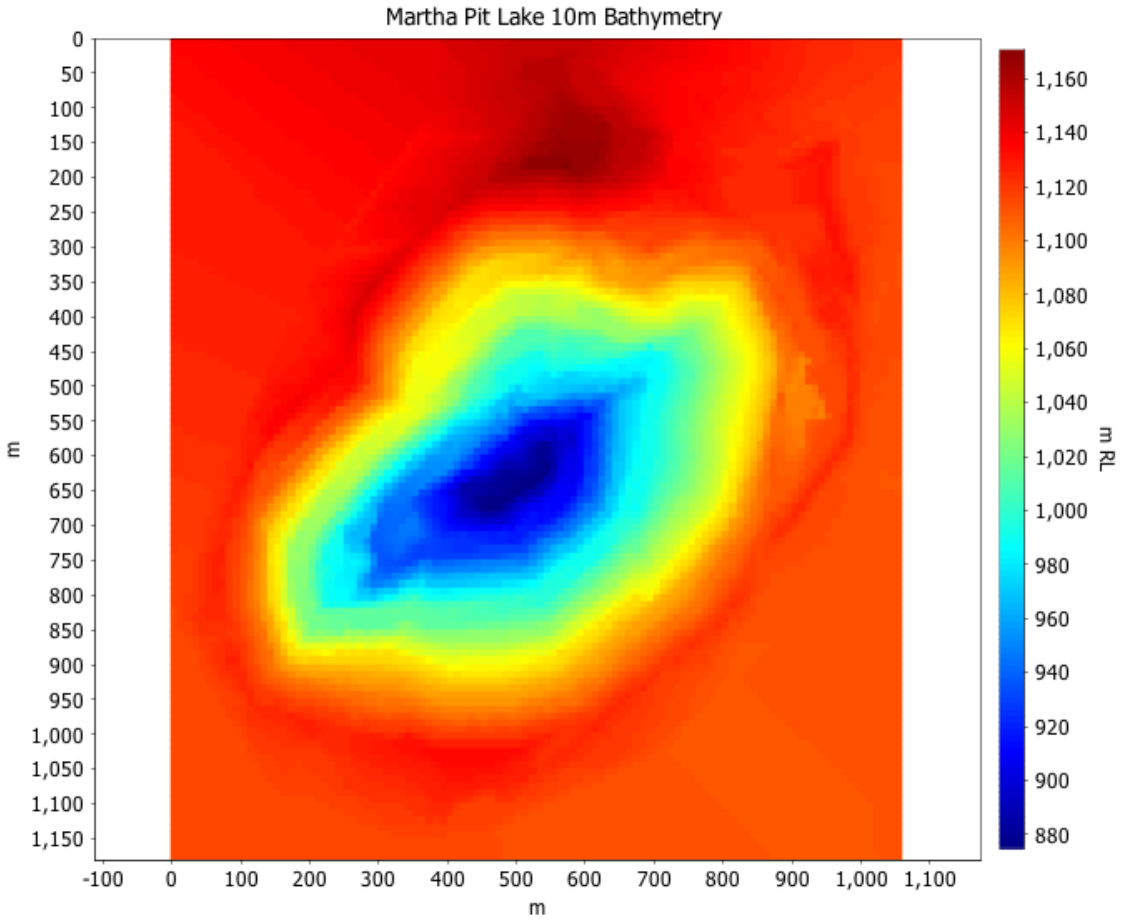

Figure 3.1 High resolution 10 x 10 m bathymetry for MPL.

Table 3.1 Model grid configurations and real to run time ratio model performance

Horizontal Grid Size (m)	Vertical Grid Size (m)	Real:Runtime ratio	Days to Simulate 10 Years
40 x 40	1	377	9.7
80 x 80	1	1377	2.7
80 x 80	2.5	2724	1.3

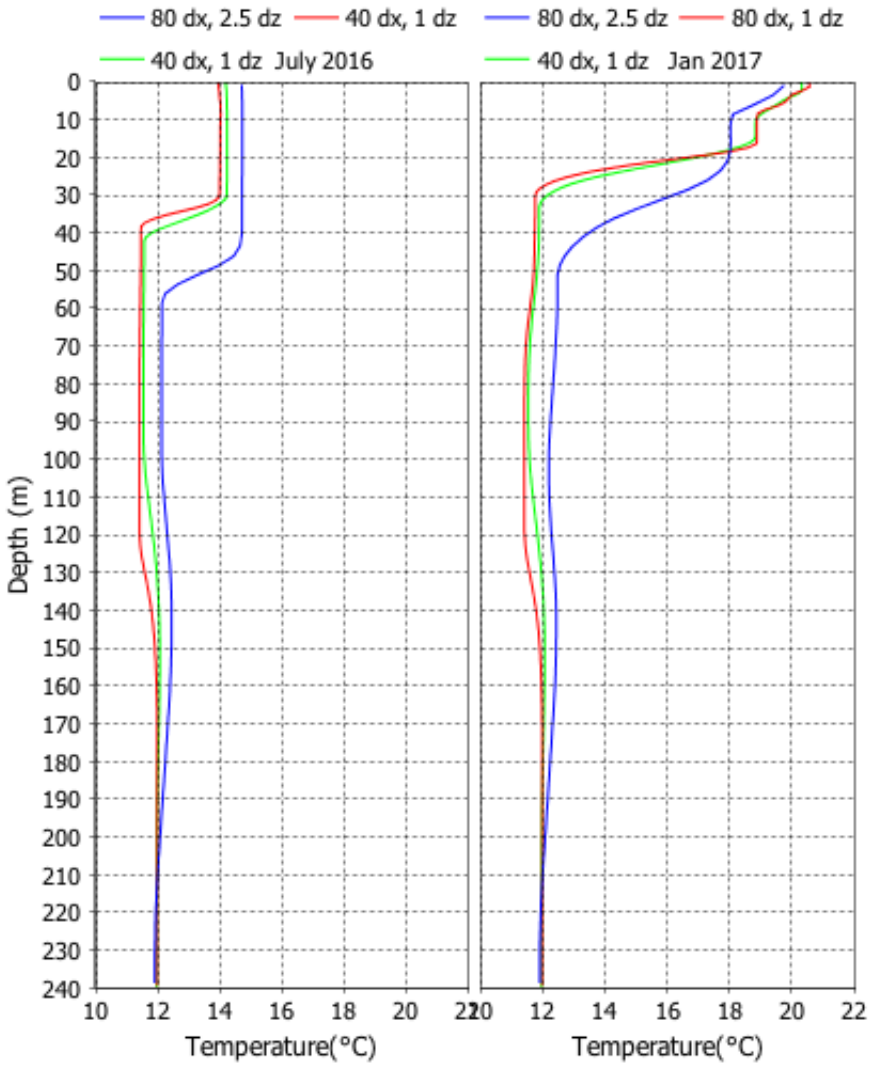

Figure 3.2 Simulated temperature profiles in MPL modelling tests for winter (left) and summer (right) for the model configured with 80 m horizontal and 2.5 m vertical grid (blue), 80 m / 1 m (red) and 40 m / 1 m (green) horizontal / vertical grid size.

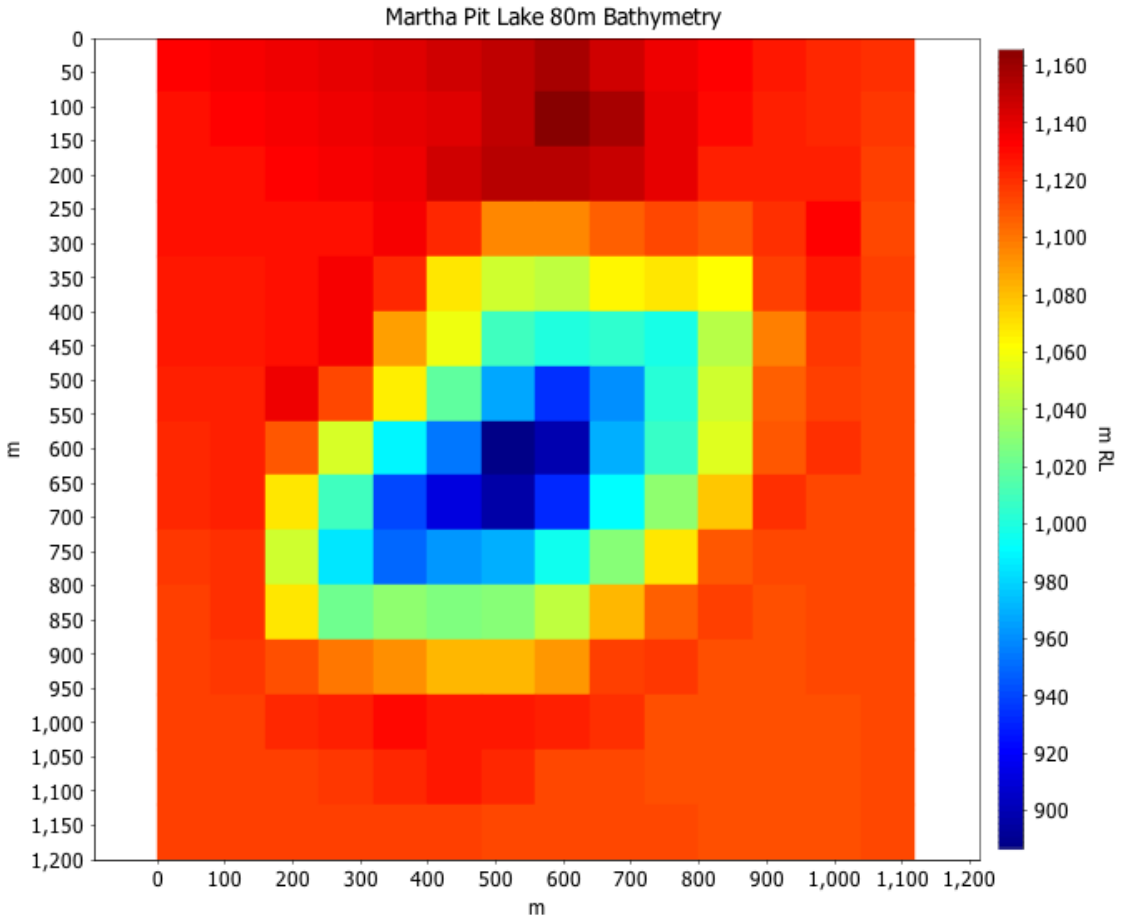

Figure 3.3 MPL model bathymetry with 80 m x 80 m horizontal grid size.

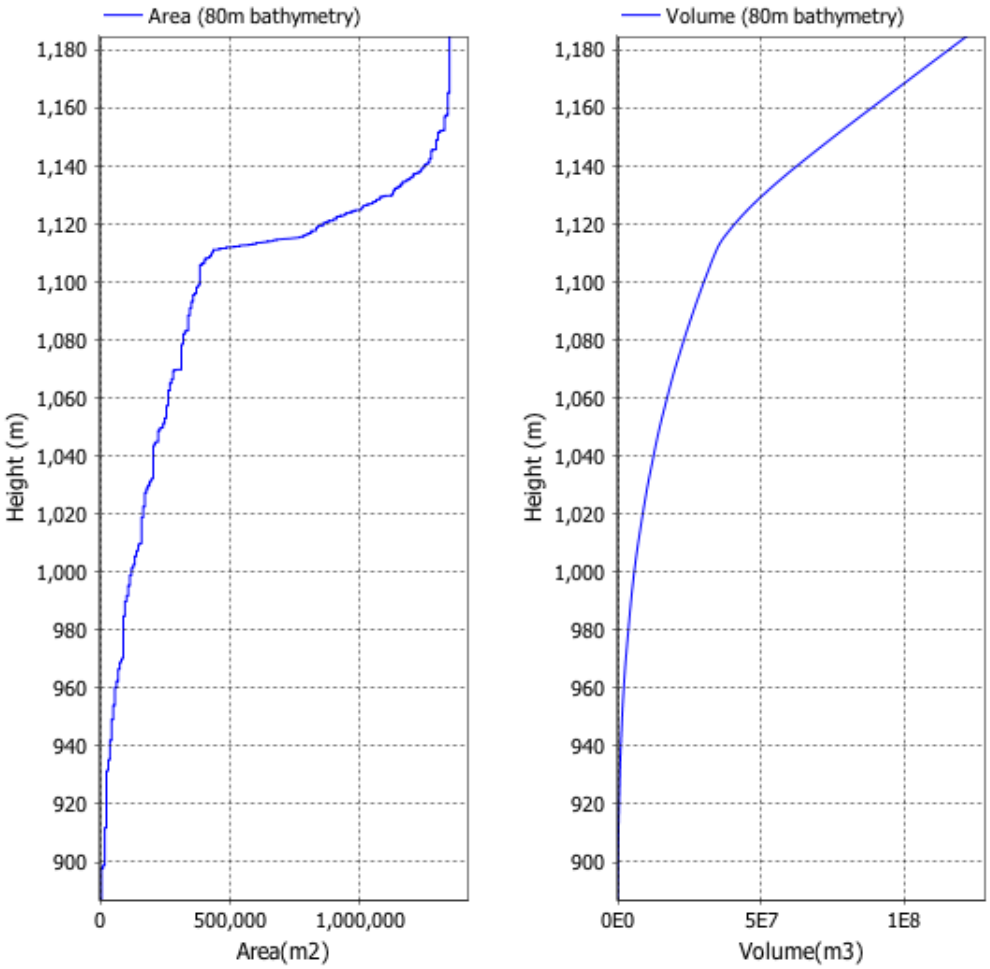

Figure 3.4 Surface area and storage curves for the 80m x 80m model grid.

3.3.2 Meteorology

Meteorological data from monitoring stations at Waihi, Golden Valley and Tauranga Airport were used to construct hourly time series of meteorological conditions required as surface boundary conditions for MPL model. The available raw data series are summarised in Table 3.2, including notes on the quality of the data. A continuous time series of each meteorological parameter data was compiled using the Waihi data as the basis and following the template provided in Table 3.3 to address the gaps in the Waihi observations.

A summary of the model time series that has been generated is provided in Table 3.4. The table indicates the model year labelling (Y01, Y02 etc.) that has been applied over the duration of the simulations. The data was looped from July 2017 (Y23) - when the latest observations were made - using data from July 2001 onwards. Detailed figures of the meteorological time series are shown in the Appendix.

Table 3.2 Summary of available meteorological data.

Parameter require by model	**Source**	**Period**	**Comments**
Solar Radiation	Waihi Mine Site (Waihi)	1994 – 2016	Minimum (overnight) value of 4.9 Wm^{-2}; quality of data prior to Sept 1994 questionable
	Tauranga Airport (TVA)	1999 – 2017	Quality/units of data prior to 1999 questionable
Cloud Cover	TVA	2004 – 2017	No gaps, code observations
Air Temperature	Waihi	1994 – 2016	Frequent spikes in data prior to Oct 1997
	TVA	1993 – 2017	
	Golden Valley (GVX)	2007 – 2017	Smaller diurnal range than Waihi and TVA
Relative Humidity	Waihi	1994 – 2016	Low maximum prior to Oct 1997
	TVA	1993 – 2017	Frequent issues with data prior to June 1994
	GVX	2007 – 2017	
Wind Direction	Waihi	1994 – 2016	
	TVA	1993 – 2017	
	GVX	2007 – 2017	
Wind Speed	Waihi	1994 – 2016	Data for 1994-2013 in ms^{-1}; data for 2006-2016 in kmh^{-1}
	TVA	1993 – 2017	Units of knots
	GVX	2007 – 2017	Units questionable – if knots correct than measurements typically substantially higher than Waihi and TVA
Rainfall	Waihi	1907 – 2017	
	TVA	1993 – 2017	

Table 3.3. Protocol that was used to fill gaps in the Waihi meteorological data.

Period of poor or missing data in Waihi record	**Parameters affected***	**Comments**
1/9/1994 - 25/10/1997	AT, RH	Filled with TVA
1-19/2/1995	S, W	W filled with TVA; S filled with subsequent fortnight Waihi
25/12/1995-6/2/1996	R	Filled with TVA
24/12/1996 - 6/2/1997	S, W	W filled with TVA; S filled with 24/12/1997 - 6/2/1998 Waihi
24/12/1996 - 25/10/1997	W	Filled with TVA
2/6/1998 - 6/2/1999	S	Filled with 2/6/1999 – 1/1/2000 Waihi and 1/1/1999 – 2/6/1999 TVA
18/6/1998 - 17/12/1998	O	Filled with TVA
6-20/11/1999	O	Filled with TVA
3-7/3/2000	ALL	Filled with TVA
30/6/2000-1/5/2002	R	Filled with TVA
29/11/2001 - 1/3/2002	O	Filled with TVA
29/11/2001 - 14/7/2002	S	Filled with 29/11/2002 – 14/7/2003 Waihi
20-22/7/2005	ALL	Filled with TVA
14/10/2011-21/3/2012	AT, RH	Filled with TVA
14/10/2011-27/4/2012	W	Filled with TVA
14/10/2011-14/4/2012	S	Filled with TVA
10/11/2011-1/2/2012	R	Filled with TVA
1/3/2012-27/4/2012	R	Filled with TVA
2/12/2013 - 3/1/2014	AT, RH	Filled with TVA
18-28/4/2014	ALL	Filled with TVA
24-27/10/2014	ALL	Filled with TVA
24/5 - 5/6/2015	AT, RH	Filled with TVA
31/12/2016 - 1/7/2017	ALL	Filled with TVA

6/12/2016 -1/7/2017	R	Filled with TVA

* AT = air temperature, RH = relative humidity, W = wind speed and direction, S = solar radiation, R = rainfall, ALL = all parameters except rainfall, O = all parameters except solar radiation and rainfall); for some Waihi solar radiation gaps, no data was available from TVA, so replication of Waihi data from subsequent year used – see comments.

Table 3.4 Annual means of variables in the meteorological time series.

Model Year	Obs. Year	Daily Max. Air Temp. (°C)	Daily Min. Air Temp. (°C)	Daily Mean Relative Humidity	Daily Total Solar Rad. (W/m2)	Daily Max. Wind Speed (m/s)
Y01	1995	18.47	10.97	0.78	3807.02	5.64
Y02	1996	18.58	10.42	0.76	4038.35	5.66
Y03	1997	18.33	10.15	0.77	4076.17	6.63
Y04	1998	19.33	11.26	0.79	4004.96	6.48
Y05	1999	18.54	9.17	0.81	3991.87	5.36
Y06	2000	18.25	9.61	0.81	4052.28	5.85
Y07	2001	18.10	9.62	0.84	3942.77	5.62
Y08	2002	17.89	9.76	0.80	4136.53	6.47
Y09	2003	18.06	9.16	0.81	3919.98	5.50
Y10	2004	17.46	8.75	0.79	3987.86	6.08
Y11	2005	18.57	9.17	0.80	4078.85	5.52
Y12	2006	17.87	8.71	0.79	4096.26	6.46
Y13	2007	18.17	9.67	0.79	3991.86	6.59
Y14	2008	18.24	9.68	0.78	4060.63	6.58
Y15	2009	17.98	8.82	0.78	4114.10	6.47
Y16	2010	18.69	9.61	0.78	4070.47	6.23
Y17	2011	18.84	10.43	0.76	4039.63	6.38
Y18	2012	18.21	9.66	0.77	4117.22	6.47
Y19	2013	19.35	10.11	0.76	4094.44	6.15
Y20	2014	18.61	9.72	0.75	4040.41	6.66
Y21	2015	18.68	9.61	0.75	4052.76	6.72
Y22	2016	18.98	10.74	0.77	3872.00	6.53
Y23	2017/01*	18.89	10.69	0.81	4132.68	6.25
Y24	2002	17.89	9.76	0.80	4136.53	6.47
Y25	2003	18.06	9.16	0.81	3919.98	5.50

Y26	2004	17.46	8.75	0.79	3987.86	6.08
Y27	2005	18.57	9.17	0.80	4078.85	5.52
Y28	2006	17.87	8.71	0.79	4096.26	6.46
Average		***18.36***	***9.68***	***0.79***	***4033.52***	***6.15***

* Repeat of meteorological data begins in July 2017 using 2001 data.

3.3.3 Water Balance

The water balance for MPL was provided by concurrent water balance modelling undertaken by GHD (Anthony Kirk, pers. comms). The water balance model outputs were provided on a daily timestep for a median flow realisation (realisation number 33 from GHD Goldsim model). A summary of the water balance provided at the time of the modelling undertaken in this study is provided in Table 3.5. Illustrations of time series of the water balance outputs are provided in the Appendix.

The total surface run-off to the pit provided in the water balance was partitioned into a series of run-off contributions from different pit wall areas (see Figure 3.5, URS 2012). The fraction of contributions from each section of the pit wall was set to change as the water level in the pit rose. A summary of the run-off contributions is provided in Table 3.6.

Table 3.5 Annual totals of model flows (ML).

Model Year	**GW to Pit**	**Pit to GW (outflow)**	**Rainfall**	**River**	**Run-off**	**Spillway (outflow)**
Y01	0	8047	1	6802	1268	0
Y02	0	6387	0	5476	952	0
Y03	1	7600	1	6437	1208	0
Y04	33	4170	33	4448	860	0
Y05	104	2447	151	5111	945	0
Y06	187	377	245	4442	718	0
Y07	77	554	469	6079	734	0
Y08	113	69	468	4491	474	0
Y09	102	8	961	7505	624	0
Y10	176	2	775	583	314	1758
Y11	181	0	1298	0	506	1985
Y12	183	0	851	0	331	1365
Y13	183	0	759	0	296	1229

Y14	182	0	772	0	300	1249
Y15	182	0	921	0	359	1468
Y16	182	0	1224	0	477	1870
Y17	181	0	772	0	300	1249
Y18	183	0	806	0	314	1294
Y19	180	0	627	0	244	1043
Y20	182	0	838	0	327	1346
Y21	182	0	889	0	346	1389
Y22	183	0	797	0	311	1290
Y23	181	0	809	0	315	1303
Y24	182	0	729	0	284	1188
Y25	182	0	729	0	284	1194
Y26	182	0	726	0	283	1187
Y27	182	0	782	0	304	1273

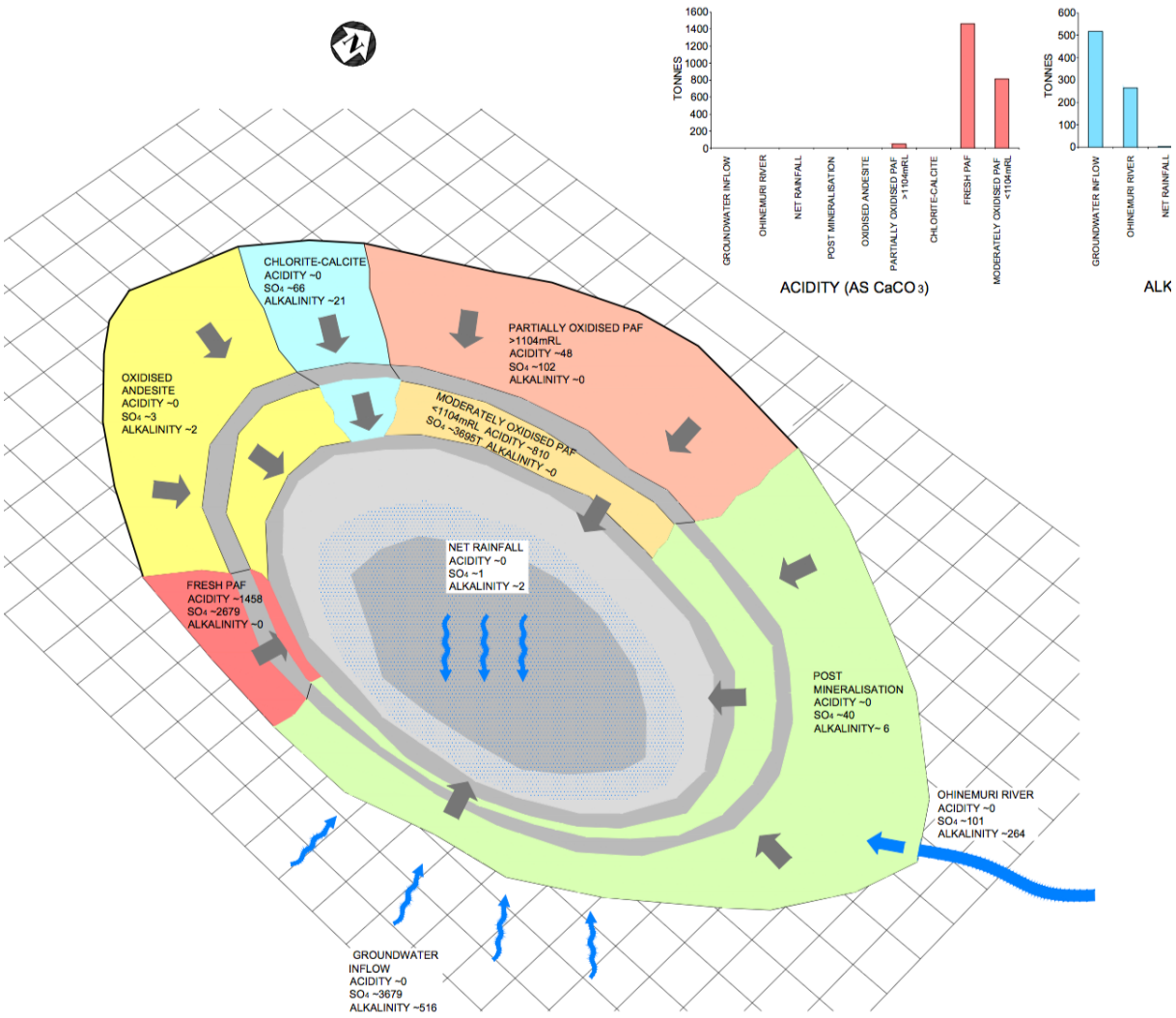

Figure 3.5 Map of predicted pit wall run-off areas (URS, 2012)

Table 3.6 Annual totals run-off (i.e. ML/yr) from the different pit-wall areas over the duration of the simulation (see Figure 3.5)

Year	Post Min	Oxidised	Partial Ox	North Fresh PAF	Chlorite Calcite	South Fresh PAF
Y01	393	179	351	24	226	95
Y02	295	134	264	18	169	72
Y03	374	170	334	23	215	91
Y04	280	125	212	17	158	68
Y05	356	159	184	22	151	72
Y06	296	144	107	21	87	63

Y07	317	165	84	26	70	72
Y08	230	154	0	32	14	45
Y09	302	202	0	42	19	59
Y10	152	102	0	21	10	30
Y11	245	164	0	34	15	48
Y12	160	107	0	22	10	31
Y13	143	96	0	20	9	28
Y14	146	97	0	20	9	28
Y15	174	116	0	24	11	34
Y16	231	154	0	32	14	45
Y17	146	97	0	20	9	28
Y18	152	102	0	21	10	30
Y19	118	79	0	16	7	23
Y20	158	106	0	22	10	31
Y21	168	112	0	23	10	33
Y22	150	101	0	21	9	29
Y23	153	102	0	21	10	30
Y24	137	92	0	19	9	27
Y25	137	92	0	19	9	27
Y26	137	92	0	19	9	27
Y27	147	99	0	20	9	29

3.3.4 Inflow Properties

The TDS for the component of the water balance items was provided from the geochemistry work of AECOM (Timothy Mulliner, pers. comms), see Table 3.7. The median TDS values were used for base case simulations, and 75th percentile TDS values for the PAF run-off contributions were used for in the sensitivity analysis described in Chapter 3.5. Salinity, as tracked by the model, was used to represent TDS using an approximation that 0.001 psu salinity is equivalent to 1 mg L^{-1} of TDS.

For the base case the water temperature of the inflows into MPL were assigned simulated in-lake temperatures; rainfall, river water and surface run-off were assigned a temperature equal to the surface water temperature of the pit lake; groundwater was assigned a

temperature equal to the bottom temperature simulated in the pit lake. Additional simulations were undertaken (see Chapter 3.5) to assess the impact of this assumption on the modelling outcomes.

Table 3.7 Inflow properties (TDS and water temperature) used in MPL model.

Groundwater			
TDS	*25th Percentile*	*Median*	*75th Percentile*
TDS (mg/L)	1410.4	1487.4	1547.7
Temperature	Bottom of Lake		
Rain			
TDS (mg/L)	2.7		
Temperature	Surface of Lake		
River Diversion			
TDS (mg/L)	55.6	57.6	61.0
Temperature	Surface of Lake		
Pit-wall run-off Contributions			
Post Mineralisation			
TDS (mg/L)	38.9	57.0	89.8
Temperature	Surface of Lake		
Oxidised			
TDS (mg/L)	23.1	33.5	52.9
Temperature	Surface of Lake		
Partially Oxidised			
TDS (mg/L)	607.7	1139	1809
Temperature	Surface of Lake		
North Wall Fresh PAF			
TDS (mg/L)	1181.6	2100.5	3619.7
Temperature	Surface of Lake		
Chlorite-Calcite			
TDS (mg/L)	270.7	418.1	556.4
Temperature (mg/L)	Surface of Lake		
South Wall Fresh PAF			
TDS (mg/L)	1181.6	2100.5	3619.7
Temperature	Surface of Lake		

3.3.5 Configuration

The MPL model was set to run for 28 years (Y01 to Y28) using a 60 second time-step. This period coincides with the beginning of the meteorological time series at Y01 (1995) and extends for the duration of the supplied water balance model (to Y28). Beyond July Y23 (2017) the available meteorological time series was repeated from July 2001 to cover the

entire time series of the water balance. The model was initiated with a surface height of 900 m RL – this is the minimum water level required for the configuration of the model. A spillway at 1104 m RL was included in the model configuration and a basic weir formula applied to calculate the rate of outflow through the spillway.

Model outputs from the deepest point in the simulated MPL have been analysed as part of results and discussion that follow.

3.4 Model Results

3.4.1 Stratification

After an initial four years of net loss of input water to the groundwater system the model predicts it will take another approximately 5 years to fill to 1104 m RL by Y10. The rate of filling may differ from the water balance model because, firstly, AEM3D makes an internal calculation of evaporation in every time-step based on the temperature of the water at the surface and meteorological conditions. This calculation will differ from the calculation used in the Goldsim water balance model provided by the GHD. Secondly, the bathymetry (and hence storage capacity) in AEM3D is influenced by the model grid size, and given that the model grid is relatively coarse, the estimate of storage capacity as a function of water level will differ from estimates made with a high spatial resolution Digital Elevation Model (DEM). However, it should be noted that these differences are unlikely to impact on the limnological behaviour predicted by the model.

By Y05 a cycle of summer temperature stratification and winter mixing develops (Figure 3.6). At the peak of summer stratification between January and February the epilimnion is 5 to 10 m deep and with temperatures of 23 to 27 ^{o}C (see Figure 3.7 to Figure 3.8). The temperature gradients in the metalimnion extend 20 to 25 m below the epilimnion, reaching down to 12 to 13 ^{o}C. In the hypolimnion temperature gradients are very weak with temperature differences of less than 1 - 2 ^{o}C spanning over the bottom 150 m.

In the autumn months the surface temperatures cool and the epilimnion deepens until the temperature gradients erode almost completely. The water cools to between 12 and 13 ^{o}C in mid-winter and in the spring, temperature gradients build again back towards peak summer stratification. Below 100 m, temperatures are maintained at 12 to 13 ^{o}C all year round, with weak gradients that occur in response to periods of deep mixing. Despite the very weak temperature gradients below 100 m, density gradients persist throughout the profile – in part due to pressure effects but also due to the elevated TDS of groundwater that seeps into the bottom of the pit and is retained near to the bottom due to the slow and weak mixing processes at operate at depth (see Figure 3.10).

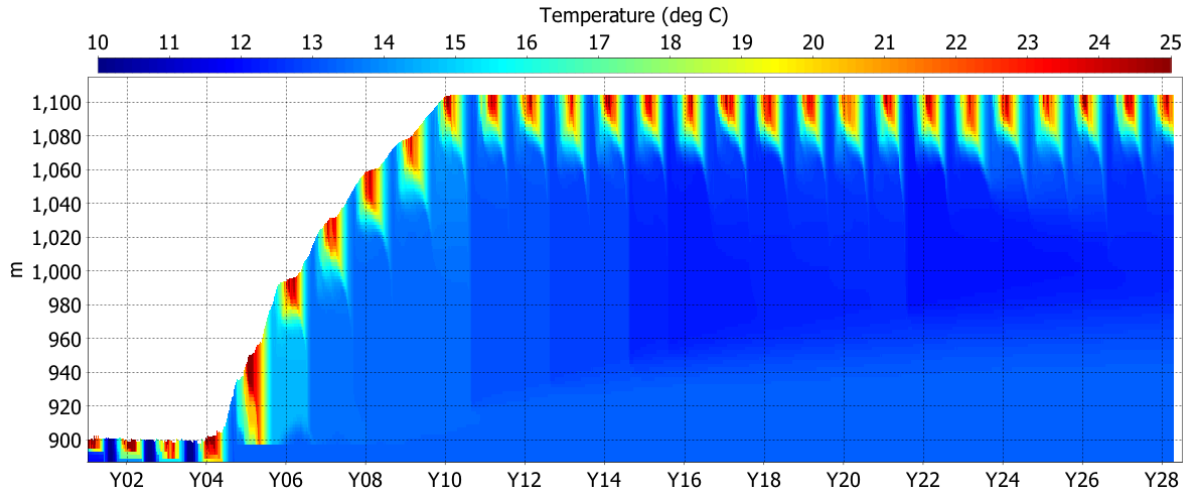

Figure 3.6 Time series contour of simulated temperature over the depth of MPL during and after filling.

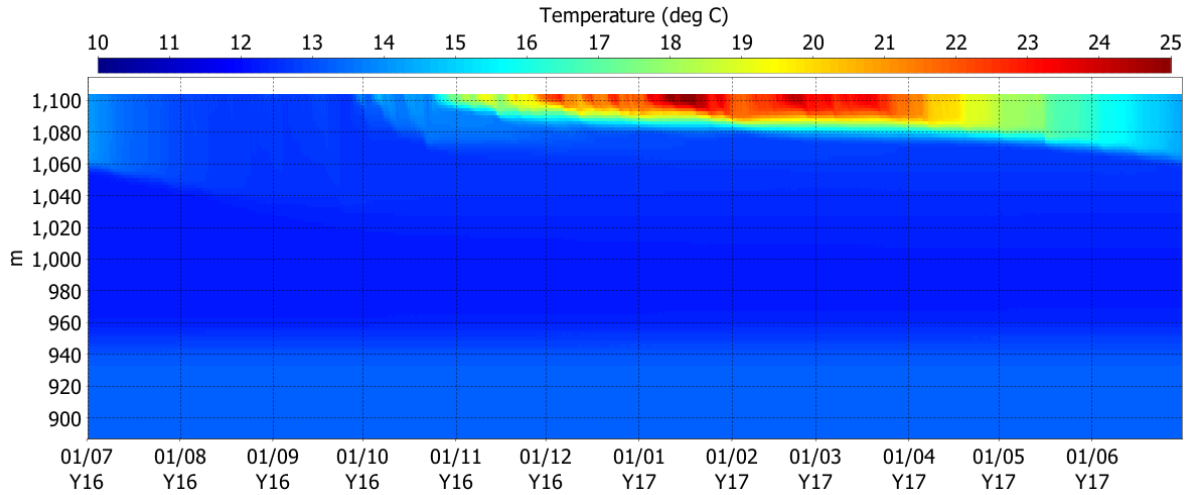

Figure 3.7 Time series contour of simulated temperature over the depth of MPL during from July Y16 to June Y17.

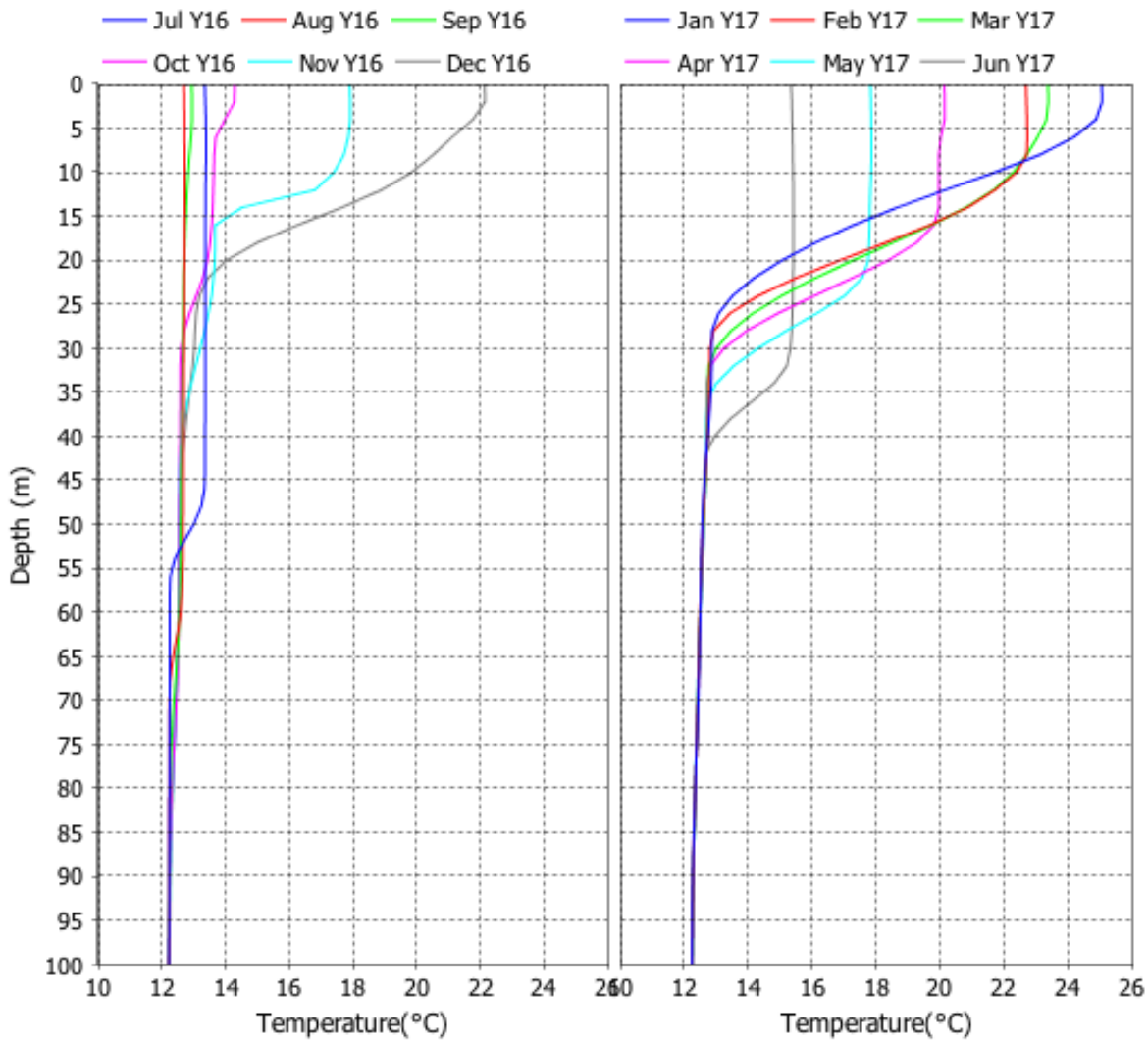

Figure 3.8 Simulated mid-month temperature profiles from July Y16 to June Y17.

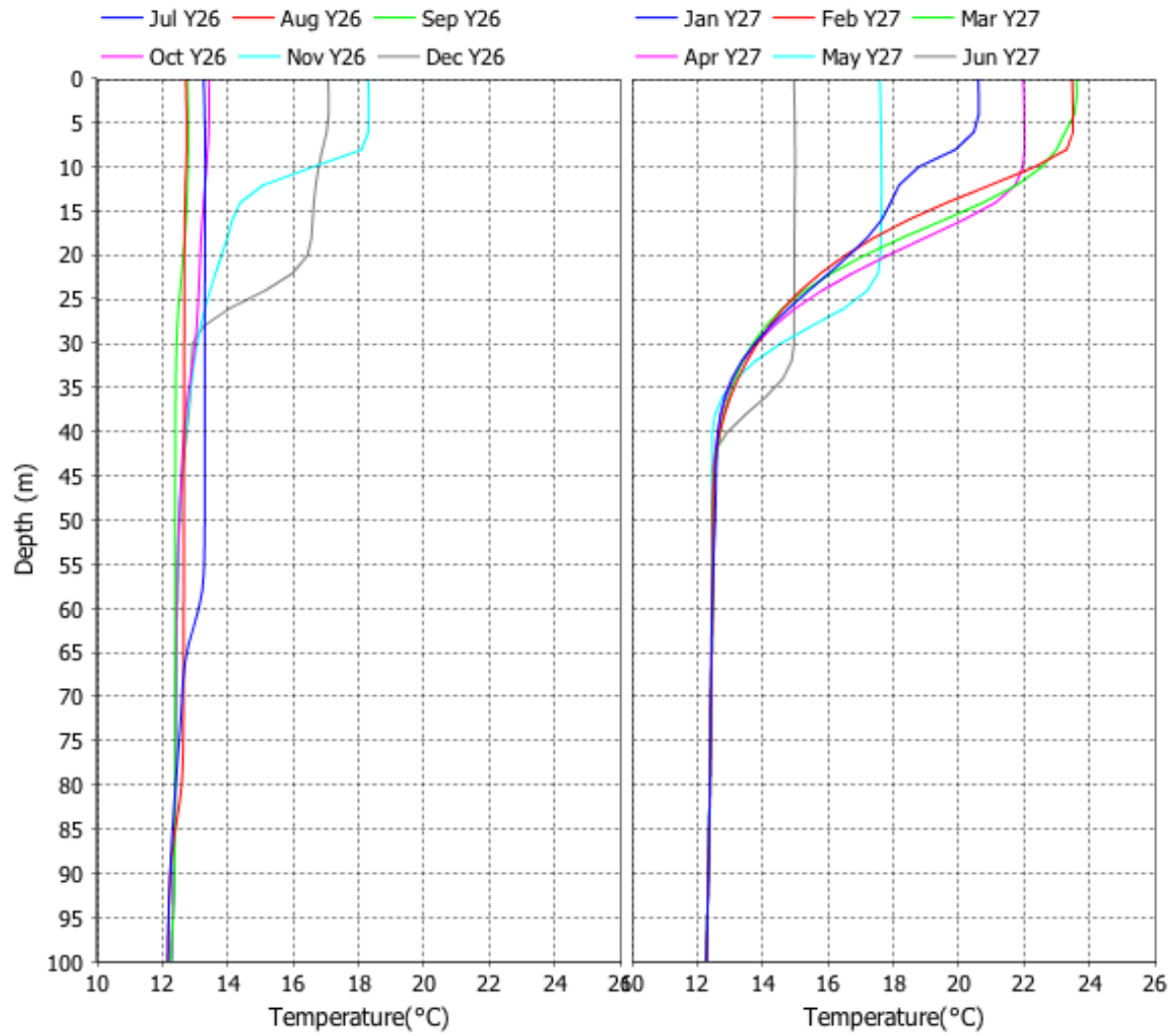

Figure 3.9 Simulated mid-month temperature profiles from July Y27 to June Y28.

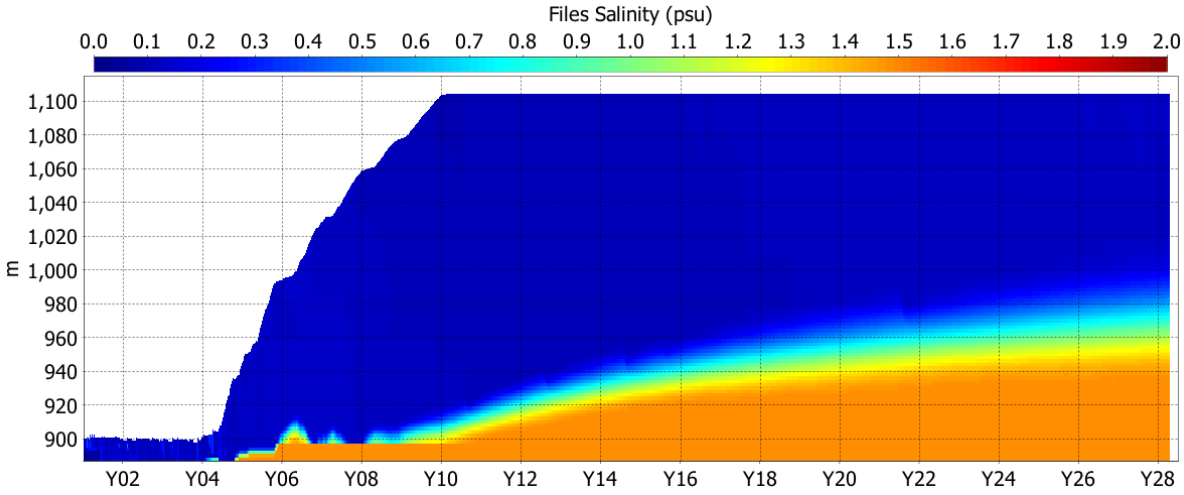

Figure 3.10 Simulated profile contour of salinity.

3.4.2 Mixing

The depth of mixing can be ascertained by examining the mixing energy profiles generated by the model and identifying the depth at which the mixing energy is no longer sufficient to cause mixing between two vertically adjacent cells. Figure 3.11 illustrates the mixing energy determined by the model over the duration of the simulation and shows the depth to which the mixing energy reaches. The model results suggest that after filling the mixing energy penetrates down to approximately 950 m RL in some years (e.g. Y21, see Figure 3.12) during the cooler winter months when the stratification is weakest. In the winter months of other years the mixing energy only penetrates to approximately 1050 m RL (e.g. Y23, see Figure 3.13).

The difference in depth of mixing between these years (the examples of Y21 and Y23) is attributable to differences in the meteorological conditions. In autumn, the initial profiles are similar, with Y21 having a slightly cooler (by approximately 1 ^{o}C) and shallower (by less than 5 m) epilimnion (see Figure 3.14). In late May of Y21 a strong wind event occurs (there is no corresponding wind event in May of Y23) so that by the beginning of June the profiles are considerably different with Y21 having a cooler (by 3^{o}C) and deeper (by 5 m) epilimnion. In June Y21, there are multiple sequences of consecutive nights with temperatures of less than 5^{o}C, compared to only one overnight temperature of less than 5^{o}C in June Y23. By the end of June the stratification in Y21 is considerably weaker compared to the end of June in Y23 so that by mid July Y21, mixing during wind events penetrates deeper into the water column. By August Y21 the temperature profile is mixed to 120 m deep. The small anomaly at the bottom of the temperature profile is related to the high TDS groundwater (as discussed above) that acts as a barrier to further mixing; at this depth there is only a small amount of mixing energy that remains and this is insufficient to overcome the buoyancy forces imparted by the denser groundwater plume. Although July Y23 has a greater number of nights with sub-zero temperatures compared to Y21, the wind speeds in Y23 are typically lower and the remnants of the temperature stratification that is not completely broken down in the preceding months acts as a barrier to deep mixing. In contrast to Y21, by August Y23, mixing has only reached 50 m deep.

The results indicate that after filling the extent of winter mixing depends on the sequence of meteorological conditions that occur over the autumn and winter months, and on the strength of the stratification that is built-up prior to the cooler months. Although this suggests that there is likely to be a continuum of different mixing depths that occur in response to the range of different meteorological conditions each year, the model results indicate some long-term sequences. Winter mixing occurs to approximately 950 m RL from Y10 to Y15, before switching to a sequence of shallower mixing winters (to 1020-1040 m RL) from Y16 to Y20, then in Y21 deeper mixing returns with cool windy autumn weather as described above. In Y22 shallower mixing returns and persists for the remainder of the simulation. The 7-day moving average temperature in late summer and autumn of Y22 (see Figure 3.15) shows considerably warmer temperatures (by 2 to 3 ^{o}C) when compared to the same period in Y21. In addition, 7-day moving average wind speed over the same period peaks at 6 ms^{-1} less in Y22 compared with Y21. After the change from deep to shallow mixing between Y21 and Y22 the 7-day moving average air temperature in late summer and autumn of Y23 (a shallow mixing year) returned to conditions similar to those observed in Y21 (a deep mixing year) but wind speeds did not peak as high. Furthermore, the temperature profiles in Figure 3.6 show a temperature gradient develops at approximately 1050 m RL after Y22 that persists until the winter of Y26. This leads to a sequence of years with a thermal stratification that is more resistant to deep mixing.

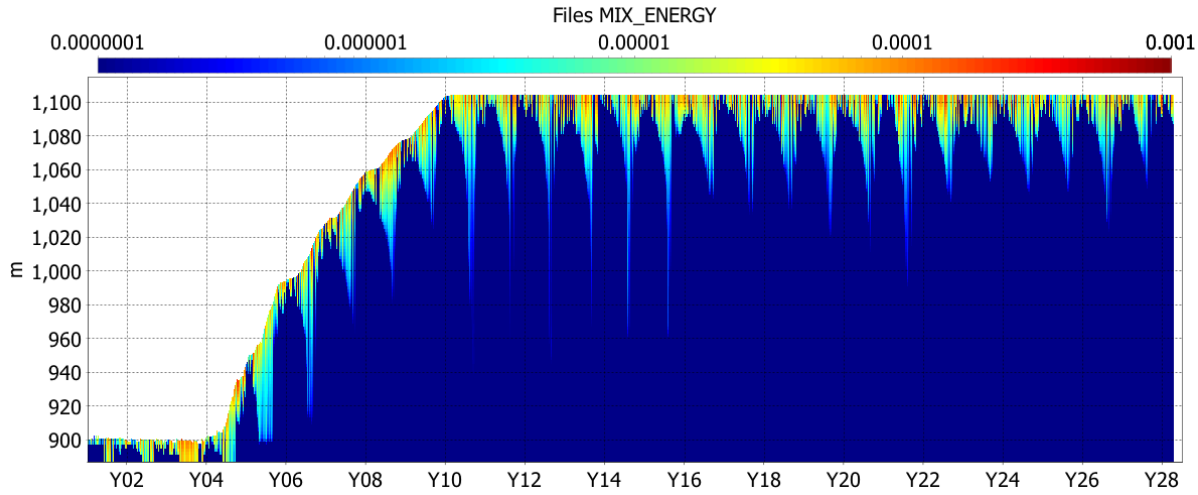

Figure 3.11 Simulated mixing energy (in units of dissipation, m^2s^{-1}) over the duration of the simulation.

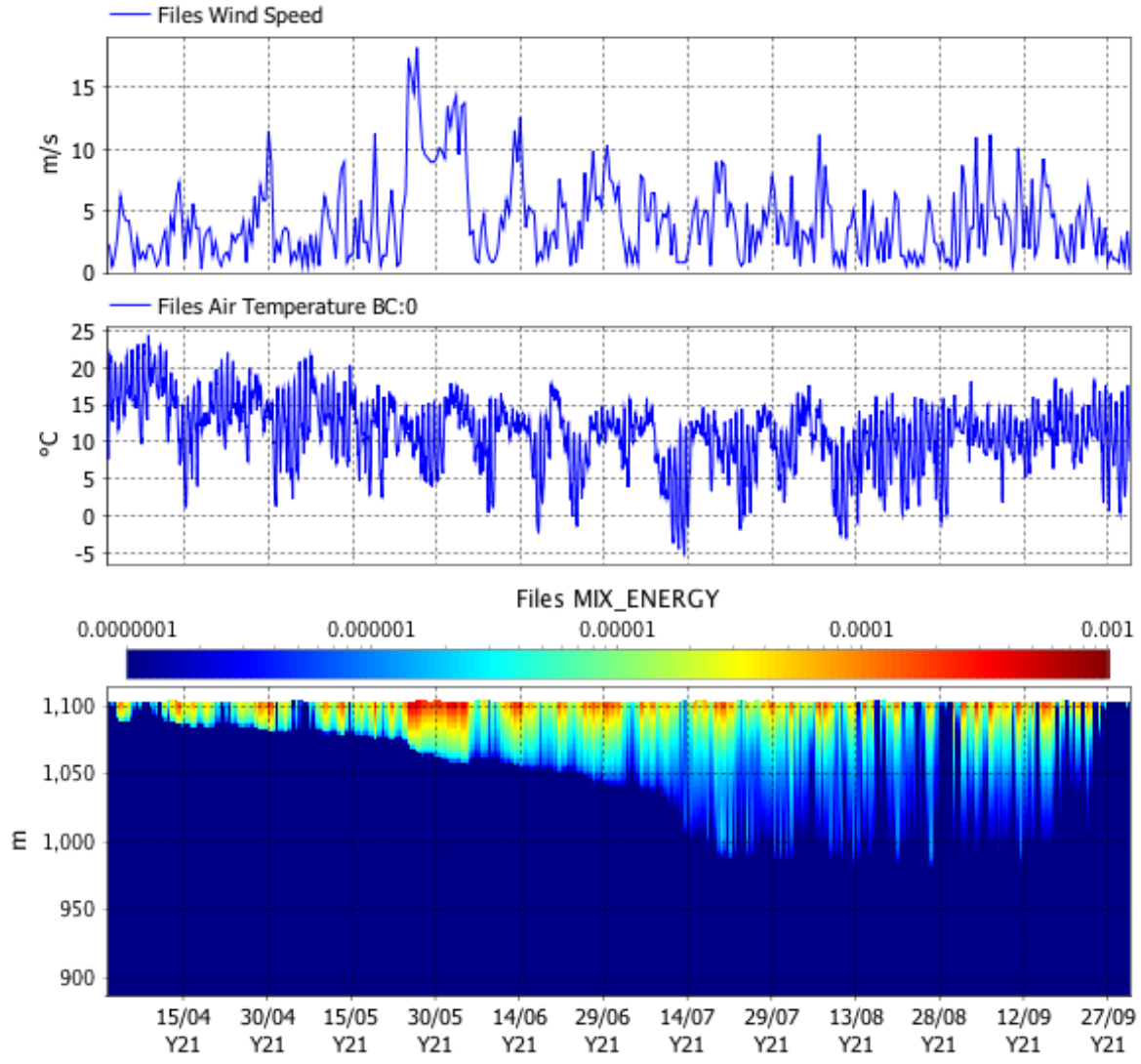

Figure 3.12 Wind speed (top panel), air temperature (middle panel) and simulated mixing energy (m^2s^{-1}) (bottom panel) from April to October Y21.

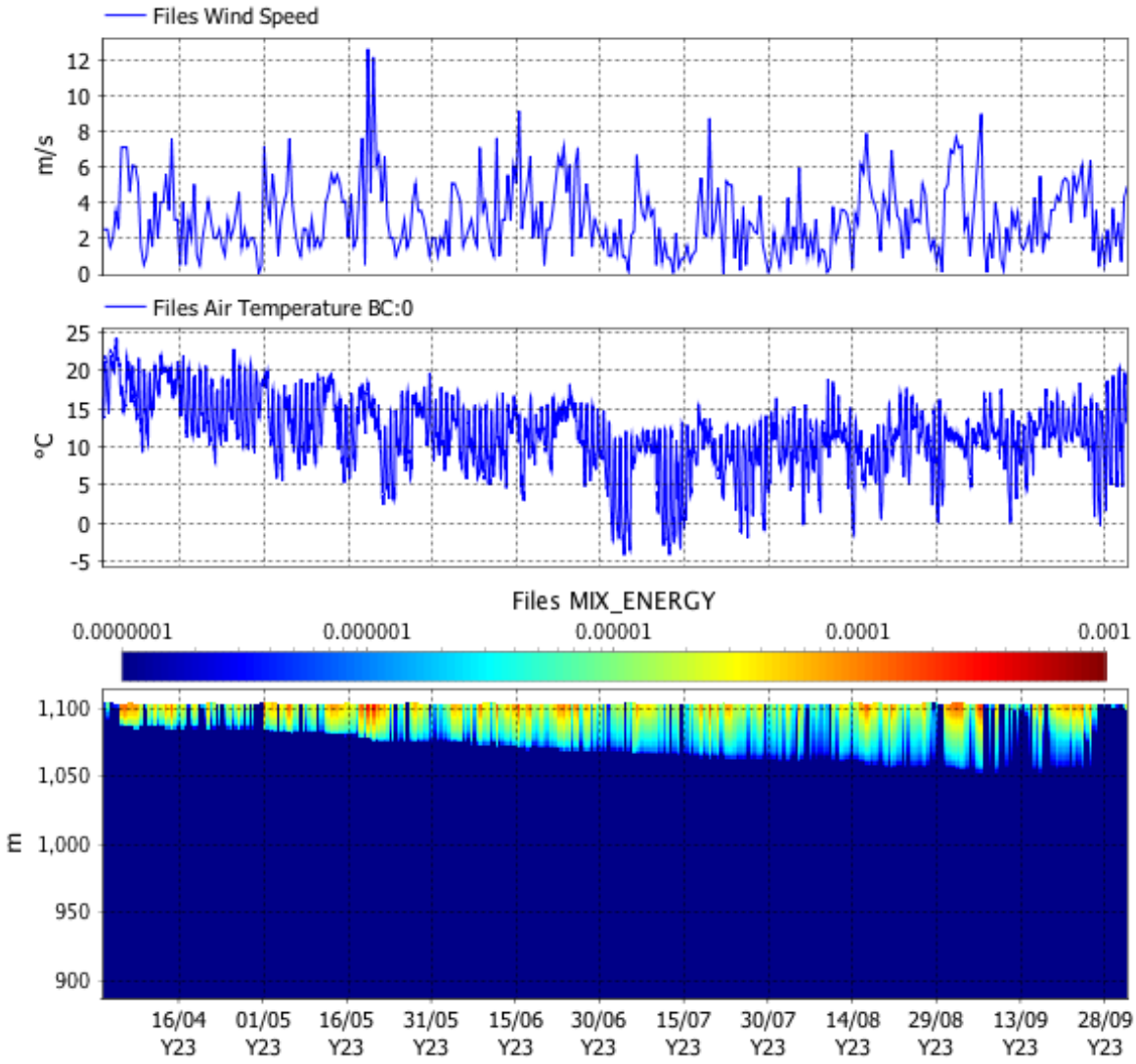

Figure 3.13 Wind speed (top panel), air temperature (middle panel) and simulated mixing energy (m^2s^{-1}) (bottom panel) from April to October Y23.

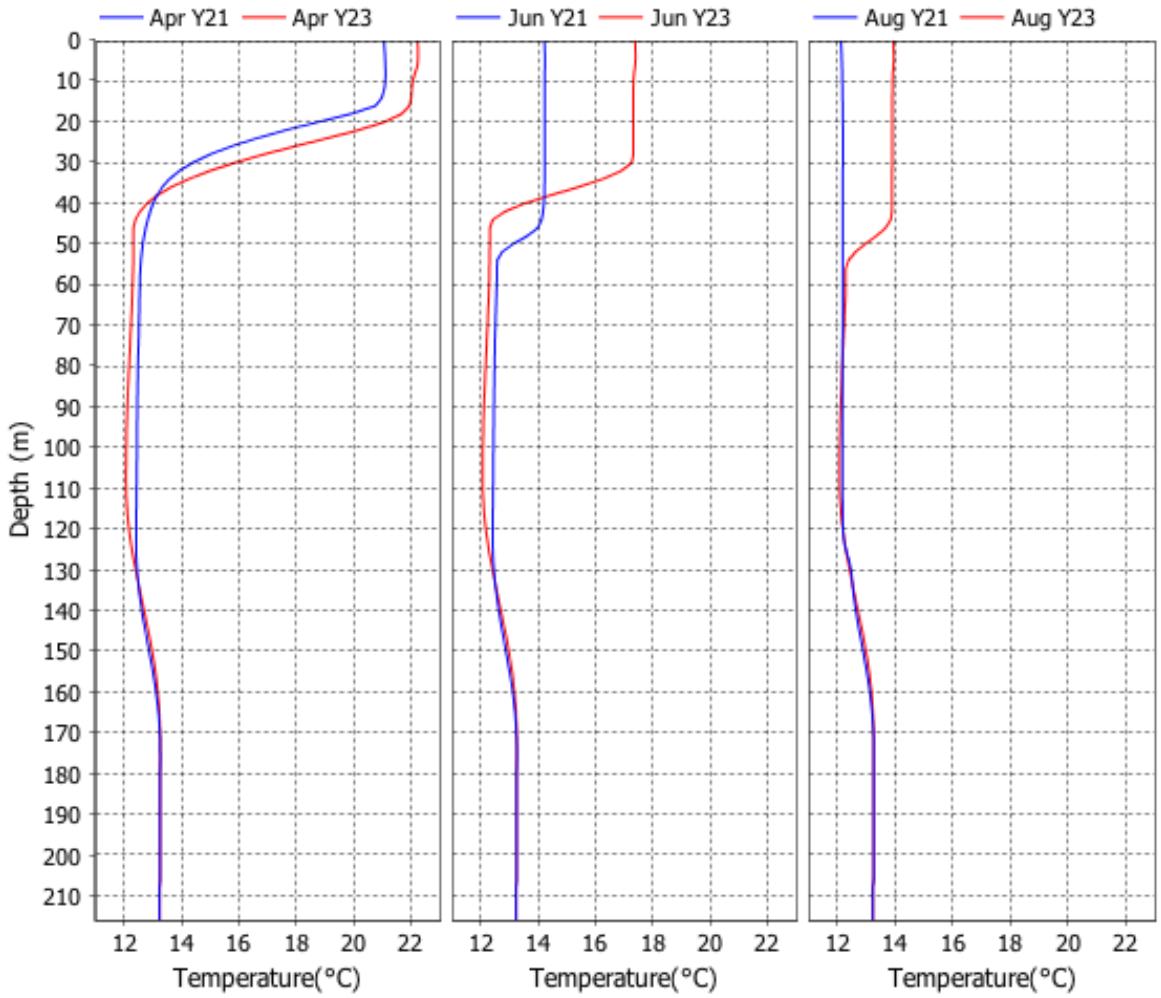

Figure 3.14 Simulated temperature profiles at the beginning of April, Jun and August in Y21 (blue profiles) and Y23 (red profiles).

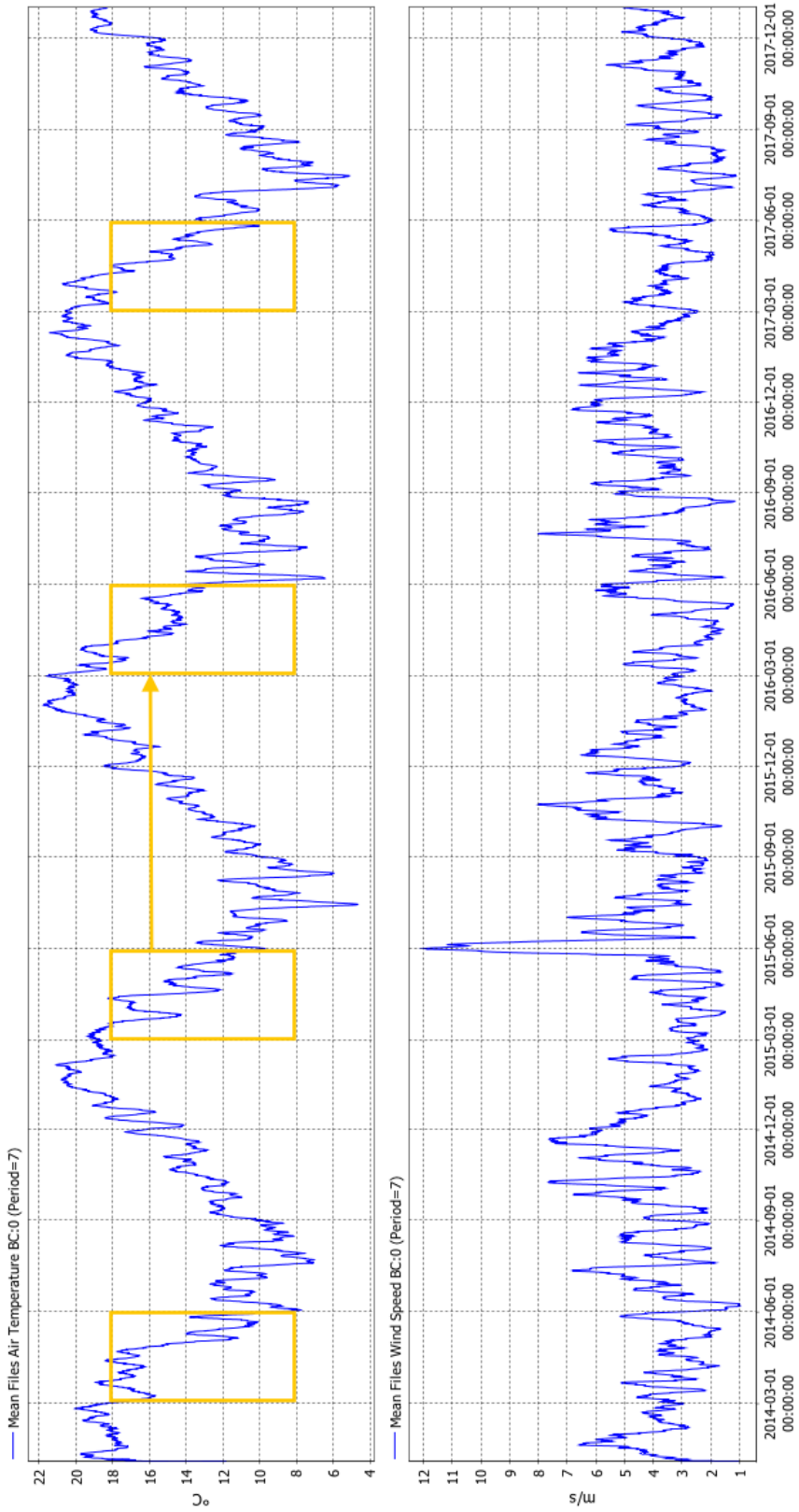

Figure 3.15 Seven-day moving average of air temperature (top panel) and wind speed (bottom panel) data from Waihi for Y20 (2014) to Y23 (2017). Yellow boxes indicate temperature from March to June. The arrow highlights the changed conditions going from a deep mixing year (Y21) to a shallower mixing year (Y22).

3.4.3 Retention Time

Figure 3.16 illustrates the predicted retention time of water in the pit lake. The retention time is determined by counting water age; water enters the pit lake at a value of zero and ages as the model progresses (i.e. for every day of simulation time the water will age by one day). When model cells mix or partially mix, the age of the mixed water is determined by calculating a volume-weighted average of the age water that is exchanged between the cells.

The results show that after filling there is a near-linear aging of the mid-depth waters (approximately in the range from 950 to 1020 m RL) because they are not regularly refreshed by the incoming waters at the surface (rainwater and run-off) or by groundwater seepage at the bottom due to the lack of vertical mixing. In the waters above there is a seasonal cycle of aging and refreshment that follows the dry months (when less water enters the pit) and wet months (when more water of zero age enters the surface as run-off), respectively. This is also impacted by the cycles of summer stratification, which isolate the waters underneath the epilimnion, and winter mixing, which brings newer water to depth. Deep in the water column (below 920 m RL) there is a continual renewal of water from the groundwater seepage that keeps the age of the water in bottom of the pit low. Above 920 m RL the groundwater slowly mixes into the far older water above leading to a sharp gradient in water age between 920 and 950 m RL.

In summary there are three layers to the water age profile that develop when the river diversion ceases and the pit lake is full. This consists of a middle layer that is irregularly and only partially mixed with the layers above and below and so undergoes little renewal over the course of the simulation. Above this the waters are periodically renewed by small run-off contributions, however on average there is an aging of this water also. At the bottom, the continual seepage of groundwater into the pit lake dominates so that the water age is considerably less near the base of the pit.

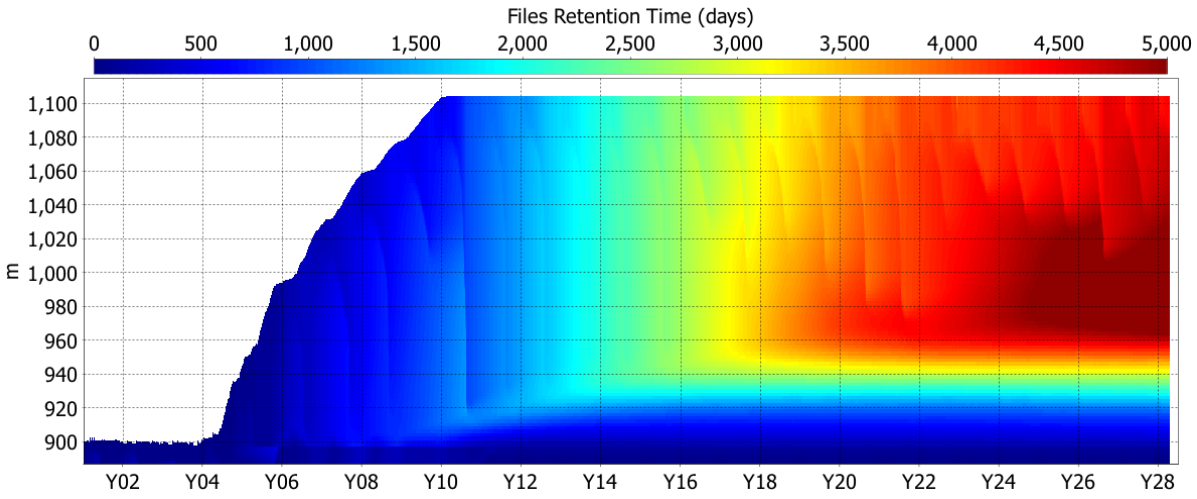

Figure 3.16 Simulated retention time (in days).

3.4.4 Fate and Transport

The mixing and stratification regime described above dictates the fate and transport of loads that enter the pit lake from the various external sources (i.e. groundwater, river water and pit-wall run-off). The fate of each individual water source has been tracked in the model with the application of inert mass-conservative tracers in each inflow, which enters at a nominal

concentration of 1 mg/L. Figure 3.17 to Figure 3.19 illustrate the tracer concentrations in the pit for inflow components described in Table 3.7. The results show that the groundwater input is initially confined to the bottom of the pit (< 900 m RL) during filling when there is a sequence of seepage into and out of the pit. After filling there is a small but consistent groundwater input that is slowly mixed into the water above over the post-filling duration of the simulation. The dense (high TDS) groundwater is primarily confined to a bottom layer in the pit lake that gradually thickens over the duration of the simulation. The contribution of groundwater to the waters above is very small because there is a lack of deep vertical mixing and the small amount of groundwater that does entrain into the waters above is greatly diluted.

The relative contribution of rainfall water in the pit increases as the surface area increases and, after filling, the river diversion ceases. The depth of mixing of the rainwater follows the mixing cycles described above. In the final years of the simulation the epilimnion consists of 40 to 50% rainwater during the stratified period.

River water dominates the inflows during filling, with the exception of the very bottom of the pit where the groundwater resides. After filling, when the diversion of the river ceases, the river water is slowly flushed from the pit lake. However, in the final years of the simulation the waters between 980 and 1020 m RL still consist of approximately 60% river water, owing to the small inflow and outflow rates from the pit and the isolation of this water from the mixing and spill that occurs above. Although this water originated from the river, by the end of the simulation it has spent 8 to 10 years in the pit and over this time the chemical properties are likely to be significantly altered.

Pit wall run-off (Figure 3.18 and Figure 3.19) makes varied contributions to the pit lake water composition that depends on the run-off area (which changes as the pit fills). The model results suggest that despite having higher TDS than the ambient pit lake water (and therefore greater density and negative buoyancy) upon ingress, the run-off partakes in the thermally controlled stratification and mixing regime of the upper waters. This is because the negative buoyancy related to higher TDS of the run-off water is negated by mixing and dilution with far larger contributions of low-TDS river water and rainfall. Whilst there is the potential for the run-off to enter as multiple sub-surface intrusions of differing density, thus creating steps in the density profile that change the mixing dynamics, assessing the potential for this would require further investigation with a high-resolution model. Given the windy conditions in Waihi it is therefore unlikely the localised gradients will exist both laterally and vertically for extended periods of time.

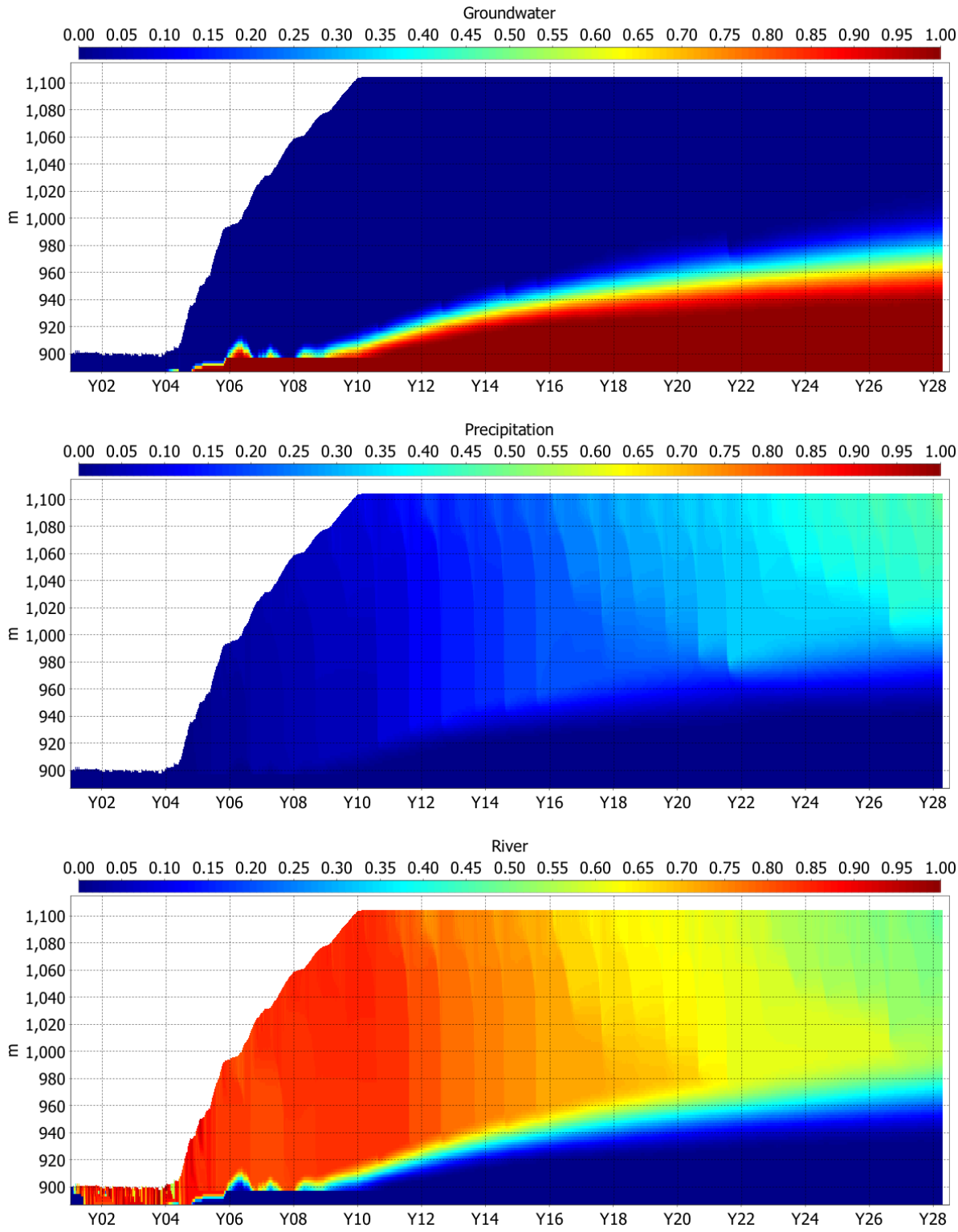

Figure 3.17 Inflow tracers for groundwater (top panel), rainfall (middle panel) and river water (bottom panel).

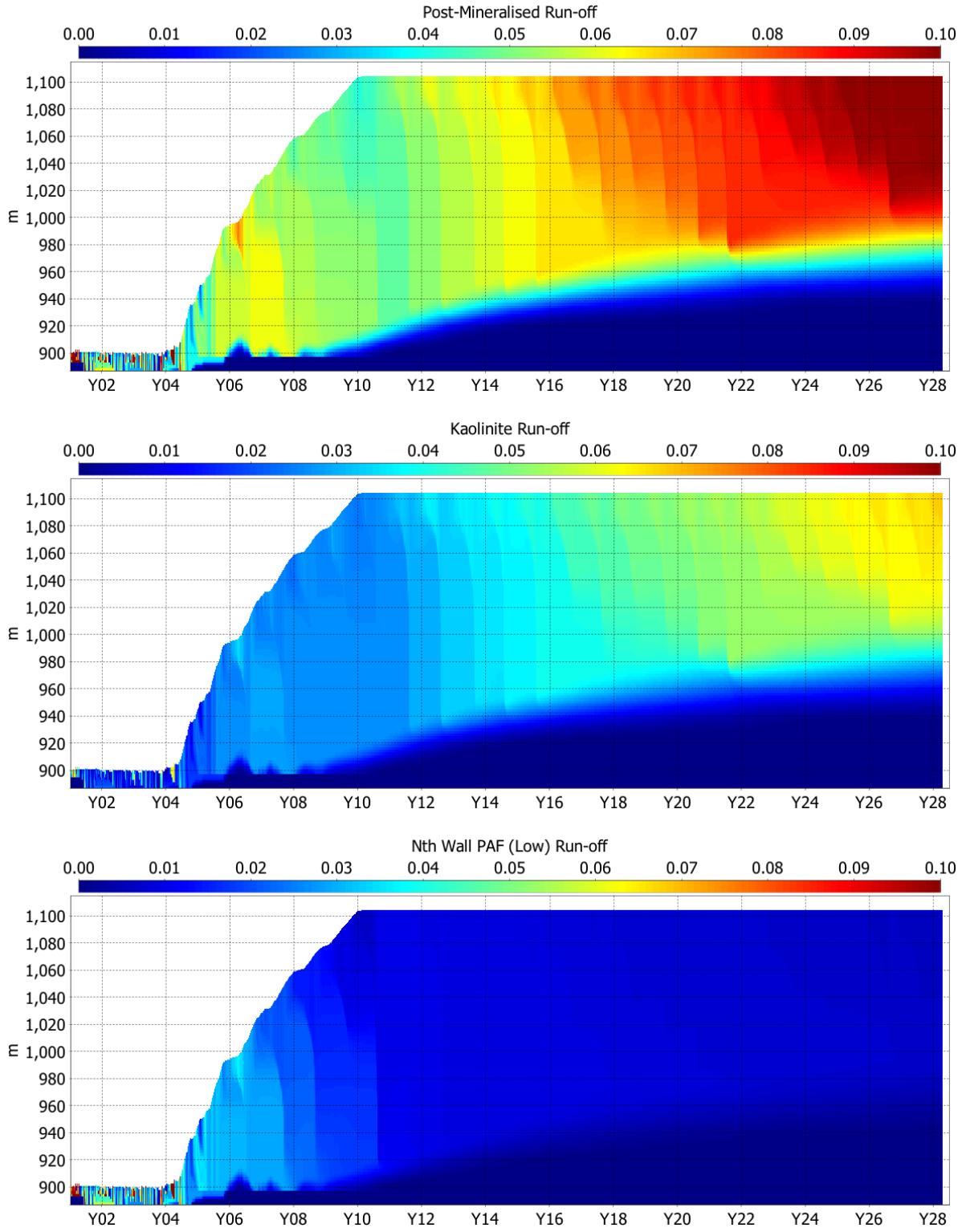

Figure 3.18 Inflow tracers for pit-wall run-off: post mineralised (top panel), Kaolinite (middle panel) and high north wall PAF (bottom panel). Note the reduced colour scale compared to tracer figures above.

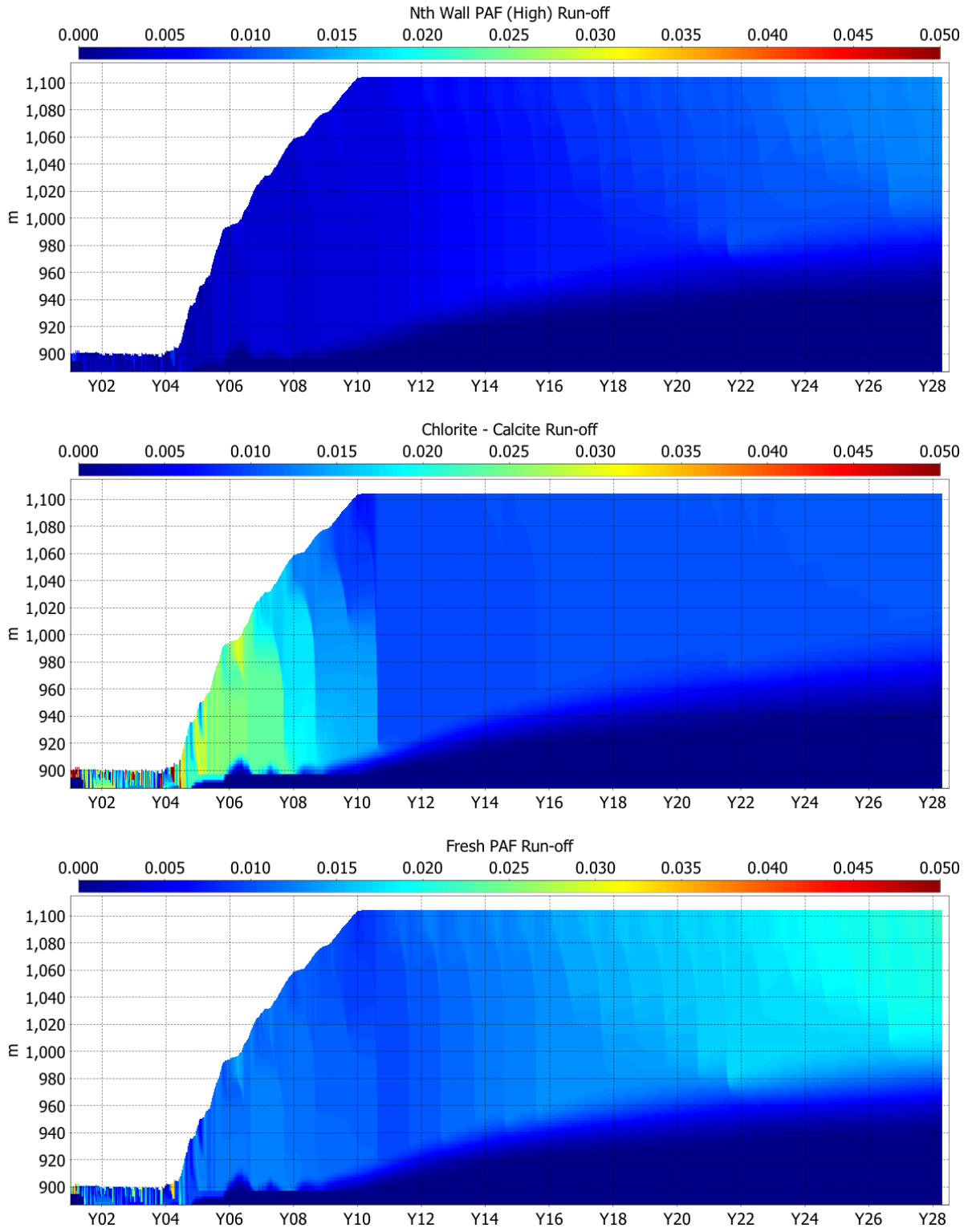

Figure 3.19 Inflow tracers for pit-wall run-off; high north wall PAF (top panel), Chlorite-Calcite (middle panel) and Fresh PAF (bottom panel). Note the reduced colour scale compared to tracer figures above.

3.5 Sensitivity Tests

3.5.1 Overview

A series of sensitivity tests was undertaken to assess how the model predictions may change in response to changes in the model set-up that are based on either statistical realisations and/or necessary assumptions. The tests are summarised in Table 3.8.

Comparisons between the tests were made using the mixing depth as a measure of the difference, given the importance of the mixing depth as a parameter that measures change in the stratification and mixing regime.

Table 3.8 Summary of sensitivity tests.

Test	Model Sensitivity Test
A	75th percentile TDS used for PAF run-off inflows
B	Light extinction coefficient reduced from 0.7 to 0.1 m^{-1}
C	3-day rolling mean air temperature used for river water temperature
D	Groundwater inflows at 24 ^{o}C
E	Groundwater inflows at 20 ^{o}C
F	Groundwater inflows at 24 ^{o}C

3.5.2 Results

Modifying the TDS of the PAF run-off (test A) did not substantially change the mixing depths (see Figure 3.20) with the exception of winter Y08, which occurs prior to complete filling of the pit lake. During winter in Y08 test A mixed less, however over the remainder of the simulation the mixing depths were consistently similar.

For the higher clarity water test (i.e. light extinction coefficient K_d = 0.1 m^{-1}, test simulation B) the summer and spring mixing depths increased 5 to 10 m (Figure 3.22). This occurs because there is deeper penetration of solar radiation into the water column when the water clarity is higher (lower extinction coefficient). The temperature gradients are therefore weaker and develop deeper in the water column. Despite the change in summer conditions, the extent of deep mixing does not significantly change after the lake is filled. Simulated winter mixing in Y07 and Y11 is in fact shallower for the case with higher water clarity. This can occur during certain cooling conditions when the trapping of heat deeper in the water column over summer maintains stratification during the cooler months because the deeper waters are insulated from heat loss to the atmosphere at the surface.

Changing the river water temperature (test C) decreases the mixing depth in some of the years during and immediately after filling (see Figure 3.21). This difference occurs because in the test simulation the incoming river water is typically cooler than the epilimnion water and therefore there is both an overall cooling of the profile and the persistence of a temperature gradient (albeit weaker) at 90 m below the surface over the cooler months (see Figure 3.24). As the simulation progresses after the river diversion has ceased, the difference between the temperature structures reduces until after Y16 the temperature profiles and mixing depth are consistent (see Figure 3.25).

Test cases with a range of groundwater temperatures (tests D to F) lead to changes in the predicted mixing depth (Figure 3.23). When warmer groundwater enters through the bottom of the pit the density anomaly between the groundwater and the remaining pit water (that is maintained by the higher groundwater TDS) weakens. In the case of groundwater of 20 ^{o}C the stratification is weakened sufficiently so that there is partial to complete mixing of the high TDS bottom groundwater into the remainder of the pit water above during the deep mixing years from Y10 to Y15 (see Figure 3.26). This is also evident in the mixing depth analysis (Figure 3.23) that shows deeper mixing events for the simulation with groundwater of 20^{o}C. The results also show that when mixing of the groundwater does take place it is into a far greater volume of lower TDS water above the groundwater and because of the large dilution there is only a small increase in the TDS of the mixed water. This leads to a gradual increase in the TDS of the pit water over time.

A simulation with a groundwater temperature of 24^{o}C (Figure 3.26, bottom panel) shows a significant change in the mixing and stratification of MPL. This occurs because when the groundwater is at 24 ^{o}C the density gradient that was maintained by cooler and high TDS groundwater applied to the previous simulations is now sufficiently reduced to allow frequent and deep mixing. As a consequence there is little or no (in the case when the groundwater is less dense that the water above) buoyancy force to overcome, and the groundwater mixes readily with the pit water above. The results indicate that for the warm groundwater case there is mixing to the bottom in two out of every three years after the pit lake is full. However, as discussed in Section 3.4.2 there are extended periods (e.g. from Y22 to Y25) when, deep mixing does not occur.

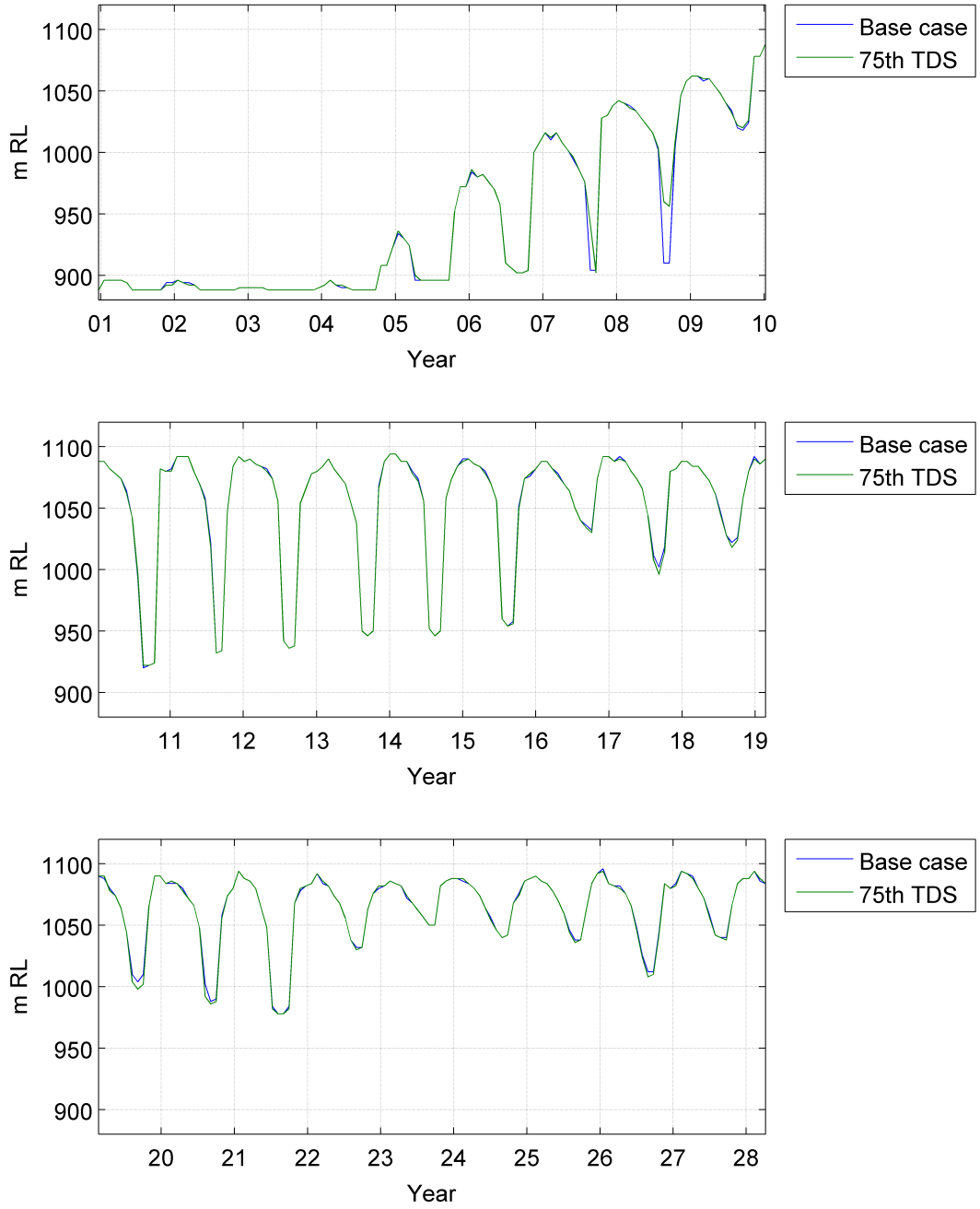

Figure 3.20 Comparison of predicted mixing depth for the base case simulation (blue) and sensitivity simulation A (green) with 75th percentile TDS used for PAF run-off inflows.

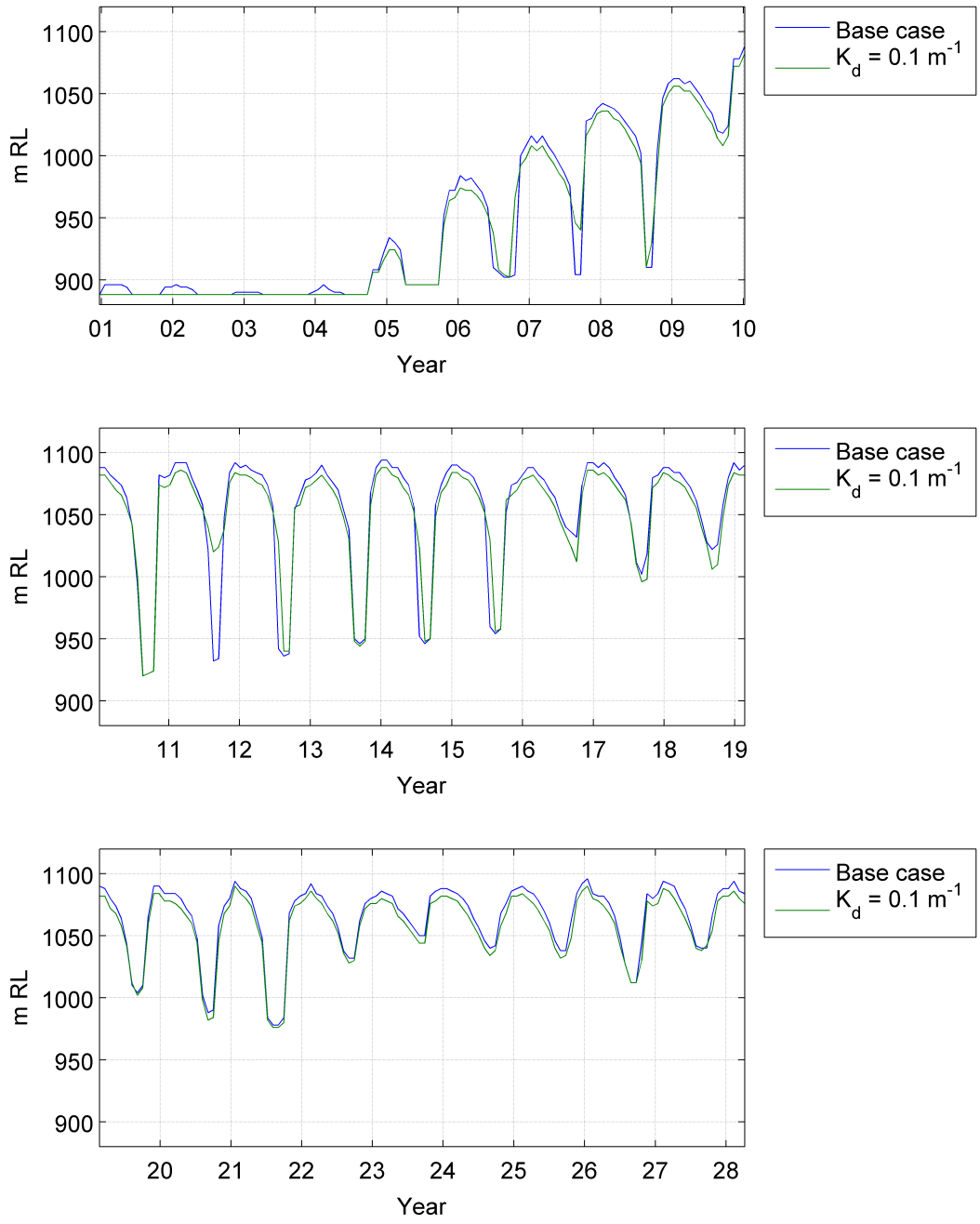

Figure 3.21 Comparison of predicted mixing depth for the base case simulation (blue) and sensitivity simulation B (green) with the light extinction coefficient reduced from 0.7 to 0.1 m^{-1}.

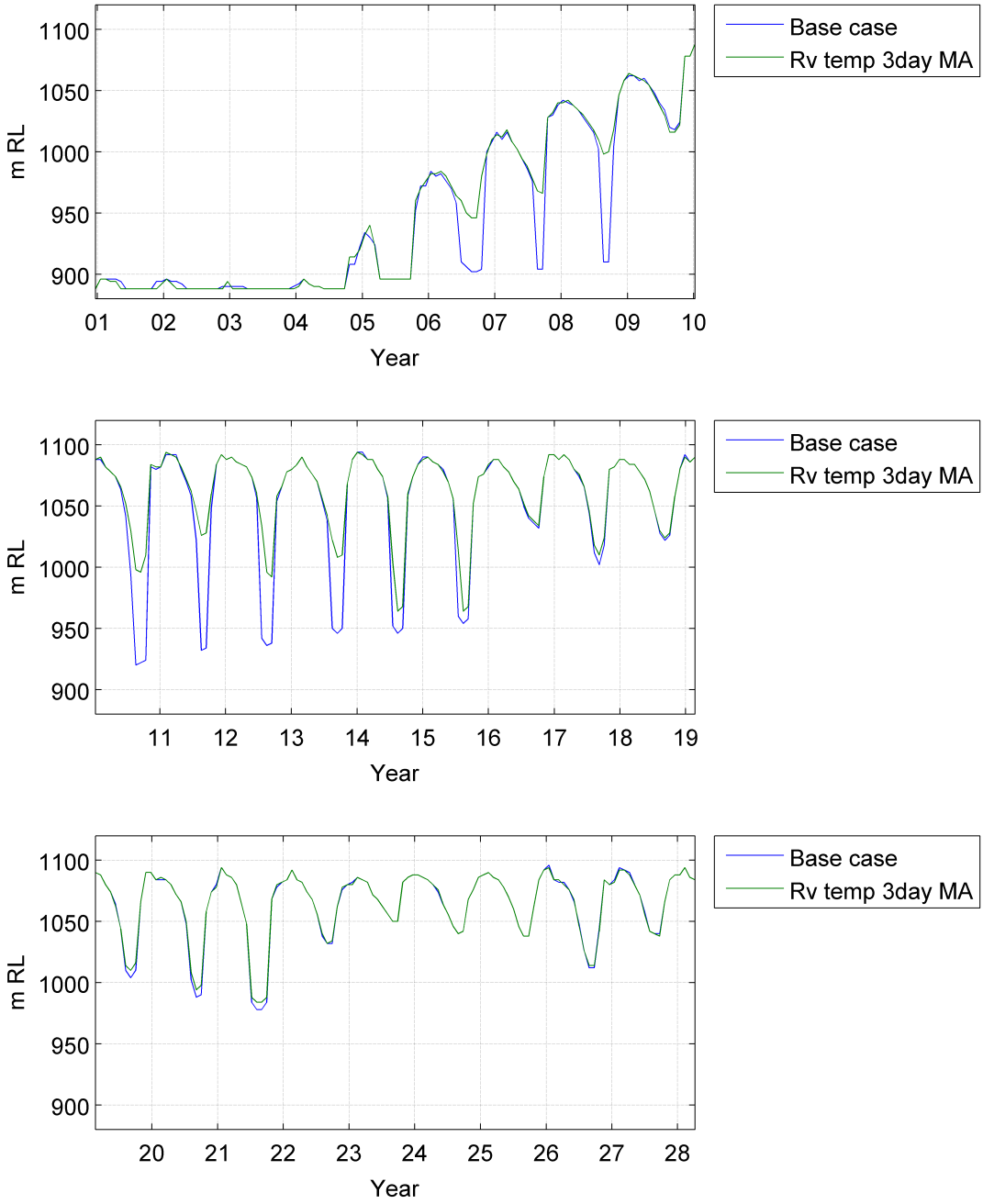

Figure 3.22 Comparison of predicted mixing depth for the base case simulation (blue) and sensitivity simulation C (green) with 3-day rolling mean air temperature used for river water temperature.

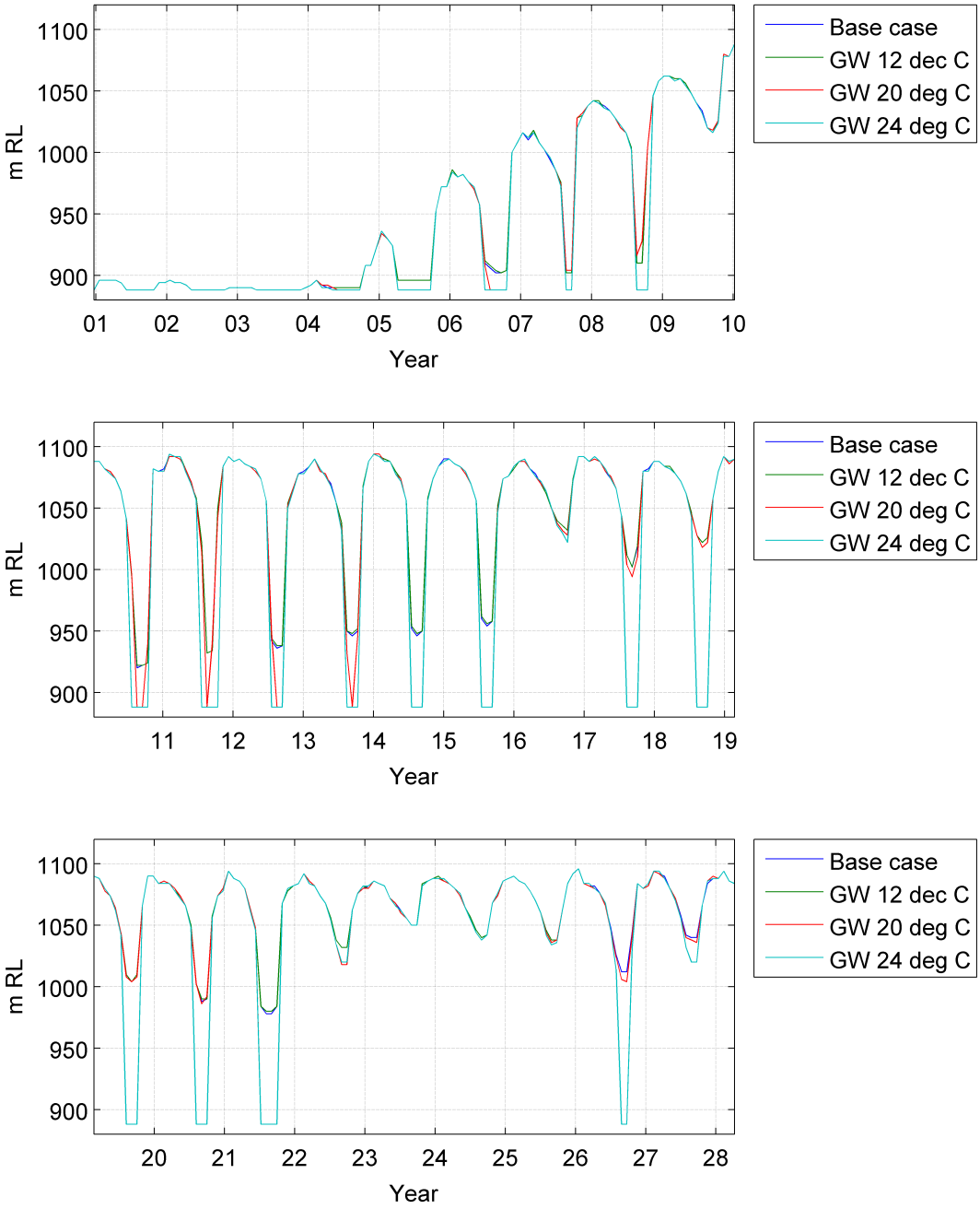

Figure 3.23 Comparison of predicted mixing depth for the base case simulation (blue) and sensitivity simulations D to F with modified groundwater temperatures.

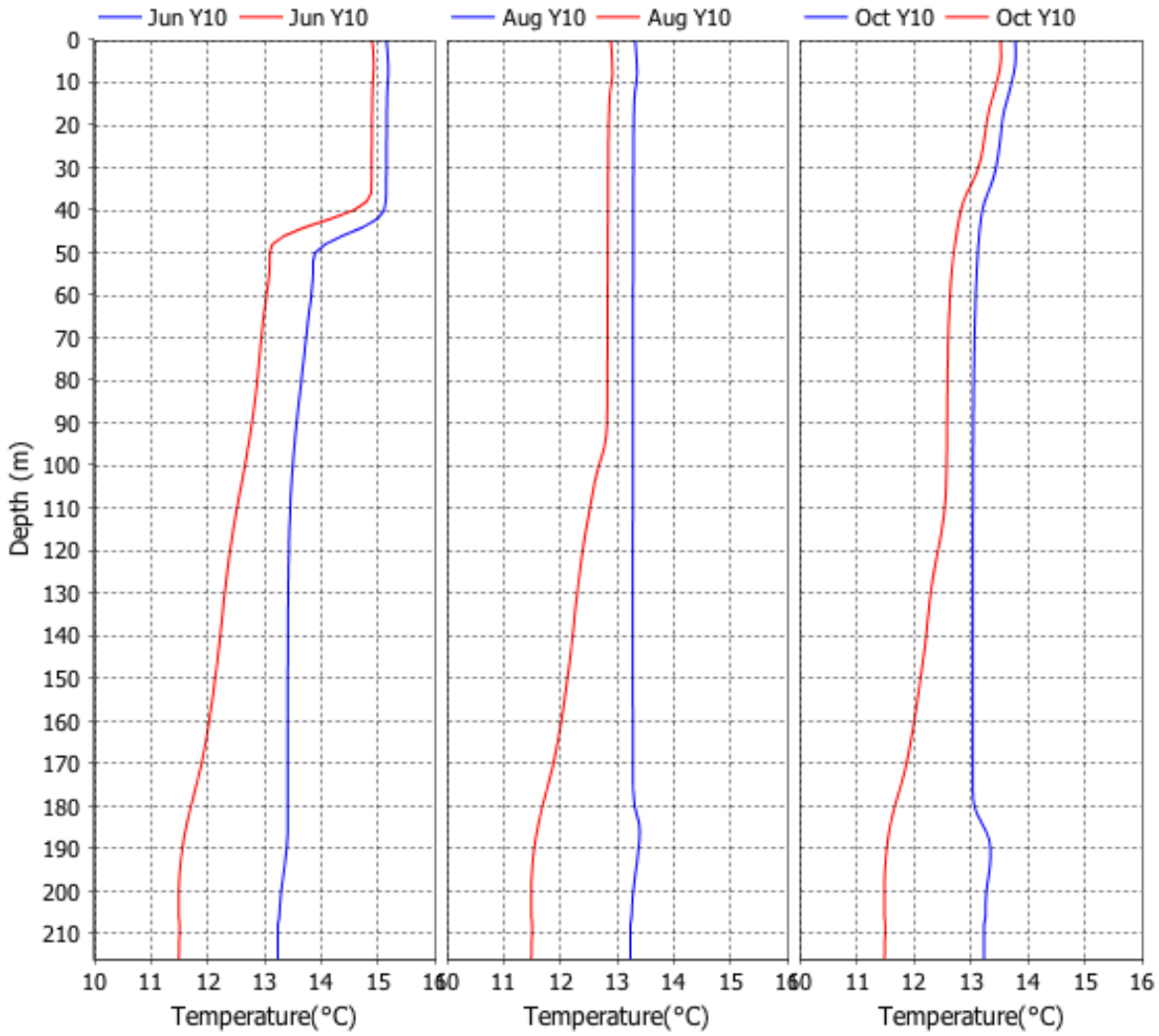

Figure 3.24 Simulated temperature profiles at the end of July (left panel), August (middle panel) and October (right panel) for the base case case (blue) and sensitivity test C (red) with a variable river diversion temperature calculated from a 3-day moving average of the air temperature.

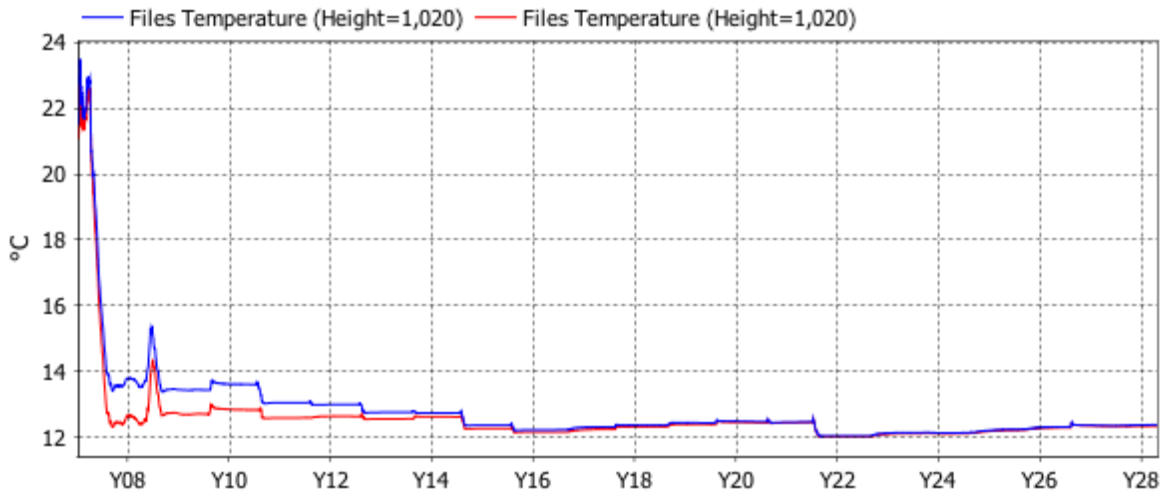

Figure 3.25 Simulated temperature at 1020 m RL for the base case case (blue) and sensitivity test C (red) with a variable river diversion temperature calculated from a 3-day moving average of the air temperature.

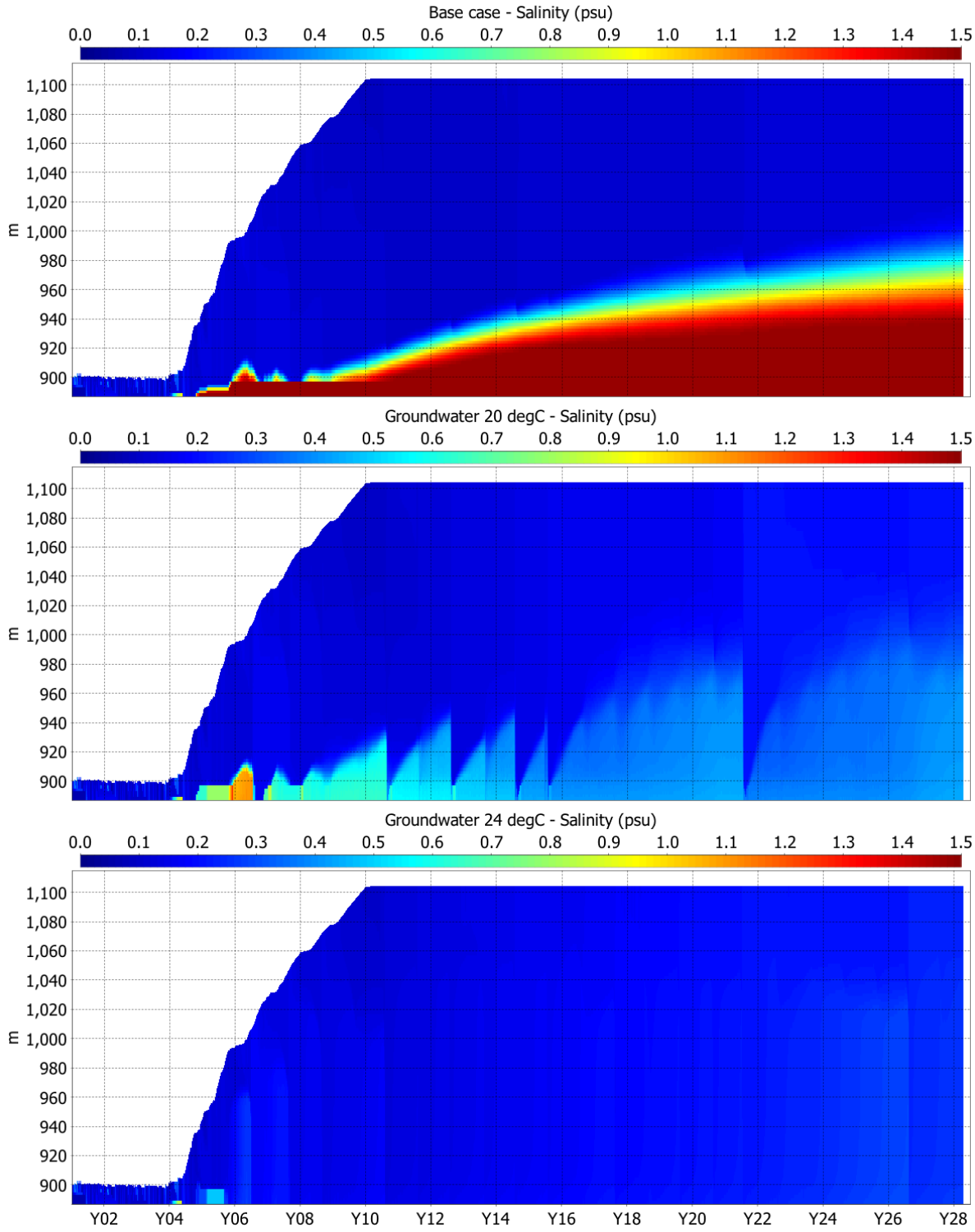

Figure 3.26 Simulated salinity for base case case (top panel), groundwater inflow at 20 °C (middle panel) and groundwater inflow at 24 °C (bottom panel). Note that different salinity scales have been used to show the gradients).

4 Discussion

4.1 Stratification and Mixing

This discussion focuses on the stratification and mixing predicted by the modelling undertaken in this study (referred to as the 'MPL model') in the context of the literature review of pit lakes and previous modelling undertaken for the Martha Pit MPL.

The simulated seasonal cycles of stratification and mixing predicted by the MPL model, and the depth of the epilimnion during summer is consistent with the estimate of 10 m that was provided within the literature. More specifically, the simulated stratification is, with some exceptions, which are discussed below, consistent with the model results of Spigel (1997).

There are two notable differences between the results of Spigel and the results of the MPL model. Firstly, the model of Spigel predicted lower hypolimnetic temperatures of approximately 10 to 11 ^{o}C. This may be related to differences in the modelling software and/or assumptions about the temperature of rainfall, run-off and, in particular, the river diversion water as these will influence the temperature of the simulated profile.

A second point of difference is that the modelling of Spigel suggests periods of complete mixing will occur every 3 to 5 years on average. In contrast, the MPL model shows a persistent stratification at depth that is formed by higher TDS (i.e. higher than the water above) groundwater that resides in the bottom of the pit. The persistent stratification acts to prevent mixing to the very bottom of the pit. The MPL model in this study is therefore more comprehensive because the influence of TDS on the stratification was assumed to be negligible in the Spigel model. In addition, the groundwater seepage was assumed to occur over a relatively large area, whereas in the MPL model a localised input at the bottom of the pit was applied.

The persistence of stratification formed by groundwater inputs at depth was considered in the more recent model of Castendyk and Webster-Brown (2007). For a case with cold groundwater the model of Castendyk and Webster-Brown (2007) predicted persistent stratification that prevented mixing to the bottom of the pit lake in winter. For warmer groundwater the stratification in the bottom began to dismantle so that complete mixing occurred in winter. Unlike changes to the groundwater salinity, sensitivity tests showed that changes to the salinity of the smaller contributions from pit-wall run-off did not alter the dynamics of the stratification and mixing. Both of these observations are consistent with the predictions from the MPL model. Castendyk and Webster-Brown (2007) applied a higher initial groundwater contribution, easing from an initial 3500 m^3/day to approximately 250 m^3/day after filling, compared to 1300 m^3/day reducing to fluctuate around 400 m^3/day for the MPL model, which established a thicker bottom layer of groundwater earlier in the simulation.

The MPL model predictions suggest that the predicted cycles of mixing and stratification are not easily described with the basic classifications (see descriptions of classifications in Chapter 2.2.3). The elevated TDS of the groundwater that seeps into the bottom of the pit develops and maintains a deep density gradient (a pycnocline) that inhibits mixing to the base of the pit unless the groundwater is warm enough (approximately 24^{o}C) to produce a weak or negative density gradient between the ambient pit water and the groundwater. In years when deep mixing occurs the pit lake behaves like a meromictic lake. Temperature stratification builds over the summer and erodes in winter but the winter mixing is not energetic enough to overcome the deep pycnocline. However, in other years, winter mixing is shallow and occurs to a depth that falls considerably short of the deep pycnocline. This regime in the upper water column is perhaps best described as oligomictic, whereby the summer temperature stratification gives way to winter mixing down to the extent of the deep pycnocline in some but not all winters. The MPL model results indicate that the likelihood of

deep mixing in a particular year may depend not only on the meteorological conditions during autumn and winter (particularly air temperatures in autumn), but potentially on the mixing and stratification experienced in the previous year(s).

In the absence of a deep pycnocline, the model of Spigel (1997) predicted oligomictic behaviour with complete winter mixing occurring every 3 to 5 years; complete mixing occurred during years with successive days of cold weather. The MPL model shows more specifically that rapid cooling in autumn appears to be a good predictor of deep winter mixing, and mild autumn conditions appear to be a precursor to shallow mixing, potentially leading to a succession of shallow mixing years due to the legacy of previous thermal stratification. The MPL model predicted that after filling, mixing occurred to a depth below 1000 m RL in 8 of the 18 years simulated, i.e. almost an average of once every two years. However, the succession of shallow mixing years at the end of the simulations indicates that the MPL model may not yet have reached a state of stable seasonal cycles after the filling period. The long-term change is discussed in Section 4.2 below.

4.2 Long-term Change

The potential for long-term change to the stratification and mixing regime was assessed by simulating an extended base case model over an additional 16 years. The input data was repeated from Y13 onwards to the end of the extended simulation (see Appendix for description). The predicted temperatures over the extended simulation are illustrated in Figure 4.1. The model results indicate that there is no significant long-term change to the temperature stratification and mixing over the additional 16 years of simulation. Repeating the analysis of mixing depth over the years of extended simulation (see Figure 4.2) shows that there for the extended series the mixing depth remains above 1000 m RL. Over time the depth of mixing reduces because of the gradual increase in groundwater at the bottom over time that pushes the pycnocline higher into the pit lake (Figure 4.3).

As the simulation progresses in the decades after filling there is a slow increase in the salinity (i.e. TDS) of the waters between 950 and 1050 m RL (Figure 4.4). The gradual increase in TDS above 1000 m RL occurs in part due to the lack of river water diversion after filling (which during filling acts to dilute higher TDS run-off) and the slow mixing of groundwater up into the water column. This will over the very long term decrease the density difference between the pit water and the groundwater, thus likely increase the depth of mixing. The rate of change in density remains slow because the loss of groundwater can only occur via slow and infrequent mixing with the waters above. In the absence of continuous groundwater seepage it would be expected that over a long period of time (perhaps many decades) the groundwater will slowly mix into the pit water above, eroding the pycnocline, so that the lake tends towards oligomixis. However, this postulation does not consider internal chemical change (including sediment-water column exchange) that has the potential to substantially alter in-situ TDS.

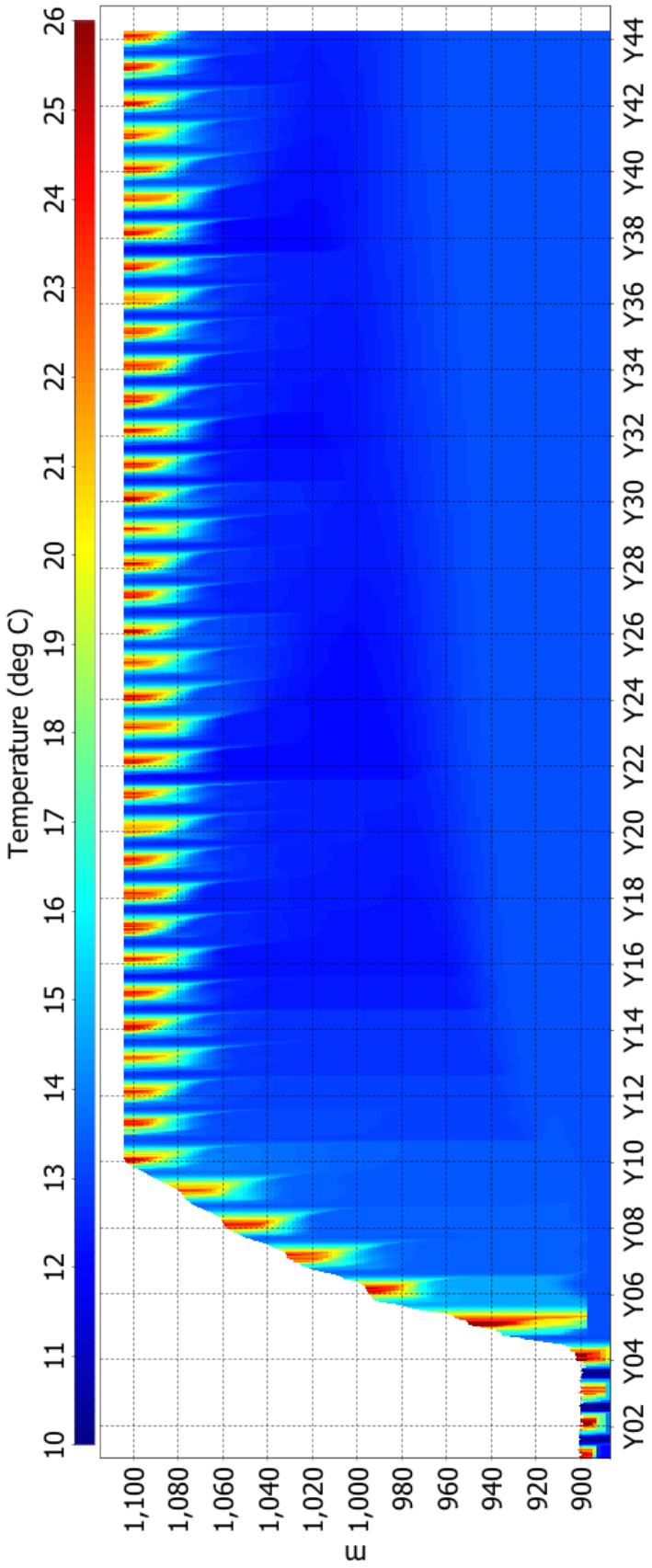

Figure 4.1 Simulated temperature for extended base case simulation.

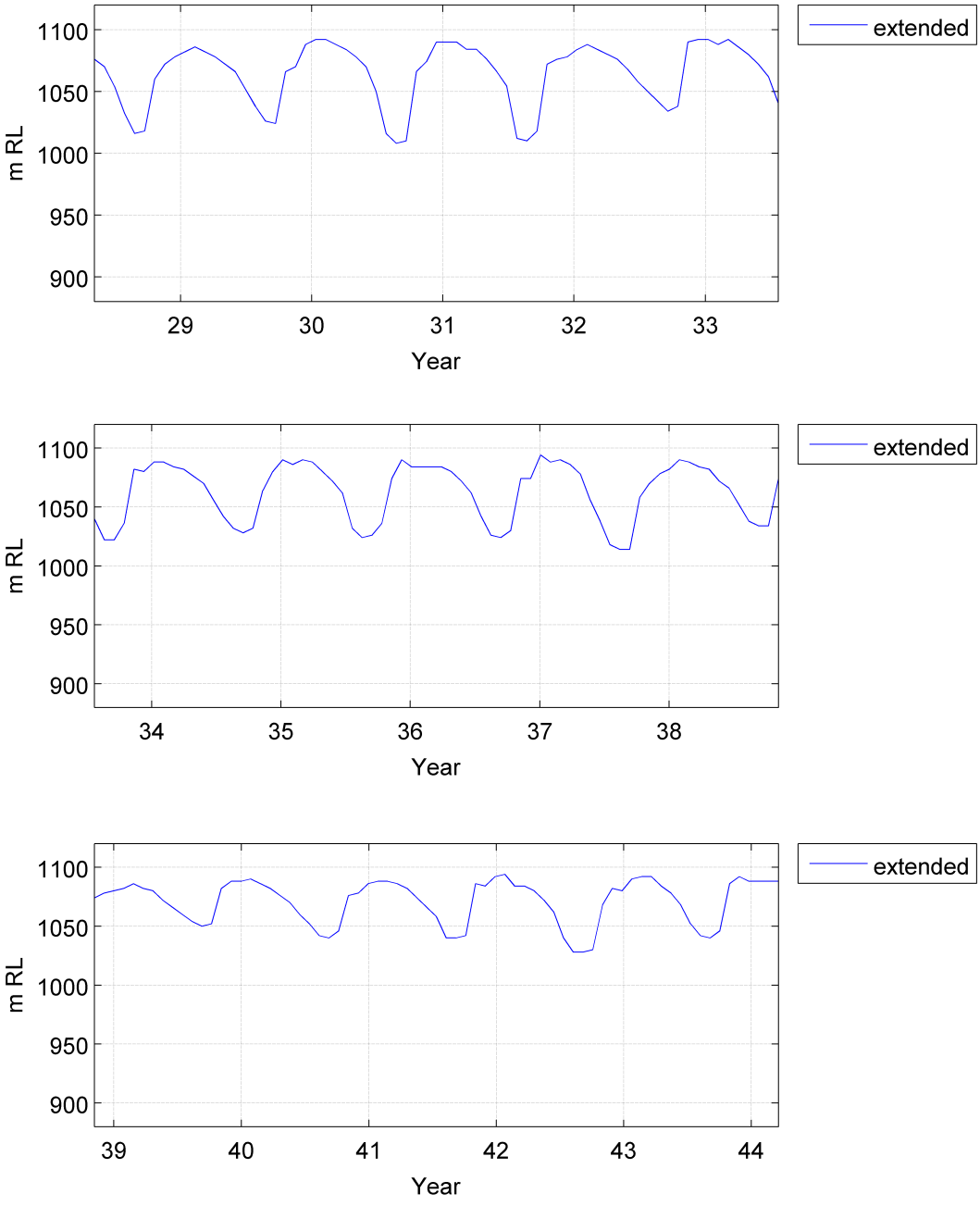

Figure 4.2 Predicted mixing depth for the extended base case simulation.

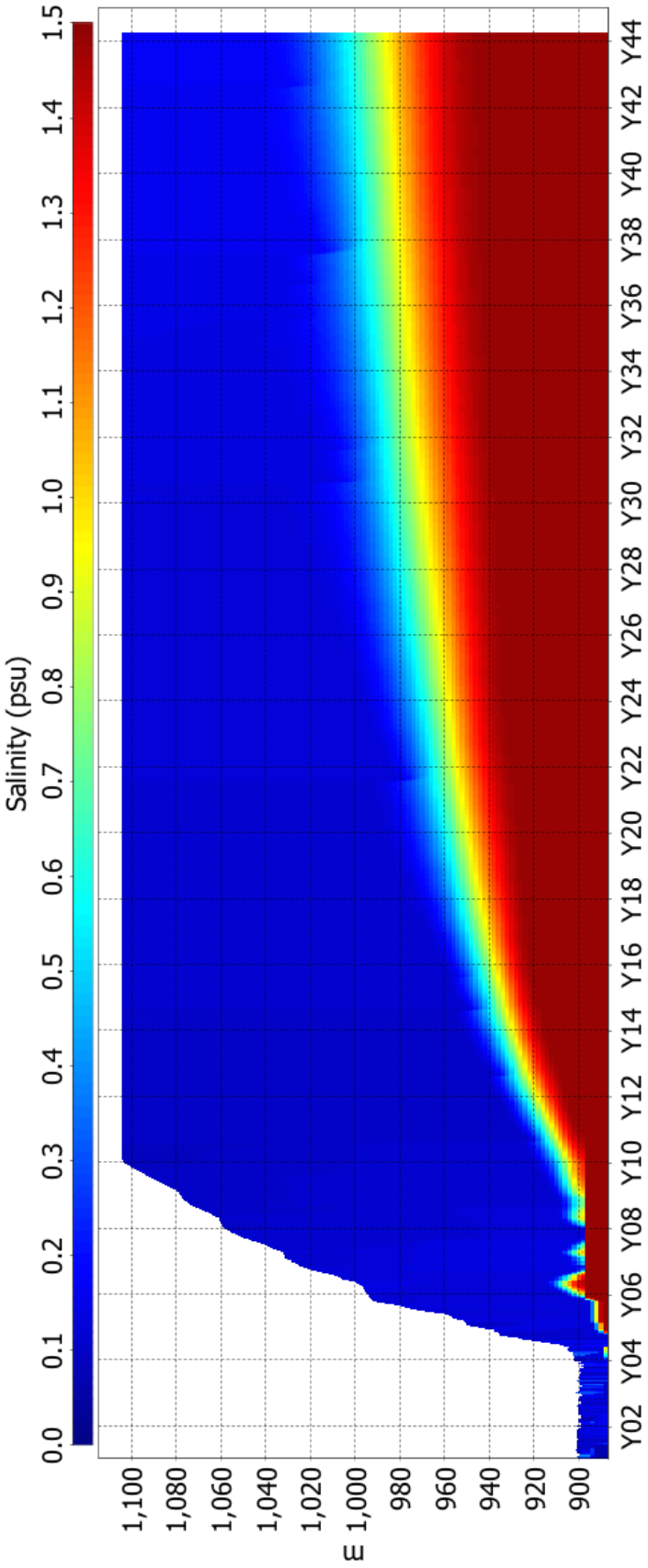

Figure 4.3 Simulated groundwater tracer for extended base case simulation.

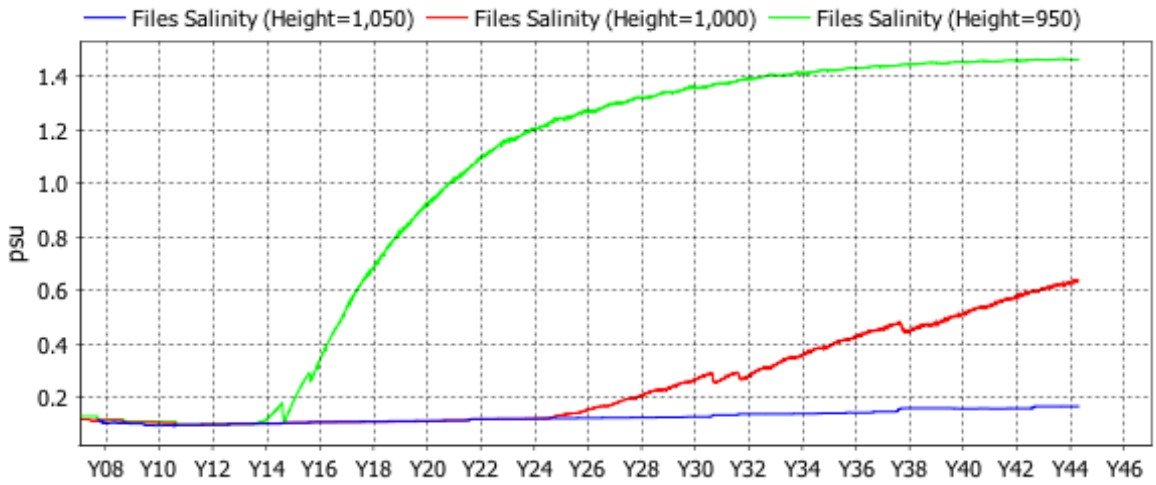

Figure 4.4 Simulated salinity at 1050 (blue line), 1000 (red) and 950 (green) m RL over the duration of the extended simulation.

4.3 Limitations and Uncertainty

There a number of important limitations to the modelling that should be noted. Firstly, the coarse resolution of the lateral grid, which enables long-term simulations in manageable timeframes, does not resolve sub-grid scale processes that may potentially alter the model outcomes. In particular the ingress of run-off from the pit wall is diffuse in the MPL model because of the coarseness of the grid. Any channelization of run-off from the pit wall has the potential to form point source inputs, which may have a different flow path and rate of mixing so as to create intrusions beneath the epilimnion. This may in turn impact on the density stratification due to the difference in TDS and temperature of the run-off water compared to the ambient pit water. However, the formation of these intrusions and potential steps in the density stratification are likely to be weak and short-lived given the small contribution from run-off and the energetic mixing that occurs on a regular basis (due to wind and cooling) near to the surface of MPL.

Another limitation to the modelling is that TDS of surface run-off and groundwater inputs do not take into account long-term change due to changes in the pit wall chemistry and changes to the groundwater chemistry over time. This can be coupled with the absence of chemical change of the waters in the pit due to precipitation and mineralisation that impact on the TDS. Whilst changes to the TDS of both the inputs and TDS within MPL are inevitable over time the sensitivity tests demonstrate that, notwithstanding large and rapid changes in TDS, changes to the cycles of mixing and stratification are likely to be subtle and very slow (over decadal time spans).

This however, lends itself to perhaps the most important limitation and that is limited length of the available meteorological forcing data and the impacts that climate change may have on future weather patterns. The 16 years of available data capture a range of conditions that importantly lead to significant changes in the extent of mixing in MPL. Whilst it is out of the scope of this report to assess the role of climate change, more frequent occurrence of unseasonal or extreme events, such as mild or very cold winter weather and storm events, is likely to change the frequency of deep mixing over time.

Some of the key uncertainties in the model set-up have been investigated with a series of sensitivity tests. Although not exhaustive, patterns emerge from the tests results. Despite a number of changes to key model parameters the predictions of mixing and stratification

remain generally consistent with the base case simulation, with the exception of the scenario with groundwater temperature of 24^{o}C. If the groundwater is of sufficiently high temperature it has the potential to alter the stratification and mixing regime because it no longer maintains a density gradient that is strong enough to inhibit mixing at the bottom of the pit.

The sensitivity results suggest that within the limits that have been tested, the uncertainty associated with the inflow TDS, water clarity and river temperature are unlikely to modify the broad prediction of the hydrodynamics. Moreover, the tests to address some the uncertainty yield results that are consistent with the findings of previous studies of MPL. To add to that, the predicted limnological behaviour is consistent with the general expectation found in a review of the literature.

5 Summary and Implications

The limnological behaviour predicted by the MPL model consists of the following attributes:

- Strong seasonal stratification in the warmer months which, in the peak of summer, consists of an epilimnion of approximately 5 to10 m thick, a metalimnion of 10 to 20 m thick and hypolimnion that extends beneath the metalimnion;
- Winter mixing erodes the temperature stratification and in years with cooler and/or stormier autumn and winter months the mixing may extend more than 150 m below the surface. In years with warmer autumn and winter months, the extent of winter mixing is less than 100 m, and typically less than 75 m;
- Mixing to the full depth of MPL is not indicated by the model because of the presence of a deep pycnocline that evolves though seepage of high TDS groundwater into the bottom of the pit and the lack of mixing energy at depth;
- This prediction holds with the exception of a case in which groundwater is warm enough (estimated to be 24^{o}C) to overcome the density differences due to TDS and increase the occurrence of mixing to the bottom of the pit to almost once in every two years (on average).
- Deep mixing below 1000 m RL is predicted to occur in approximately 50% of years in the first 18 years after filling. The model results suggest sequential years of deep and shallow mixing because of the legacy effects of, in particular, years with warm autumn and winter conditions. Therefore, extended periods of no deep mixing are expected;
- Mixing below 1000 m RL was not indicated in the extended 16 years of simulation because of the increasing height of the pycnocline associated with the continual groundwater inputs into the base of the pit; and
- Of the limitations and uncertainties associated with developing a predictive model of MPL, the groundwater temperature (as noted above) presents as the uncertainty that is likely to impact on the predicted outcomes.

The predicted physical limnology has a number of associated implications that should be considered in accompanying studies. They are:

- The chemistry associated with very long, and potentially indefinite, periods of isolation (i.e. a lack of refreshing from mixing processes) of the waters beneath the deep pycnocline from the waters above;
- Long periods (possibly decades) of isolation of waters below 70 to 100 m and above the pycnocline. Unlike the water beneath the pycnocline (which is refreshed by new groundwater seepage), there is no renewal of these waters. Substantial chemical change is expected over this time;
- Mixing of waters beneath 70 to 100 m into the surface water during deep mixing years, has the potential to rapidly and substantially change the surface water chemistry and the chemistry of the released water;
- By the same physical mechanism, a lack of deep mixing for long periods may lead to deteriorated surface water chemistry due to a lack of dilution of poor quality run-off waters; and
- MPL will take some time to adjust to a run-off, rainfall and groundwater dominated system after a filling period dominated by diverted river water so it is likely that the

physical limnology will gradually change over decadal timeframes, with associated long-term evolution of the water chemistry.

6 References

AECOM, 2018. Martha Pit Lake Management Strategy. Martha Pit Lake – Modelling, Mitigation and Management Assessment.

Amorocho, J. and Devries, J.J. 1980. A new evaluation of the wind stress coefficient over water surfaces. J. Geophys. Res. 85, pp. 433–442.

Bernudez, A, Delgado, J.L., Garcia-Garcia, L.M., and Quintela, P. A three layer model ro Estimate Pit Lake Water Quality. 2007. IMWA Symposium 2007: Water in Mining Environments, R. Cidu and F. Frau (Eds), 27-31 Mar 2007, Caliari, Italy.

Boland, K.T. and Padovan, A.V. Seasonal stratification and mixing in a recently flooded mining void in tropical Australia. 2002. Lakes and Reservoirs: Research and Management, 7, pp. 125-131.

Castendyk, D.N. and Eary, L.E. (Eds). 2009. Mine Pit Lakes: Characteristics, Predictive Modeling and Sustainability. Volume 3. Published by Society for Mining, Metallurgy and Exploration.

Castendyk, D.N. and Webster-Brown, J.G. 2007. Sensitivity analysis in pit lake prediction, Martha Mine New Zealand 1: Relationship between turnover and input water density. Chemical Geology 244, pp 42-55.

Casulli, V. and Cheng, R.T. 1992. Semi-implicit finite difference methods for three-dimensional shallow water flow. *Int. J. Numer. Methods Fluids*. 15, pp. 629–648.

Czop, M., Matyka, J., Sracek, O. and Szuwarzynski, M. 2011. Geochemisrty of the Hyperalkaline Gorka Pit Lake (pH>13), in the Chrzanow Region, Southern Poland. Water Air Soil Pollut, 214, pp. 423-434.

Dowling, J. Atkin, A. Beale G. and Alexander G. 2004. Development of Sleeper Pit Lake. Mine Water and Environment, 23, pp 2-11.

Doyle, F.W. & Davies, S.J.J.F. (1999). Creation of a wetland ecosystem from a sand mining site: a multidisciplinary approach. In, Wetlands for the future, McComb, A. J. & Davis, J. A. (eds.) pp 761-772.

Doyle, G.A., and Runnells, D.D. 1997. Physical limnology of existing mine pit lakes. Mixinf Engineering, Dec 1997, pp. 78-80.

Fisher, T.S.R. 2002. Limnology of the meromictic island copper mine pit lake. PhD Thesis, Uni. of British Columbia.

Hodges, B.R., Imberger, J., Saggio, A. and Winters, K.B., 2000, Modeling basin-scale internal waves in a stratified lake, Limnology and Oceanography, 45(7): 1603-1620.

Imberger, J. and Patterson, J.C. 1981. A dynamic reservoir simulation model - DYRESM 5. Transport models for inland and coastal waters H. Fischer (ed.). Academic Press., pp. 310– 361

Integral Consulting Inc. 2007. Appendix B-1: Draft Ecological Investigations for the Pit Lake Operable Unit. Prep. for Atlantic Richfield Company.

Jacquet, J. 1983. Simulation of the thermal regime of rivers. Mathematical modeling of water quality: Streams, lakes and reservoirs: G.T. Orlob (ed.). Wiley-Interscience.

Jewell, P.W. 2009. Stratification controls of pit mine lakes. Mining Engineering Technical Paper February 2009, pp 40-45.

Kumar, R.N., McCullough, C.D., Lund M.A. and Larranaga, S.A. Assessment of factors limiting algal frowth in acidic pit lakes – a case study from Western Australia, Australia. Environ. Sci. Pollut. Res., 23 pp. 5915 - 5924.

Levy, B.B., Custis, K.H., Casy, W.H. and Rock, P.A. 1997. The Aqueous Geochemistry of the Abandoned Spenceville Copper Pit, Nevada County, California. J. Environ. Qual., 26 pp. 233-243.

Moreira, S., Boehrer, B. Schultze, M. and Samper, J. 2009. A Coupled Hydrodynamic-Geochemical Model of Meromictic Pit Lake Waldersee. Proc. International Mine Water Conference, October 2009, pp. 892-897.

Parshley, J.V. and Bowell, R.J. 2003. The Limnology of Summer Camp Pit Lake: A Case Study. Mine Water and the Environment, 22, pp. 170-186.

Pieters, R., Codey, W. Ashley, K.I. and Lawrence, G.A. Artificial circulation od a mine pit lake. Can. J. Civ. Eng, 42, pp. 33-43.

Schultze, M. and Boehrer, B. 2008. Development of Two Meromictic Pit Lakes – a Case Study from the Former Lignite Mine Mersebirg-Ost, Germany.

Soni, A.K, Mishra, B. and Singh, S. 2014. Pit Lakes as an end use of mining: A review. Journal of Mining and Environment, Vol 5 (2), pp. 99 -111.

Spigel, R.H. 1997. Density Stratificaiton and Mixing in the Proposed Waihi Pit Lake. Report prepared for Woodward-Clyde (NZ) Ltd.

Stevens, C.L. and Lawrence, G.A. 1997. The effect of sub-aqueous disposal of mine tailings in standing waters. Jounrnal of Hydraulic Research, 35(2), pp. 147-159.

Stevens, C.L. and Lawrence, G.A. 1998. Stabilty and meromixis in a water-filled mine pit. Limnology and Oceanography, 43(5) pp. 946-954.

Yusta, I and Sanchez Espana, J. 2013. Hydrochemistry and stratification of the Blondis lake: the “invisible fingerprint” of historical iron mining in La Arboleda (Bizkaia). Boletín Geológico y Minero, 124 (4), pp. 639-655.

Zhao, L.Y.L, McCullough, C.D. and Lund, M.A. 2009. Mine Voids Management Strategy (I): Pit Lake Resources of the Collie Basin. Prepared for Dept. of Water (WA) by Centre for Ecosystem Management, Edith Cowan University.

7 Appendix

7.1 Pit Lake Review

Table 7.1 Summary of pit lake characteristics reported in the literature.

Pit Lake Name	Depth (m)	SA (ha)	Country/Region	Stratification	Reference
Island Copper	350	171	British Columbia, Canada	Meromictic	Fisher 2002
Martha	244	66	Waihi, New Zealand		
Berkeley	242	290	Butte, Montana USA	Meromictic	Doyle and Runnells 1997
Lignitos de Meirama	200	333	A Coruna, Spain	Meromictic	Bermudez et al. 2007
Caland	180	120	Ontario, Canada	Meromictic	McNaughton 2001
Sleeper	177	127	Nevada, USA	Holomictic	Dowling et al. 2004
Hogarth	160	100	Ontario, Canada	Meromictic	McNaughton 2001
Brenda	150	44.18	British Columbia, Canada	Meromictic	Stevens and Lawrence 1997
Enteprise	140	27	Northern Territory, Australia	Holomictic	Boland and Padovan 2002
Athabasca Basin, Gunnar	110	70	Saskatchewan, Canada	Meromictic	Doyle and Runnells 1997
Zone 2	110	17	Yellowknife, Canada	Meromictic	Pieters at al. 2014
Blowout	71	3.38	Iron Mountain, Utah, USA	Holomictic	Castendyk and Jewel 2002
Lake Kepwari	65	103	Collie, Western Australia	Holomictic	Kumar et al. 2016
Wollaston Lake, B-Zone	55	290	Saskatchewan, Canada	Holomictic	Doyle and Runnells 1997
Yerington	40	57	Nevada, USA	Holomictic	Integral 2007
Lake Rassnitz	36	230	Halle, Germany	Meromictic	Schultze and Boehrer 2008
Lake Wallendorf	27	280	Halle, Germany	Meromictic	Schultze and Boehrer 2008
Blondis	27	164	Bilbao, Spain	Holomictic	Yusta and Espana 2013
Blackhawk	26.5	1.6	Iron Mountain, Utah, USA	Holomictic	Castendyk and Jewel 2002
Athabasca Basin, D Pit	26	16	Saskatchewan, Canada	Holomictic	Doyle and Runnells 1997
Summer Camp	24	N/A	Nevada, USA	Meromictic	Parshley and Bowell 2003
Blue Waters	24	13.7	Collie, Western Australia	Holomictic	Zhao et al. 2009
Gorka	18	3.1	Chrzanow, Poland	Meromictic	Czop et al. 2011
Spnceville	17	0.2	Nevada, Canada, USA	Potentially Meromictic	Levy et al. 1997
Lake Stockton	15.4	47	Collie, Western Australia	Holomictic	Zhao et al. 2009
Mine Lake 111	10.7	10.2	Lusatia, Germany	Meromictic	Karakas et al. 2003
Black Diamond A	8	4.6	Collie, Western Australia	Homothermal	Zhao et al. 2009
Centaur	7	4.5	Collie, Western Australia	N/A	Zhao et al. 2009
Black Diamond B	5	2.6	Collie, Western Australia	N/A	Zhao et al. 2009
Waldsee	4.7	0.6	Dobern, Germany	Meromictic	Moreira at al. 2014
Duncan	3	0.65	Iron Mountain, Utah, USA	Holomictic	Castendyk and Jewel 2002

7.2 Model Flows

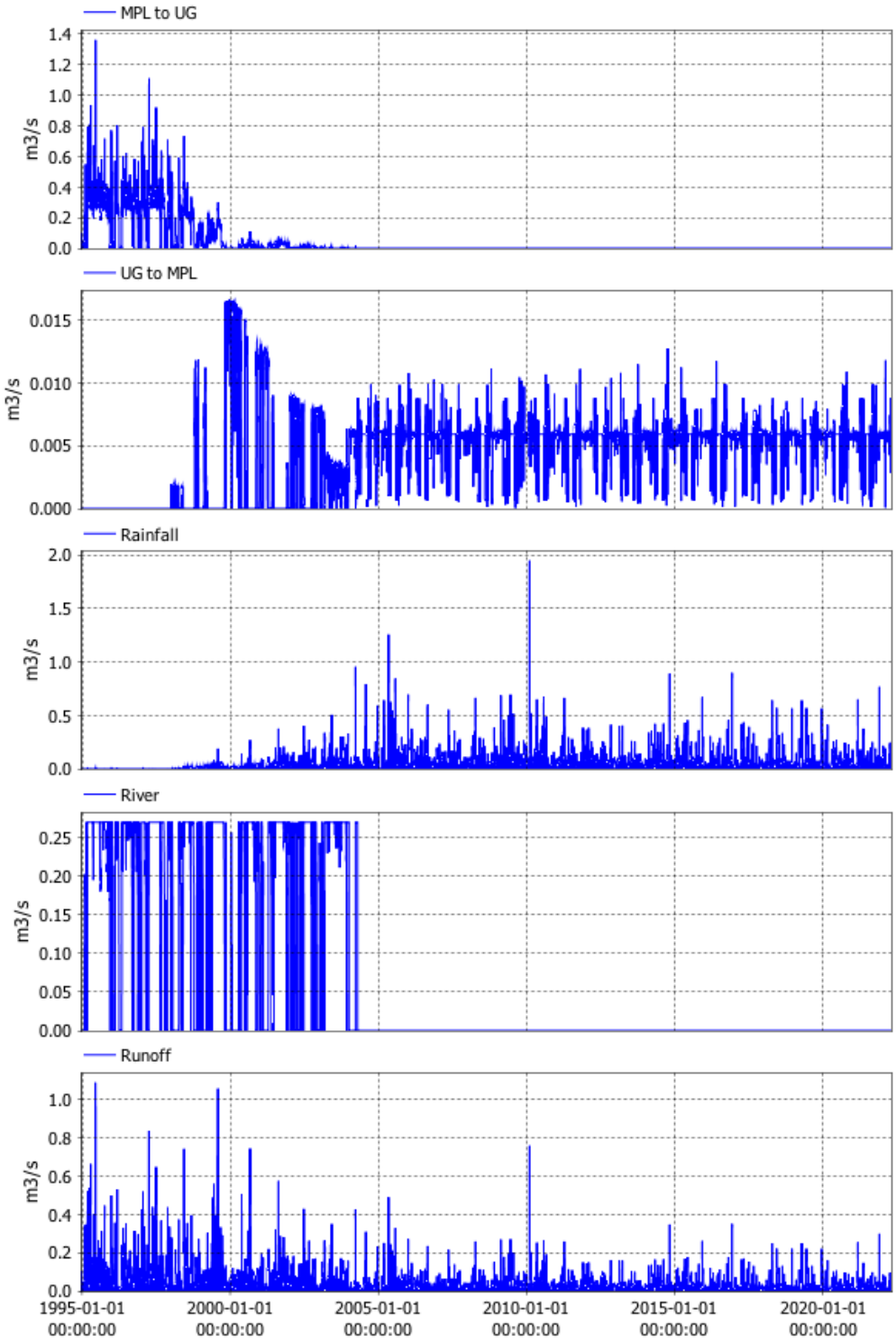

Figure 7.1 Time series of flow inputs to model (extraction in the case of MPL to UG).

7.3 Model Meteorological Forcing

Table 7.2 Annual means of key characteristics of 40-year meteorological time series.

Model Year	Obs. Year	Daily Max. Air Temp. (°C)	Daily Min. Air Temp. (°C)	Daily Mean Relative Humidity	Daily Total Solar Rad. (W/m2)	Daily Max. Wind Speed (m/s)
Y01	1995	18.47	10.97	0.78	3807.02	5.64
Y02	1996	18.58	10.42	0.76	4038.35	5.66
Y03	1997	18.33	10.15	0.77	4076.17	6.63
Y04	1998	19.33	11.26	0.79	4004.96	6.48
Y05	1999	18.54	9.17	0.81	3991.87	5.36
Y06	2000	18.25	9.61	0.81	4052.28	5.85
Y07	2001	18.10	9.62	0.84	3942.77	5.62
Y08	2002	17.89	9.76	0.80	4136.53	6.47
Y09	2003	18.06	9.16	0.81	3919.98	5.50
Y10	2004	17.46	8.75	0.79	3987.86	6.08
Y11	2005	18.57	9.17	0.80	4078.85	5.52
Y12	2006	17.87	8.71	0.79	4096.26	6.46
Y13	2007	18.17	9.67	0.79	3991.86	6.59
Y14	2008	18.24	9.68	0.78	4060.63	6.58
Y15	2009	17.98	8.82	0.78	4114.10	6.47
Y16	2010	18.69	9.61	0.78	4070.47	6.23
Y17	2011	18.84	10.43	0.76	4039.63	6.38
Y18	2012	18.21	9.66	0.77	4117.22	6.47
Y19	2013	19.35	10.11	0.76	4094.44	6.15
Y20	2014	18.61	9.72	0.75	4040.41	6.66
Y21	2015	18.68	9.61	0.75	4052.76	6.72
Y22	2016	18.98	10.74	0.77	3872.00	6.53
Y23	2017	18.89	10.69	0.81	4132.68	6.25
Y24	2002	17.89	9.76	0.80	4136.53	6.47

Y25	2003	18.06	9.16	0.81	3919.98	5.50
Y26	2004	17.46	8.75	0.79	3987.86	6.08
Y27	2005	18.57	9.17	0.80	4078.85	5.52
Y28	2006	17.87	8.71	0.79	4096.26	6.46
Y29	2007	18.17	9.67	0.79	3991.86	6.59
Y30	2008	18.24	9.68	0.78	4060.63	6.58
Y31	2009	17.98	8.82	0.78	4114.10	6.47
Y32	2010	18.69	9.61	0.78	4070.47	6.23
Y33	2011	18.84	10.43	0.76	4039.63	6.38
Y34	2012	18.21	9.66	0.77	4117.22	6.47
Y35	2013	19.35	10.11	0.76	4094.44	6.15
Y36	2014	18.61	9.72	0.75	4040.41	6.66
Y37	2015	18.68	9.61	0.75	4052.76	6.72
Y38	2016	18.98	10.74	0.77	3872.00	6.53
Y39	2017	18.89	10.69	0.81	4132.68	6.25
Y40	2002	17.89	9.76	0.80	4136.53	6.47

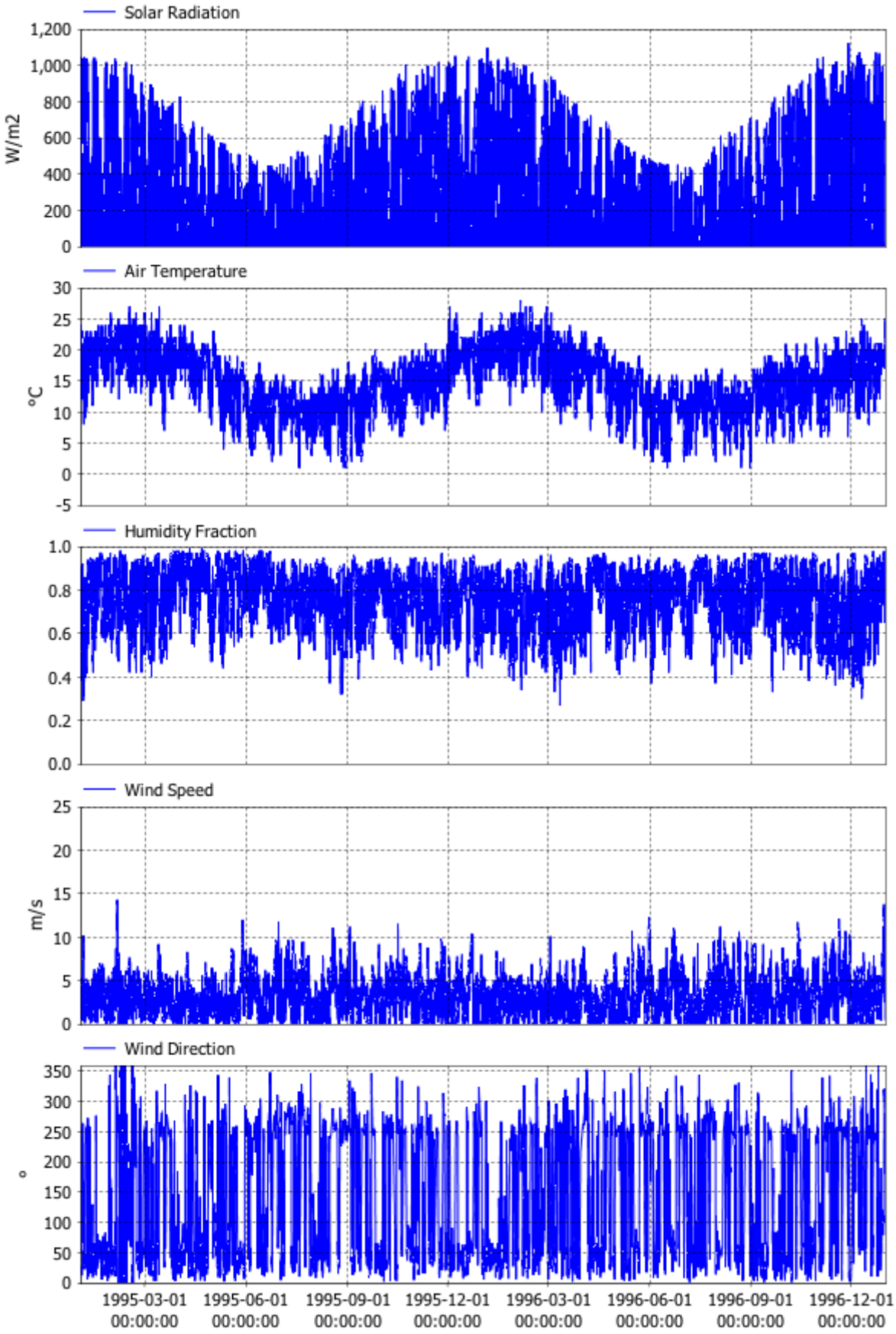

Figure 7.2 Model meteorological forcing for 1995 and 1996.

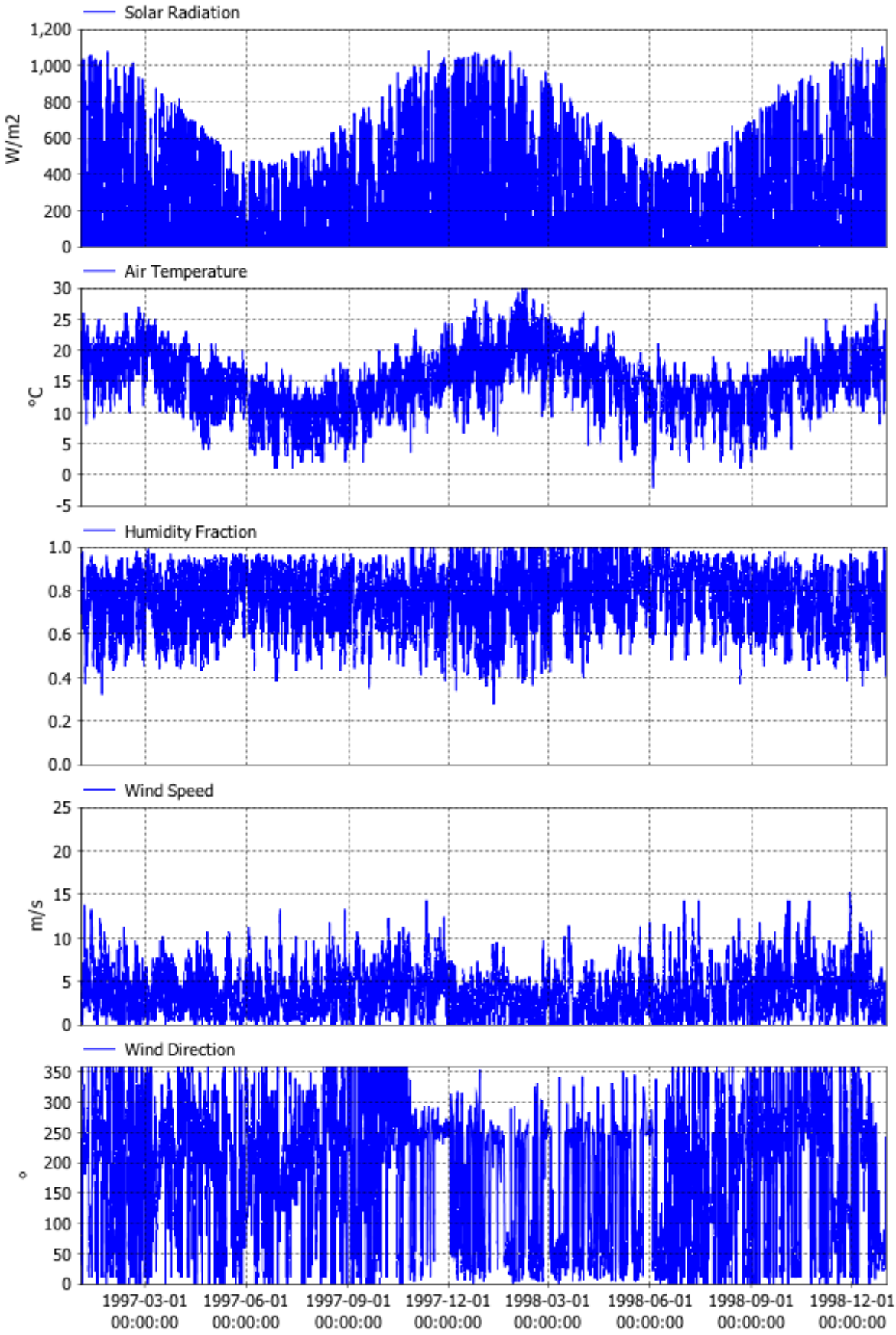

Figure 7.3 Model meteorological forcing for 1997 and 1998.

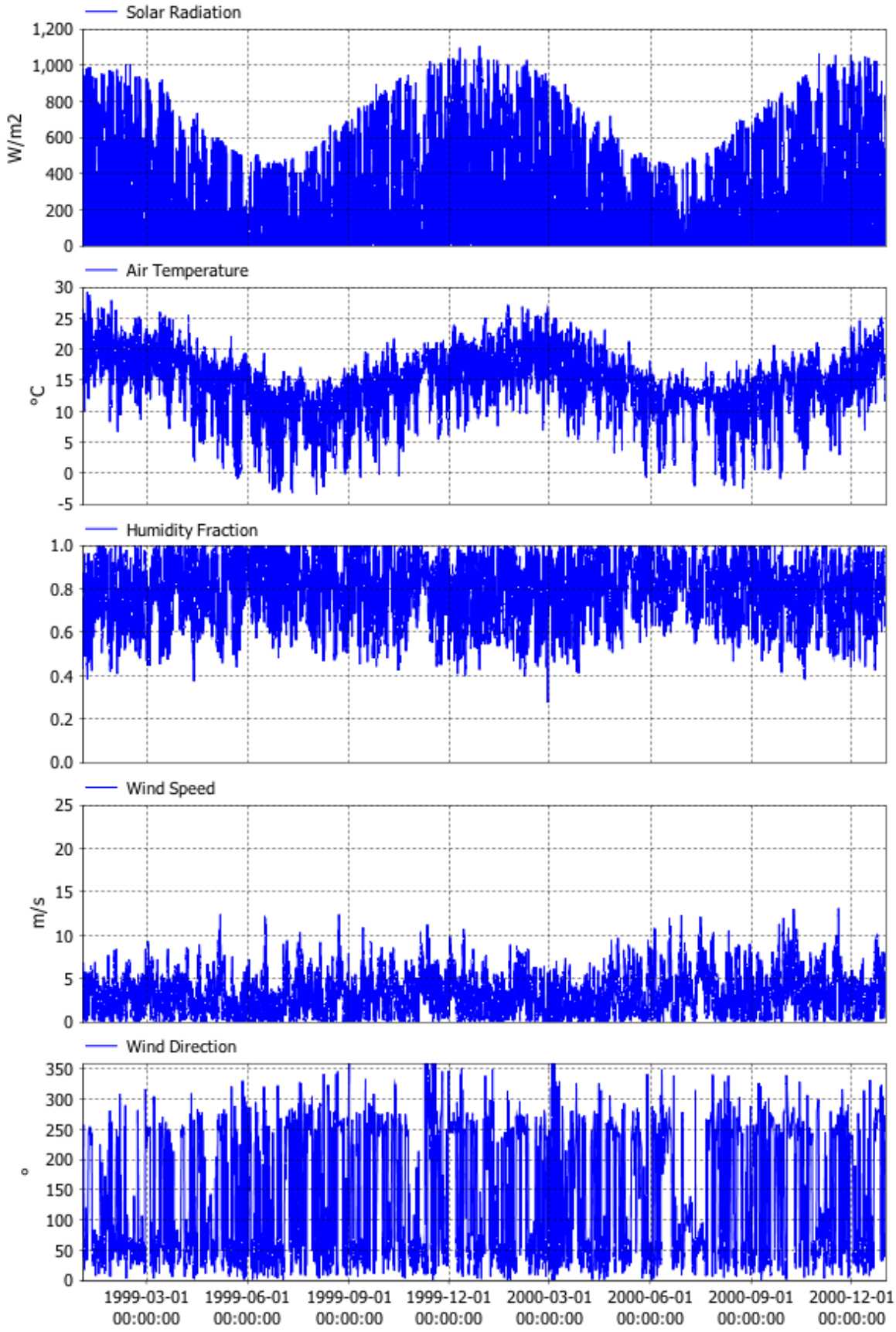

Figure 7.4 Model meteorological forcing for 1999 and 2000.

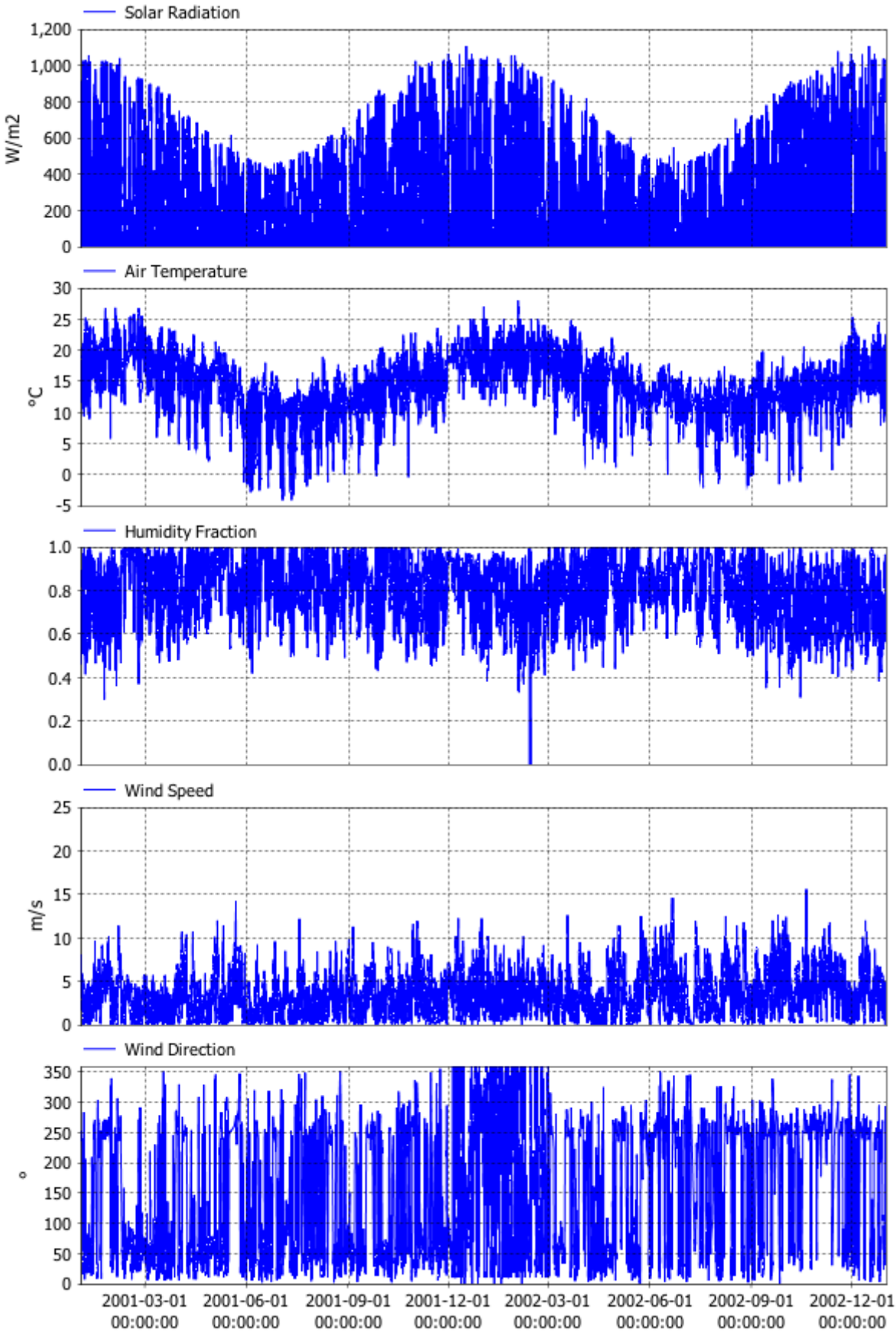

Figure 7.5 Model meteorological forcing for 2001 and 2002 (also 2017 and 2018).

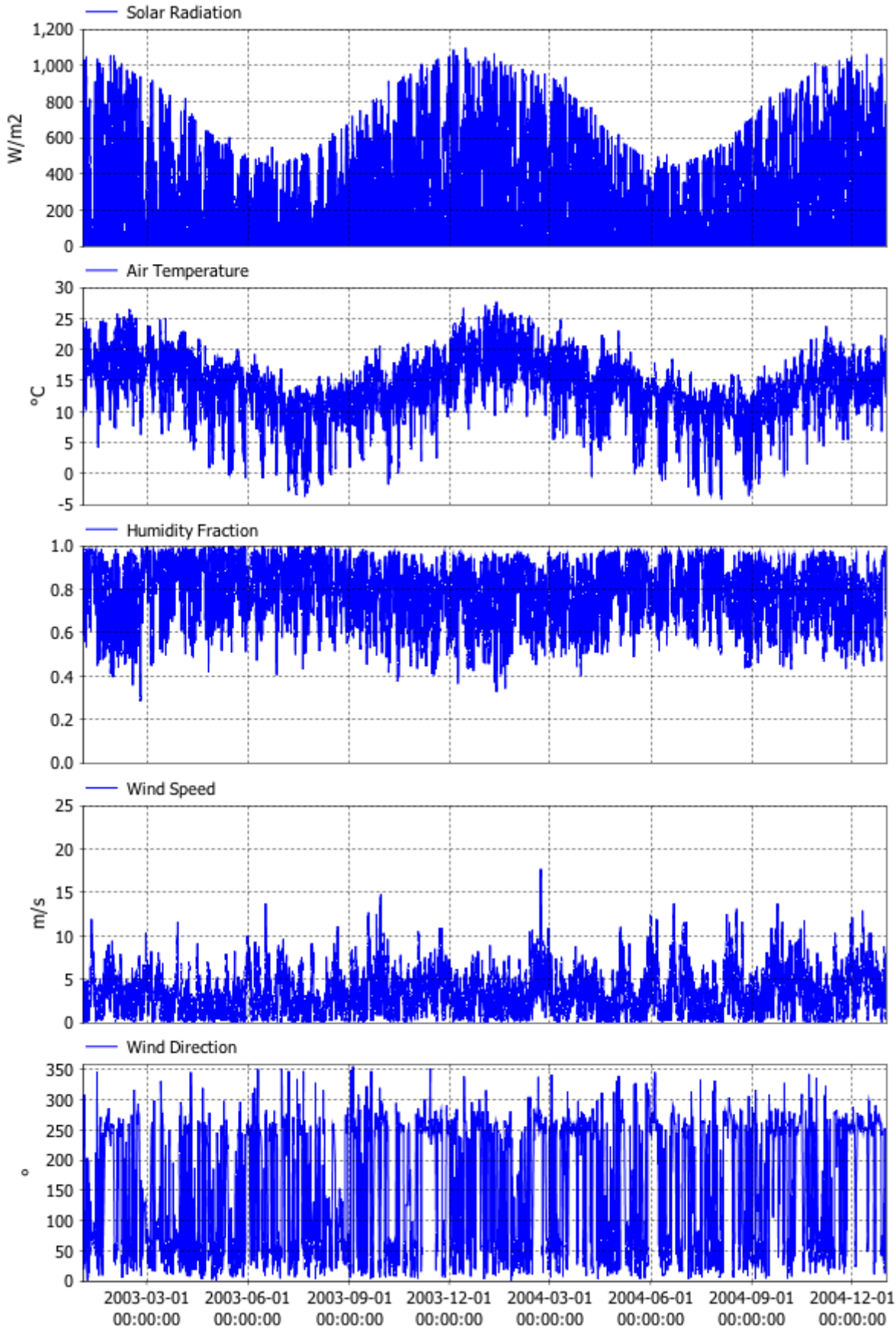

Figure 7.6 Model meteorological forcing for 2003 and 2004 (also 2019 and 2020).

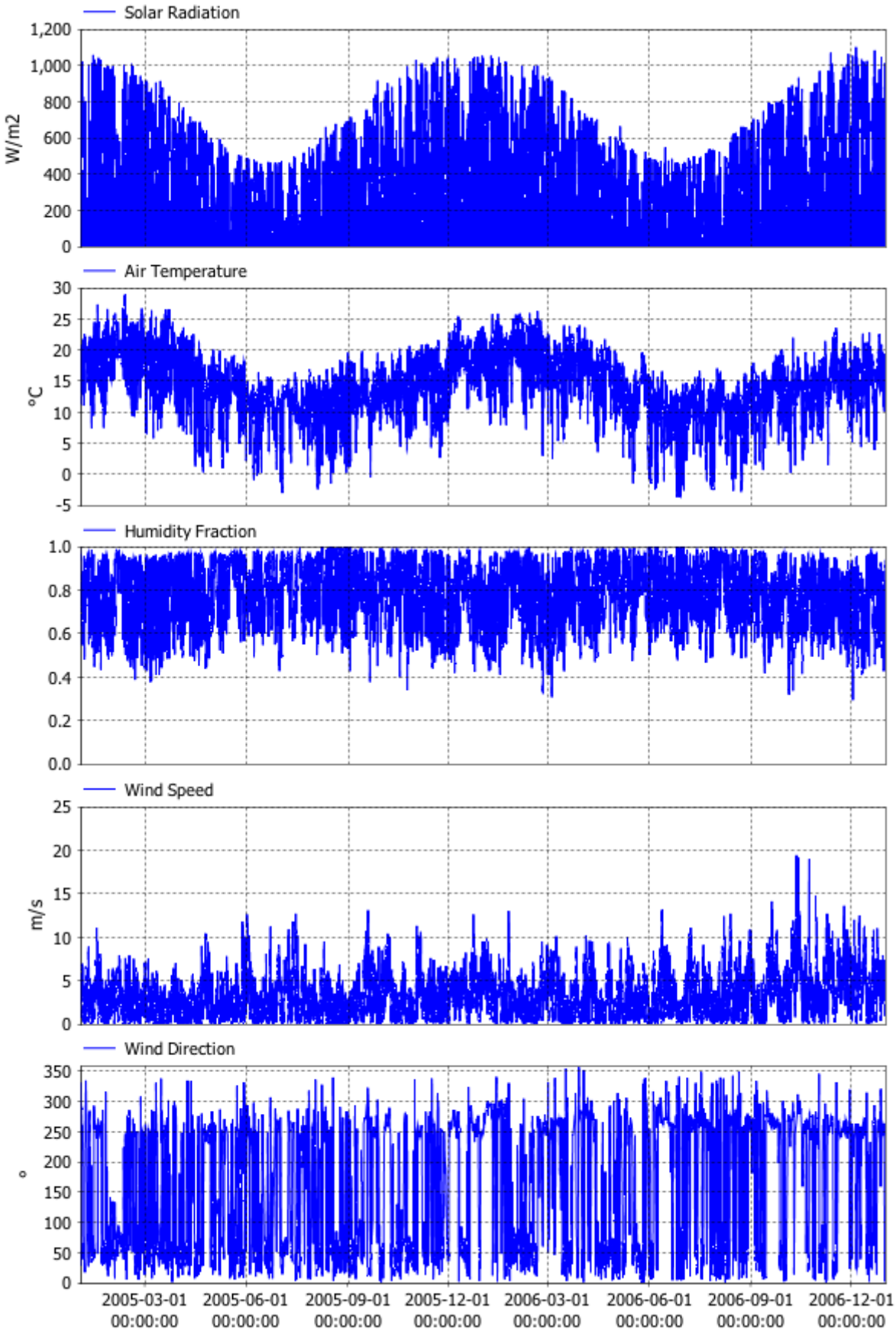

Figure 7.7 Model meteorological forcing for 2005 and 2006 (also 2021 and 2022).

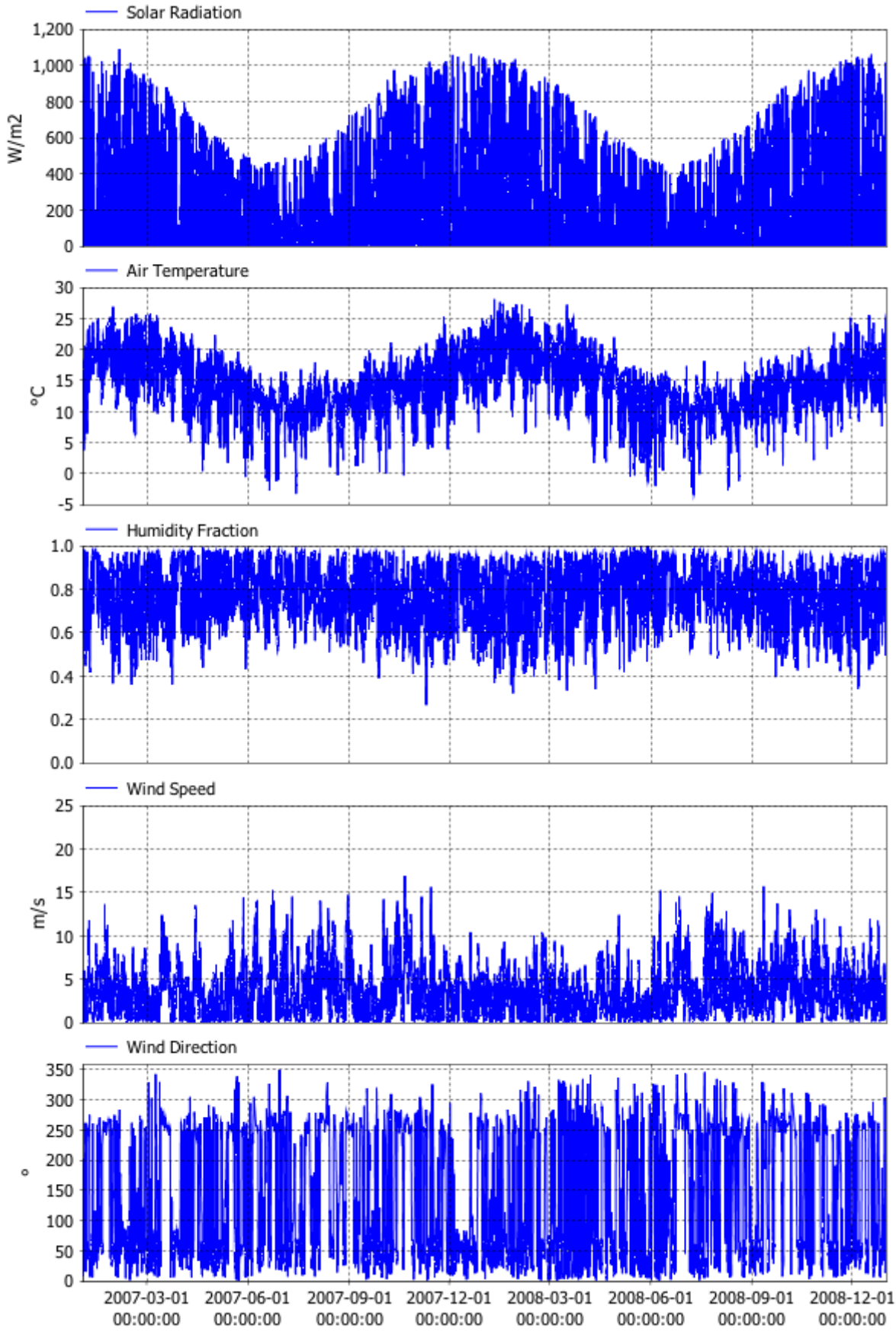

Figure 7.8 Model meteorological forcing for 2007 and 2008 (also 2023 and 2024).

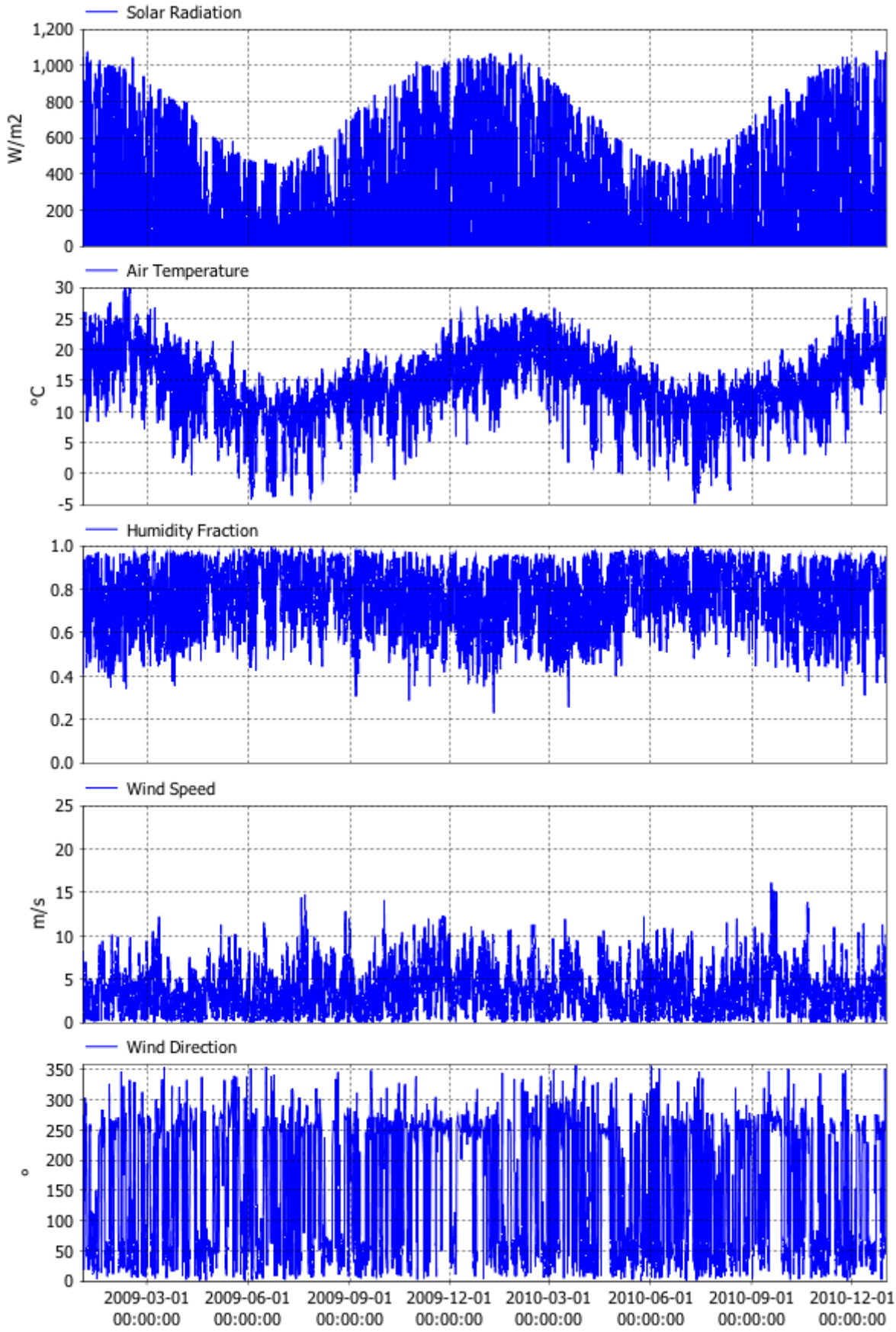

Figure 7.9 Model meteorological forcing for 2009 and 2010 (also 2025 and 2026).

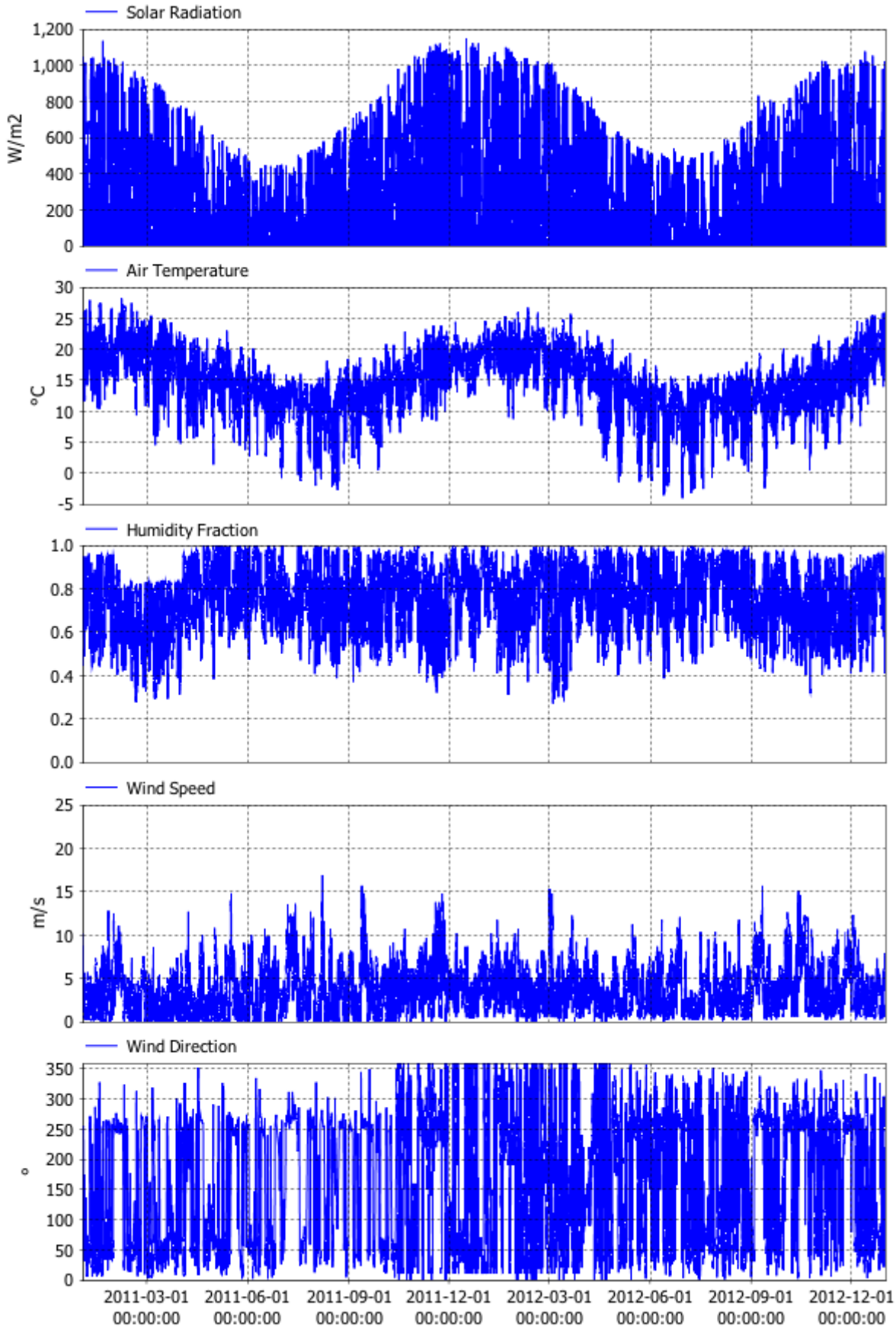

Figure 7.10 Model meteorological forcing for 2011 and 2012 (also 2027 and 2028).

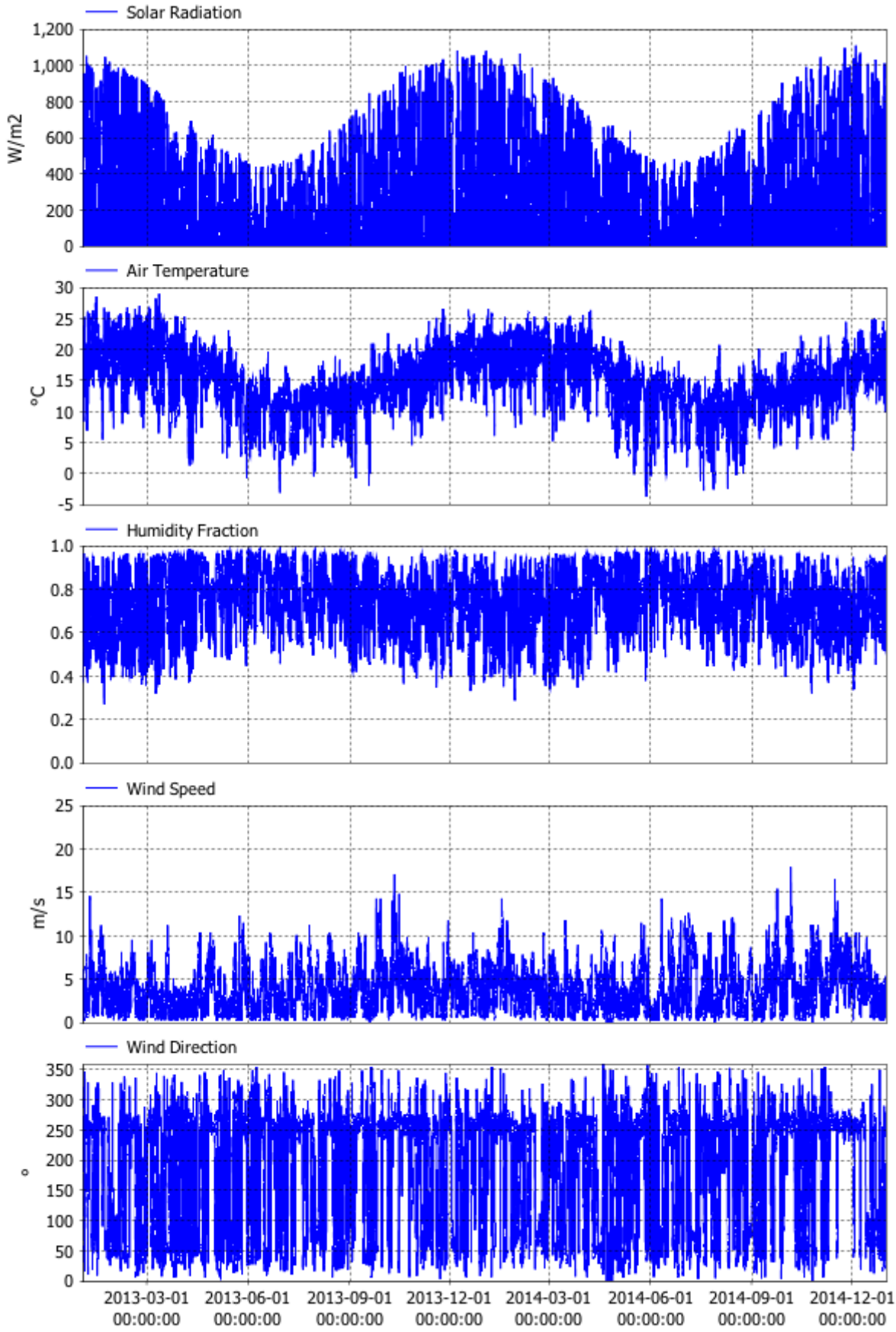

Figure 7.11 Model meteorological forcing for 2013 and 2014 (also 2029 and 2030).

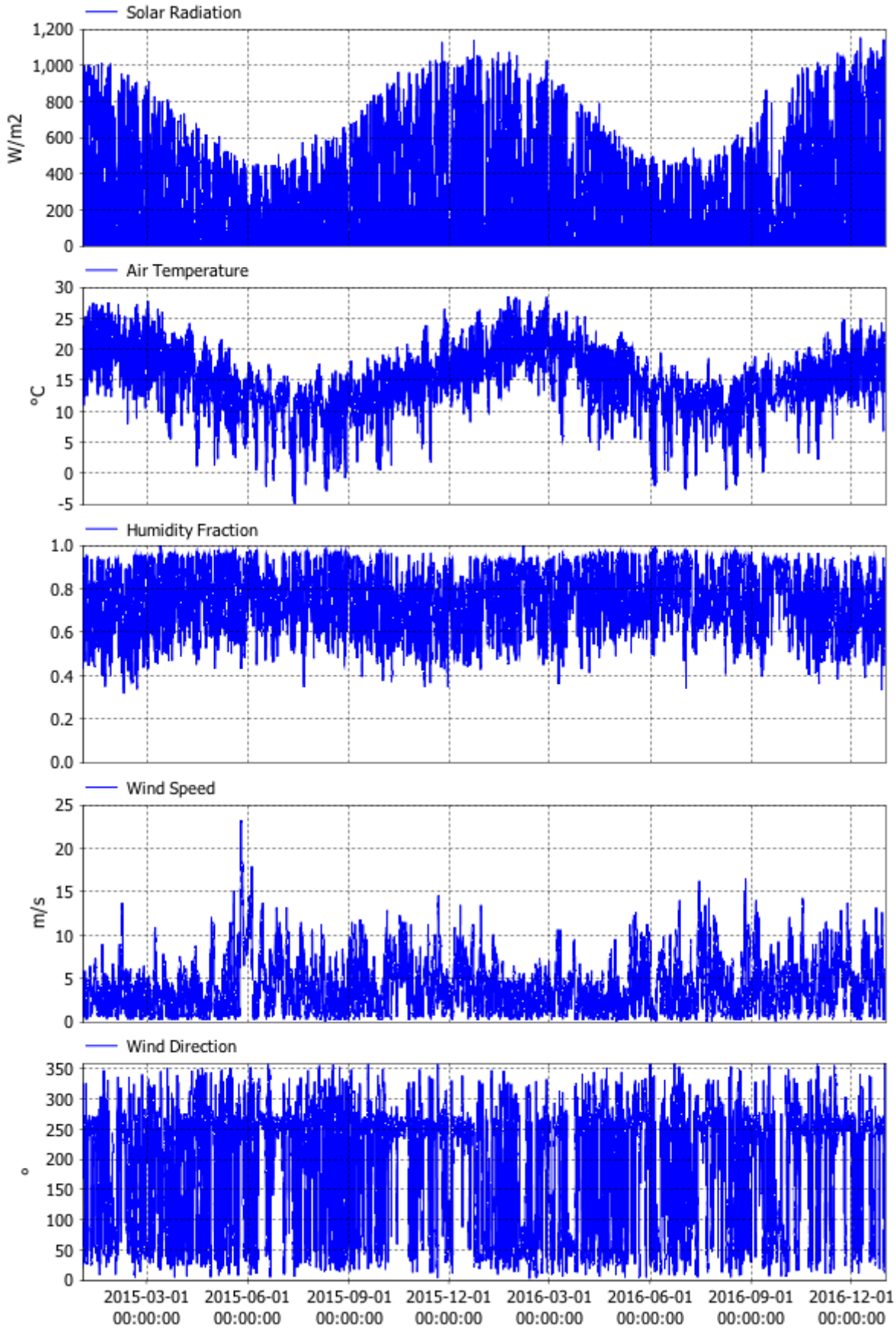

Figure 7.12 Model meteorological forcing for 2015 and 2016 (also 2031 and 2032).

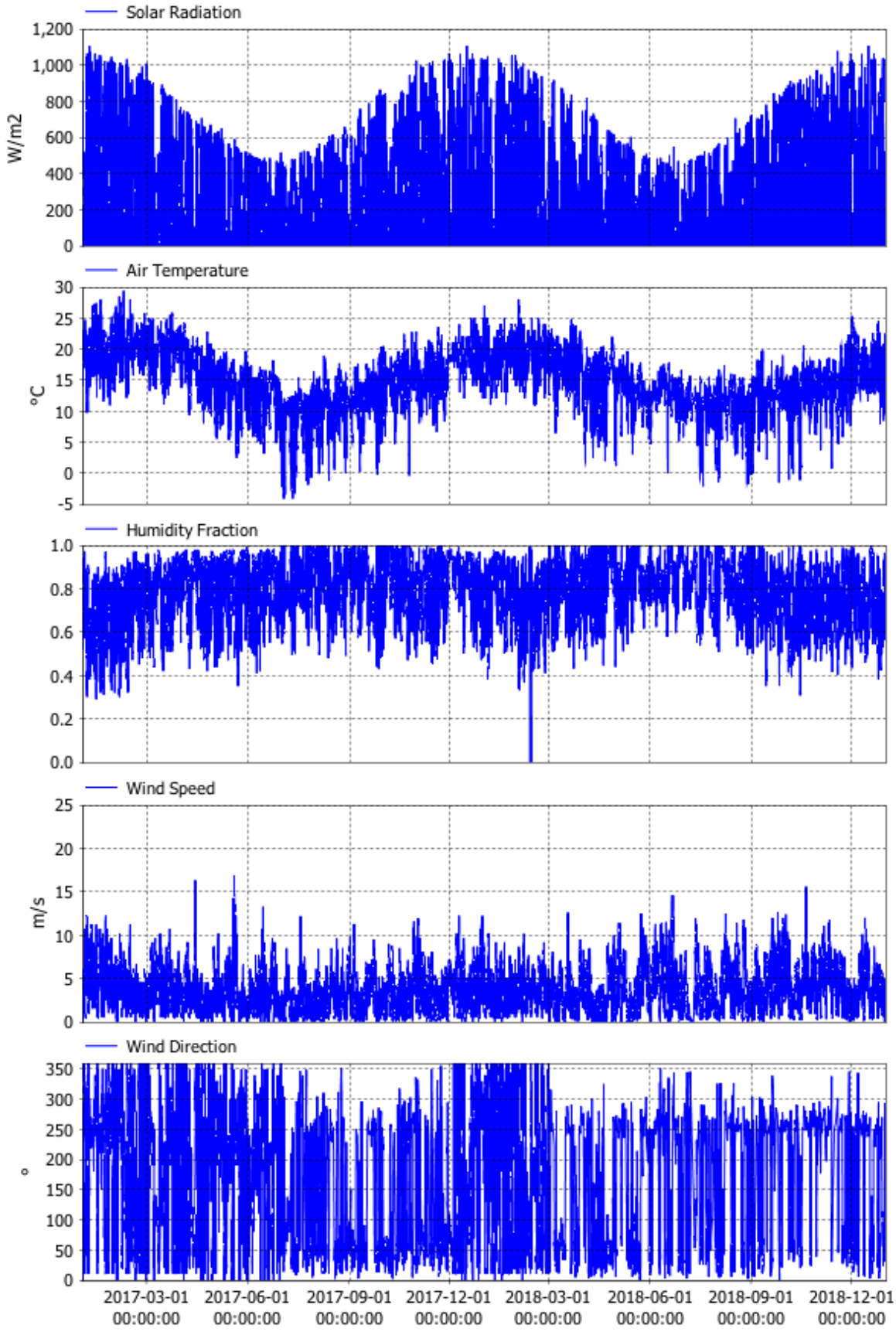

Figure 7.13 Model meteorological forcing for 2017 and 2018 (also 2033 and 2034).